Jovian Dynamics. Part I: Vortex Stability, Structure, and Genesis

G. P. WILLIAMS

Geophysical Fluid Dynamics Laboratory/NOAA, Princeton University, Princeton, New Jersey

(Manuscript received 7 December 1995, in final form 24 April 1996)

ABSTRACT

The vertical structure of Jupiter's atmosphere is probed and isolated by evaluating the stability characteristics of planetary vortices over a wide parameter range. The resulting structures lead to simulating the genesis of single and multiple vortex states in Part I of this paper and the genesis of an equatorial superrotation and midlatitudinal multiple jets in Part II.

The stability and genesis of baroclinic Rossby vortices, the vortices associated with long solitary Rossby waves in a stratified fluid, are studied numerically using a primitive equation model with Jovian and oceanic parameters and hypothetical structures. Vortex stability, that is, coherence and persistence, depends primarily upon latitude location and vertical structure and is used to deduce possible stratifications for Jupiter's atmosphere. The solutions suggest that Jupiter's large-scale motions are confined to a layer of depth h and are bounded by an abyss with an impermeable interface at a depth H, such that $h/H \leq 1/20$. Consequently, they also extend earlier results derived with the reduced-gravity, shallow-water model, particularly the explanation for the origin, uniqueness, and longevity of the Great Red Spot (GRS).

Beginning at the equator, stable anticyclones are seen to exist only when they have the Hermitian latitudinal form, the Korteweg–deVries longitudinal form, the confined exponential vertical structure $\exp(Nz/H)$, and the amplitude range as prescribed by the analytical theory of Marshall and Boyd for $N = 8$. Soliton interactions occur between equatorial vortices of similar horizontal and vertical form.

In middle and low latitudes, shallow anticyclones with an exponential structure of $N = 20$ exist quasi-stably for a variety of sizes. Such vortices remain coherent but tend to migrate equatorward (where they disperse) at rates that depend upon their size, location, and vertical structure: large and medium anticyclones propagate primarily westward while migrating slowly, whereas small storms just migrate rapidly and then collapse. The migration of these large, shallow vortices can be reduced, but not stopped, in low latitudes by an easterly jet with the same vertical structure.

Anticyclones are stabler when they are thinner relative to the abyss. Thus, when $N = 60$, their migration is sufficiently slow that it can be stopped by a weak easterly jet. Furthermore, absolute stability sets in when $N = 90$ and migration ceases completely for the large, thin anticyclones that now just propagate westward. Such flows may also be usefully represented by a vertical structure that is *linear* in z for the velocity and static stability in the thin upper layer and vanishes in the abyss.

Large, thin ($N \geq 90$) anticyclones can exist indefinitely either freely or when embedded within an anticyclonic zone of alternating jet streams of similar vertical structure. This holds true for the confined linear-z representation also. The permanence of GRS-like, low-latitude vortices in Jovian flow configurations occurs in a variety of lengthy calculations with thin structures. Ocean vortices are less persistent because the thermocline is relatively thick.

The baroclinic instability of easterly jets is nonquasigeostrophic and takes on the form of solitary rather than periodic waves when the jets have a thin exponential ($N \geq 90$) or confined linear-z structure. Such nonlinear waves develop into vortices that exhibit a variety of configurations and evolutionary paths. In most cases multiple mergers tend toward an end state with a single large vortex. Two types of merging occur in which a stronger vortex either catches a weaker one ahead of it or reels in a weaker one from behind. This duality occurs because propagation rates depend as much on local as on global conditions. In a further complication, vortices generated by an unstable easterly tend to have an exponential structure for exponential jets but a first baroclinic eigenmodal structure for confined linear-z jets.

Single vortex states resembling the GRS, with sizes ranging from 15° to 50° in longitude and with temperature gradients, velocities, and propagation rates near the observed range, can be generated either directly through the growth of a local front in a marginally unstable easterly jet or indirectly through a series of mergers of the multiple vortices generated by a more unstable easterly jet. Sets of vortices can be produced simultaneously in the anticyclonic zones centered about latitudes −21°, −33°, and −41°, and have the same relative scales as Jupiter's GRS, Large Ovals, and Small Ovals. Thin anticyclones can also be generated at the equator by the action of vortices lying in low latitudes. Equally realistic long-lived vortices can also be generated by jets with structures matching the recent *Galileo* spacecraft observations by using other hyperbolic forms and greater depth scales.

1. Introduction

This two part study is concerned with trying to improve our definition and understanding of the global circulations of the atmospheres of Jupiter and Saturn. The approach adopted is one of using the highly selective behavior of planetary vortices to examine hypothetical vertical structures for the planets to see whether such structures favor the mutual genesis of vortices, equatorial superrotation, and multiple midlatitude jets.

To understand these phenomena and eventually to simulate Jupiter's circulation requires, at this stage, that

Corresponding author address: Dr. Gareth P. Williams, Geophysical Fluid Dynamics Laboratory/NOAA, Princeton University, P.O. Box 308, Princeton, NJ 08542.

four interconnected fundamental questions be addressed in order.

1) What atmospheric structures allow vortices to be absolutely stable[1] and so last much longer than in Earth's oceans?
2) What processes generate single and multiple long-lived vortex states?
3) How are multiple midlatitude jets generated in a way that is consistent with vortex stability and genesis?
4) How is an equatorial superrotation produced in coexistence with multiple jets and vortices?

These problems are studied numerically using a three-dimensional, primitive equation (PE) model, mainly with Jovian parameters and hyperbolic vertical structures.

a. Approach

Given that a simple PE model may not be particularly relevant to Jupiter, we begin the calculations with the intent of systematically evaluating the behavior of planetary vortices with baroclinic and barotropic components, with and without zonal currents, at the equator and in middle and low latitudes. Such modes are at least of intrinsic value. However, the selective existence of absolutely stable vortices also allows them to be used very effectively as an atmospheric probe to deduce the preferred vertical structure, qualitatively and even, perhaps, quantitatively. Our presentation follows this systematic approach to show how and why we reach the conclusion we do, that the motions occupy a relatively thin layer.

The main hypothesis invoked, that the atmospheric circulations are relatively shallow and driven by a baroclinicity supplied by the sun and the planet, was first put forward two decades ago and has since been examined with a wide range of standard geophysical fluid dynamics (GFD) models (Williams 1975a,b; 1978; 1979; 1985b; 1988a,b). For a recent review of the current status of Jovian dynamical theory, see Gierasch and Conrath (1993). To apply this hypothesis to the primitive equation model requires that the motions be confined to an upper thermocline layer of indeterminate thickness that is underlain by a deep abyssal layer, rather like the ocean.

We are concerned mainly with isolating the vertical parameters and structures that yield Jovian circulations for the PE model. Until the global relevance of any model is established, any detailed analyses seem premature and are avoided. Many calculations in parameter space are needed to achieve this goal because the phenomena and system are so completely nonlinear that existing GFD theory provides little guidance. Consequently, we work with a Boussinesq model, idealized to a periodic channel, to provide the simplest, fastest, most complete dynamical model. This follows the minimalist approach of making the least number of assumptions necessary to get a model to produce flows relevant to Jupiter. The PE model is essentially a 3D dynamical process model for vortices and jets. Some additional calculations with an atmospheric model (see Part II of this paper) indicate that compressibility and upper boundary conditions have no fundamental influence on these phenomena.

The vertical structure is probably the factor that has the most influence on flow form. Fortunately, the parameters and structures that yield absolutely stable vortices with realistic amplitudes are so narrowly defined that they should be relevant to Jovian conditions. The fact that such structures also make superrotation and multiple jets possible provides an independent cross-check on their relevance. For the vortex problems discussed in Part I, we specify existing geostrophically balanced flows and follow their evolution. Then, using the vertical structures derived in Part I, we try in Part II to reproduce complete circulations in flows developed from rest with simple heating functions.

b. Planetary views

The vortex phenomena that we primarily need to reproduce and explain are the size, stability, and singularity of the Great Red Spot (GRS) centered at latitude $\phi = -21°$, as well as the existence of the three Large Ovals at $\phi = -33°$ and the dozen or so Small Ovals at $\phi = -41°$ [see Audouze and Israël (1994) for a review of the observations]. We denote the related Rossby vortices as RV_1, $3RV_2$, and $12RV_3$, where the prefix refers to the numbers of storms and the suffix indicates the anticyclonic zone in which they lie. Indeed, we use indexes to refer to most phenomena by zone or latitude rather than use the geographical terminology devised by observers. Thus, starting at the equator, for the zonal currents we use W_0 for the superrotating westerly at $\phi = 0°$, followed by W_1 and E_1 for the low-latitude westerly and easterly at $\phi = -8°$ and $-15°$, and, thereafter, by W_i and E_i ($i = 2, 3, 4 \cdots$) for the numerous midlatitude currents. Whether the W_1, E_1 jets really are separate phenomena from those in Jupiter's midlatitudes is an issue that arises and is dealt with during the study. The equatorial plumes may also be vortices related to nonlinear planetary waves such as the Rossby soliton.

Jupiter's atmosphere in fact displays many forms of motion, some coherent and long-lived, others irregular and transient. The ubiquitous waves and turbulence occur on the smaller scale and the steady zonal currents on the larger scale, while the GRS, ovals, and plumes occur on intermediate scales. Because of their vastly different scales, the various phenomena probably lie in

[1] In this paper the term "stability," when applied to vortices, refers to coherence plus persistence.

different dynamical regimes (Williams and Yamagata 1984). More recent ideas about the vertical structure and circulation as derived from analyses of the variations in the radiative emission between belts and zones are thoroughly discussed by Carlson et al. (1994). But as Gal-Chen (1988) has so clearly argued, the state of an atmosphere can never be described from observations alone and a predictive model must be fully involved for the problem to be well posed.

Jovian motions may also have much in common with those of the ocean: a strong energy conversion by the small eddies, activity over a wide range of scales, a weak dissipation rate, coherent and turbulent forms, and similar nondimensional parameter ranges. Differences occur not so much in the basic modes of motion but rather in their forcing mechanisms and boundary conditions. Vortices lying between the alternating jet streams on Jupiter last much longer than those occurring in the oceans near the Gulf Stream for reasons that need to be delineated. In particular, we need to find out what structures and environments allow vortices to exist so much longer in the Jovian system and why they are also conducive to jet and superrotation formation.

Such planetary-scale motions are predominantly geostrophic but can take on different forms depending on their size relative to the Rossby deformation radius L_R. Quasigeostrophic (QG), intermediate geostrophic (IG), and planetary geostrophic (PG) motions occur at the small, medium, and large scales, respectively. These flow regimes are subsets of a general geostrophic system and can coexist if their scales are sufficiently separated (Yamagata 1982; Williams 1985a), although the governing equations have been derived only for the shallow-water and two-layer systems so far (Cushman-Roisin et al. 1992).

In the GFD (thin atmosphere) view of Jupiter proposed earlier (Williams 1985b), the zonally banded form of circulation, with its multiple easterly and westerly jets, is essentially a characteristic of quasi-horizontal turbulence on a rapidly rotating sphere. The flow is energized by small, Rossby L_R-scale, baroclinic eddies that cascade energy toward the larger, Rhines (1975) L_β scales, where they generate the planetary waves that evolve into zonal currents. These jets can become unstable at larger scales and generate solitary waves resembling Jovian vortices. The many developments made in jet theory over the last two decades are thoroughly discussed by Rhines (1994) and James (1994). Elsewhere, at the equator a superrotating westerly current can be produced by eddy energy cascading from low latitudes (Williams 1978, 1988a); the probable source of these eddies is identified in Part II.

c. *Models past*

This GFD view of the circulation has been explored with a variety of models. In particular, barotropic models of planetary turbulence show that zonally aligned flows are the preferred end state of eddy-driven, quasi-horizontal, nonlinear cascades on a rapidly rotating planet (Williams 1978). Studies of QG turbulence further show that baroclinic instability can energize the eddies that drive the multiple Jovian jets provided that the baroclinicity ΔT achieves a modest level, further implying that in midlatitudes Jupiter behaves like a larger, faster-spinning Earth (Williams 1979; Panetta 1993; Vallis and Maltrud 1993; Pierrehumbert and Swanson 1995). Calculations with a global circulation model for Earth's atmosphere in which the rotation rate is increased do, in fact, produce multiple jets and equatorial westerlies, all resembling Jupiter's winds in latitudinal form (Williams and Holloway 1982).

Studies of coherence have progressed best with the reduced-gravity shallow-water (SW) model and show that long-lived Rossby vortices can exist indefinitely in the single-layer system at the larger planetary scales, both in midlatitudes and at the equator (Williams and Yamagata 1984; Williams and Wilson 1988, hereafter WW88). Vortices in the two regions are related through their basis on the long solitary divergent Rossby wave. Their different characteristics stem from their different forms of Rossby wave and nonlinearity. Only anticyclones achieve a balance and a permanence, and merge during encounters in midlatitudes but behave like solitons at the equator. Shallow-water vortices can be generated by unstable easterly jets. Nezlin and Sutyrin (1994) provide an overview of recent developments in planetary vortex theory, while Flierl (1987) and McWilliams (1991) review theories, mainly quasigeostrophic, for oceanic vortices.

Overall, these early models provide viable but preliminary explanations for the phenomena active on Jupiter. They are limited to the extent that they concentrate on the horizontal processes involved and simplify or ignore vertical aspects, partly out of necessity due to the limited observations, but mainly out of the need to progress systematically. Clearly, a synthesis and additional analyses are needed. Furthermore, given that we regard the motions as being mostly confined to an upper layer, the solutions to the GFD models must be reinterpreted and applied accordingly. Of immediate concern is whether the SW model, a model based on a single vertical mode, is relevant for a nonlinear phenomenon such as the Rossby vortex or whether interactions among vertical modes limit the solutions.

d. *Models present*

The new calculations with the PE model, in seeking answers to the four basic dynamical issues, cover a range of phenomena and conditions. In Part I, using geostrophically balanced initial states, we first isolate the structures that favor absolute vortex stability and examine the coexistence of stable vortices and stable jets. We then proceed to study vortex genesis by unstable jets and examine a variety of evolutionary paths.

Later, in Part II, after adding a heating function to the PE model, we look at the conditions that lead to the onset of an equatorial superrotation and to the generation of multiple midlatitude jets and vortex sets. These solutions give answers to the four basic problems that are mutually consistent and synthesize or extend earlier studies of the thin atmosphere hypothesis.

After describing the numerical model in section 2 and the theoretical basis in section 3, we begin our calculations in section 4 at the equator. We start there because a correspondence has been established for that region between the shallow water and continuous systems by Marshall and Boyd (1987), hereafter MB87, who have derived a nonlinear analytical solution for Rossby solitons with a first baroclinic eigenmodal structure and stratifications of the form $\exp(Nz/H)$, where the integer $N = 8$ for ocean parameters. Although specialized, the MB87 solution offers hope that the shallow-water theory for vortex stability and genesis may also be physically meaningful in all regions. But in doing so, it also makes the $N = 8$ structure seem too representative and the issue look too easy, and therein lie pitfalls that are not immediately overcome.

The calculations, initialized in section 4 with the MB87 analytical solution, examine the existence, stability, and interactions of equatorial vortices for both the ocean and Jupiter. These yield a preliminary parametric and structural system, which we denote as $P_0(N8)$ when $N = 8$, with which to begin exploring Jupiter.[2] Then in section 5, we examine the stability of vortices of diverse size in the simpler, less dispersive midlatitudes using a slightly shallower $P_1(N20)$ structure, but find that a stable regime does not exist in this region.

This leads us to low latitudes, where all processes and problems are more acute, and in section 6 we proceed to examine whether zonal currents can conditionally stabilize the $P_1(N20)$ storms by blocking their equatorward migration. Because they cannot, we vary the structure in a more extreme way in section 7. We then find that vortices can be made conditionally stable (by jet blocking) if they are thinner, as in the $P_2(N60)$ regime, and even made absolutely stable if they are very thin, as in the $P_3(N90+)$ regime. Very thin flows may also be represented by a "confined linear" structure that is linear in z over an upper layer of depth h and vanishes in the abyss, and is denoted as $L_3(D20+)$ when the thickness factor $D = H/h$ equals or exceeds 20. Given that absolutely stable vortices can exist for the P_3 and L_3 systems, we then examine whether they can coexist indefinitely with zonal currents of like structure.

We then proceed in section 8 to examine whether long-lived vortices can be generated in the P_3 and L_3 systems by the baroclinic instability mechanism. A variety of solutions are needed to determine whether the single vortex state arises directly at the beginning or evolves indirectly from a series of mergers, or whether other end states are more likely. Finally, in section 9, we describe how long-lived vortices can also be generated in modified hyperbolic structures that are consistent with the vertical wind variations recently observed by the *Galileo* spacecraft probe. We reserve for Part II the discussion of how the jets themselves are generated and how the character of multiple vortex sets varies with latitude, as well as how to generate simultaneously the equatorial superrotation, the multiple jets, and vortex sets in a full circulation model.

2. The primitive equation model

Our numerical studies use the primitive equations of motion with a Boussinesq equation of state, solved for a regional channel by finite-difference methods. This formulation provides the simplest, most computationally efficient, three-dimensional model. The model is made physically minimal to compensate for the large number of cases that parameter-varying studies require, while the simple geometry and numerics let us concentrate on regional phenomena with a high resolution and avoid the complexity of atmospheric GCMs. Testing the model with the nonlinear analytical MB87 solution confirms that the model conserves vortices accurately, even with modest resolutions.

Physically, the PE model provides an excellent representation of basic dynamical mechanisms such as the Charney and Eady baroclinic instabilities and the jet and vortex geneses. Although the validity of a Boussinesq model is normally limited to small vertical extents when applied formally to atmospheres, comparison with compressible GCM solutions (in Part II) shows that the PE model flows can be applied directly if mapped from vertical to pressure coordinates (cf. Held and Hou 1980). For a thorough discussion of the topic of oceanic analogs to atmospheric motions, see Charney and Flierl (1981).

a. System of equations

The primitive equation model for a thin hydrostatic fluid is specified by the zonal, meridional, and vertical velocity components u, v, and w, and by the pressure, density, and temperature fields p, ρ, and T. The equations are standard but we present the finite-difference form so as to document recent changes in the formulation of the advection terms. For the Boussinesq equation of state, these are written in spherical coordinates and with the central difference operator (δ) notation as

$$\delta_t \bar{u}^t + L(u) - v(f + mu) = -\frac{1}{ac\rho_0}\delta_\lambda \bar{p}^\phi + F^u \quad (1)$$

[2] Terms such as $P_i(N)$ are used, for convenience, to symbolize parametric regimes with distinct forms of behavior over certain N ranges, where $i = 0, 1, 2, 3$.

$$\delta_t \bar{v}^t + L(v) + u(f + mu) = -\frac{1}{a\rho_0}\delta_\phi \bar{p}^\lambda + F^v \quad (2)$$

$$\delta_t \bar{T}^t + L'(T) = Q + F^T \quad (3)$$

$$\delta_z p = -g\bar{\rho}^z, \quad \rho = \rho_0[1 - \alpha(T - T_0)], \quad (4)$$

where, for $q \equiv u$ or v, at the horizontal velocity grid points,

$$L(q) = \frac{1}{ac}[\delta_\lambda(U\bar{q}^\lambda) + \delta_\phi(c'V\bar{q}^\phi)] + \delta_z(w\bar{q}^z) \quad (5)$$

$$U = \bar{u}^{\lambda\phi\phi}, \quad c'V = \overline{c\bar{v}^{\lambda\lambda}}^{\phi} \quad (6)$$

and where, at the temperature grid points,

$$L'(T) = \frac{1}{ac'}[\delta_\lambda(\bar{u}^\phi \bar{T}^\lambda) + \delta_\phi(c\bar{v}^\lambda \bar{T}^\phi)] + \delta_z(w'\bar{T}^z) \quad (7)$$

with the identities $L(1) = 0$ and $L'(1) = 0$ for the mass conservation defining the w and w' fields. Primes distinguish items evaluated at the temperature grid points from their values at the velocity grid points.

The dissipation terms are for computational control and use simple biharmonic and second-derivative forms in the horizontal and vertical, respectively:

$$F^u = \nu_4\nabla^4 u + \nu_2\delta_{zz}u \quad (8)$$

$$F^v = \nu_4\nabla^4 v + \nu_2\delta_{zz}v \quad (9)$$

$$F^T = \nu_4\nabla^4 T + \frac{\nu_2}{\gamma}\delta_{zz}T, \quad (10)$$

where the coefficient ν_4 is negative; the parameter γ, which equals 1 for $T_z \geq 0$ and 0 for $T_z < 0$, indicates that convective adjustment is implemented when the fluid is vertically unstable; and

$$\nabla^2 q = \frac{1}{a^2c^2}\delta_{\lambda\lambda}q + \frac{1}{a^2c}\delta_\phi(c'\delta_\phi q) \quad (11)$$

is the Laplacian for $q \equiv u$ or v and also for $q \equiv T$ when c and c' are switched.

In the above notation, $f = 2\Omega\sin\phi$, $m = (1/a)\tan\phi$, and $c = \cos\phi$ define the Coriolis and two map parameters[3] at the velocity grid points. In addition, L is the advection operator; λ, ϕ, and z represent the longitude, latitude, and height; g is the gravity; Ω and a are the planetary angular velocity and radius; while ρ_0, T_0, and α denote two reference values and the thermal expansion coefficient for the Boussinesq equation. The heating function $Q(\lambda, \phi, z)$ is set to zero in Part I but is defined and used in Part II.

The equations are solved using the leapfrog time differencing scheme and a Robert filter with a coefficient α_R for variables defined on the so-called B grid. In the horizontal, this grid places u and v together at the corners of boxes centered about the T points and, in the vertical, places w between the $u-v$ points and w' between the T points (Bryan 1969). The two vertical velocity fields are closely linked by the identity $w = \overline{w'}^{\lambda\phi}$. This consistency follows from the new form of the momentum advection operator (5) derived by Smith et al. (1992) and it leads to better mass conservation and behavior, especially at the equator. Improvements also come from using the complete-column convective adjustment scheme of Rahmstorf (1993) to help control regions with very active convection.

The computational domain is usually a channel of sufficient width and breadth to isolate the main modes of interest from the boundaries. Boundary conditions assume periodicity in longitude and one of two optional states on the northern and southern walls: one for mid-latitude domains and one for low-latitude domains. In the first system, we assume that no-slip, no-flux conditions hold on both walls so that

$$(u, v, T_\phi) = 0 \quad \text{at} \quad \phi = \Phi_S, \Phi_N. \quad (12)$$

For the second system, the northern boundary lies at the equator, where we assume symmetry prevails so that

$$(v, T_\phi) = 0 \quad \text{at} \quad \phi = \Phi_N, \quad (13)$$

while the southern wall retains the no-slip, no-flux condition of (12). For both systems, the walls lie at $u-v$ grid points. In the vertical, on the other hand, both surfaces are taken to be horizontal rigid lids lying at w grid points with free-slip, no-flux conditions so that

$$(w, u_z, v_z, T_z) = 0 \quad \text{at} \quad z = 0, -H, \quad (14)$$

where H is the thickness of the fluid layer. An option to include a drag at the lower surface, to help equilibrate the flow, is never activated.

b. *Method of solution*

To actually solve (1)–(4) for a rigid lid system, we follow the classic method of eliminating the surface pressure by splitting the velocity into the internal (baroclinic) and external (barotropic) modes (Smagorinsky 1958; Bryan 1969):

$$(u, v) = (u^*, v^*) + (\tilde{u}, \tilde{v}),$$

where

$$(\tilde{u}, \tilde{v}) = \frac{1}{H}\int_{-H}^{0}(u, v)dz. \quad (15)$$

The procedure then involves time marching a reduced set of momentum equations with the pressure p replaced by its hydrostatic component. This yields a shifted internal mode that is then normalized so as to have a zero vertical mean and give the baroclinic mode.

[3] After section 2b, the variable c refers to the phase speed and primes generally denote eddies.

To obtain the barotropic component, we define a streamfunction $\psi(\lambda, \phi)$ at the temperature grid points such that

$$\tilde{u} = \frac{-1}{aH}\delta_\phi\psi, \quad \tilde{v} = \frac{1}{acH}\delta_\lambda\psi. \tag{16}$$

This leads to a two-dimensional Poisson equation for the vertically averaged flow change:

$$\frac{1}{(ac')^2}[\delta_{\lambda\lambda}\dot{\psi} + c'\delta_\phi(c\delta_\phi\dot{\psi})] = \frac{H}{ac'}[\delta_\lambda\overline{GV}^\phi - \delta_\phi(c\overline{GU}^\lambda)], \tag{17}$$

where $\dot{(\ )}$ denotes $\partial/\partial t$ and GU, GV represent the vertical means of the nonlinear and diffusion terms driving the internal momentum changes in (1) and (2).

The boundary conditions in (17) require that there be no net cross-flow on the northern and southern walls so that

$$\dot{\psi} = \begin{cases} 0 & \text{at} \quad \phi = \Phi_N \\ aH\displaystyle\int_{\Phi_S}^{\Phi_N} \overline{GU}\,d\phi & \text{at} \quad \phi = \Phi_S, \end{cases} \tag{18}$$

where $\bar{(\ )}$ denotes the zonal mean. The Poisson equation is solved exactly using a fast trigonometric transform in longitude and the Thomas recursion algorithm in latitude to invert the tridiagonal matrix for the Fourier coefficients. This requires less than 1% of the total computer time.

c. *Initialization procedure and parameter values*

The vertical structure of the vortices and jets presented in sections 4–7 is mainly set to that of the first baroclinic normal mode, as given by solutions to the equation for the vertical velocity eigenvector $\hat{w}_k$ of order k:

$$\delta_{zz}\hat{w}_k + \frac{B_S(z)}{c_k^2}\hat{w}_k = 0, \tag{19}$$

where $\hat{w}_k = 0$ at $z = 0, -H$; $B_S(z) = \alpha g(dT_S/dz)$ is the Brunt–Väisälä stability parameter based on the background hydrostatic lapse rate; and c_k is the eigenvalue phase speed.

Differencing (19) over the PE model's vertical grid gives a generalized eigenvalue problem of the form $\mathbf{A}\hat{\mathbf{w}} = \lambda\mathbf{B}\hat{\mathbf{w}}$, where $\mathbf{A}$ is a diagonal matrix and $\mathbf{B}$ is a tridiagonal symmetric matrix. This problem is solved for all $k = 1, K$, where K is the vertical resolution, using the EISPACK code (Garbow et al. 1977) for the QZ algorithm (Moler and Stewart 1973). The normal mode relations for geostrophic flows, $\hat{v} \sim \hat{p} \sim \hat{w}_z$ and $\hat{T} \sim B_s\hat{w}$, then give the vertical forms of the initial fields. In practice, only the first baroclinic mode is used, to which a small barotropic component is sometimes added to make the abyssal flow vanish. For exponential stratifications, the eigenmodes simplify to Bessel functions.

We calculate, using parameter values that are thought to be appropriate for Jupiter's atmosphere, values that produce flows with the amplitudes and propagation rates comparable to those observed at cloud level. The parameter values evolve as the calculations progress toward more relevant solutions. The following set represents typical values about which variations are made (see Tables 1–4). The planetary parameters $a = 71\,400$ km, $\Omega = 1.76 \times 10^{-4}$ s^{-1}, and $g = 26$ m s^{-2} remain fixed, but the fluid thickness H changes from an initial 100 km to 600 and 1200 km in later cases, and ends up at 10 000 km in responding to the *Galileo* data. The Boussinesq coefficient is somewhat arbitrary for this process model but is kept at $\alpha \sim 1/T_o = 0.005$ K^{-1}. Most importantly, the motions are confined to an upper layer of thickness $h = 30$–500 km by stability structures $B_e(z)$ that vary greatly in steepness by setting the background hydrostatic temperature to $T_s = T_c + T_a \exp(Nz')$, where $T_c = 1$–4 K, $T_a = 3$–45 K, $N = 8$–300, and $z' = z/H$.

The computational diffusion parameters, set at $\nu_4 = -10^{17}$ m^4 s^{-1} and $\nu_2 = 10^{-8}$ m^2 s^{-1}, provide a minimal energy loss as well as equilibrium in most cases. Because the vertical diffusion only becomes active when $\nu_2 \sim 10^{-5}$ m s^{-1}, it is essentially zero. The Robert time-filter coefficient is fixed at $\alpha_R = 0.005$.

Domains cover 60°–180° in longitude and 40°–50° in latitude and are centered either in northern midlatitudes at $\phi = 40°$ or in southern low latitudes at $\phi = -20°$. The standard resolution has $66 \times 42 \times 20$ points in the λ, ϕ, z directions, with grid increments of $\Delta\lambda \sim 1°$–$3°$ and $\Delta\phi = 1°$ and with a time step of $\Delta t = (1/50)$ day. The vertical grid varies exponentially in its spacing so as to put most points aloft in the active layer. In particular, the early cases with $N = 8$–20 and $H = 600$ km vary Δz as $\exp(3z')$ to go from 5–8 km near the top to 60–90 km near the bottom. Likewise, the later cases with $N \geq 60$ and $H = 1200$ km vary Δz as $\exp(5z')$ to go from 2–5 km aloft to 130–260 km in the abyss (as in Fig. 20). For the confined linear structure L_3, a simple split grid has 10 points in the upper $1/20$th of the fluid and 10 points in the remainder, so that $\Delta z_1 = 6$ km aloft and $\Delta z_2 = 114$ km below when $H = 1200$ km.

All calculations are made on a Cray YMP or C90 with matlab and xlib graphics running in parallel on an SGI workstation to provide flow animation. Colored and animated versions of some solutions may be viewed on the Internet at http://www.gfdl.gov/~gw. All figures use dashed lines for the negative contour values and solid lines for the positive or zero values. The right side of each figure contains a profile of the field averaged over the abscissa and scaled to unity by its amplitude. Frames are referenced from the top, with the left column first. Altitude is measured in kilometers

in the vertical cross sections. In the figure captions, the contour intervals are denoted by Δ and the field, while the scales of the means are denoted by the field and an asterisk. The coordinates denote the position at which the cross section is taken, with the variable $Z = H - z$ being introduced to indicate the depth below the top surface. The captions also list the vortex properties c, U, T, and B, which give approximately the amplitudes of the phase velocity, zonal velocity, temperature variation, and Brunt–Väisälä stability at the end of each calculation.

3. Theoretical considerations

Large planetary-scale vortices have a very restricted existence, occurring only in certain parts of Earth's oceans for limited periods and in the Jovian atmospheres for lengthy periods. To date they seem to occur and survive best theoretically in shallow-water (SW) models with Jovian parameters. Unlike jets and waves, which are ubiquitous phenomena, planetary vortices are an exotic species whose reproduction by the SW model provides the strongest guide to and constraint on dynamical theories of the Jovian atmosphere. We now briefly summarize the SW vortex theory, noting some limitations and some connections with the continuous primitive equation (PE) system.

a. Shallow-water vortex theory

Away from the equator, geostrophic motions in the SW system are governed by a single equation for the geopotential thickness h:

$$h_t - \nabla(f^{-2}h\nabla h_t) + (f^{-1})_y h h_x - \mathrm{J}(h, h\zeta f^{-2}) - J(hf^{-1}, K) = 0, \quad (20)$$

where

$$\zeta = \nabla(f^{-1}\nabla h), \; K = 0{\cdot}5 f^{-2}(\nabla h)^2,$$

and

$$J(h, q) = (\cos\phi)^{-1}(h_x q_y - h_y q_x)$$

define the vorticity, kinetic energy, and advective Jacobian for the coordinates $x = a\lambda$ and $y = a\phi$ (Williams 1985a).

The dispersion and the vorticity advection dominate in (20) for the small planetary scales of the quasigeostrophic regime, whereas the nonlinear divergence (steepening) due to the interface displacement dominates for the large-scale planetary geostrophic regime and while the dispersion and the divergence act in balance for the intermediate scale regime. Although simple Korteweg–deVries (KdV) balances are not possible in this general geostrophic system, the KdV terms—dispersion and steepening—do control aspects of the nonlinear solitary waves that (20) allows, particularly the size, strength, shape, and speed of many large vortices. The advection and the twisting caused by the latitudinally varying phase speed tend to prevent soliton forms of interaction and encourage vortices to merge instead.

The generalized geostrophic equation (20) cannot describe processes that act across the equator, and no equivalent simple equation exists for that region. Nevertheless, a special class of nonlinear analytical solutions to the SW equations at the equator that includes stable anticyclones describable by a KdV dynamics does exist (Boyd 1980). In these, the vorticity advection rather than the steepening produces most of the KdV nonlinear term through the self-interaction of components lying on both sides of the equator.

The existence and stability of Boyd's equatorial Rossby solitons are supported by the numerical SW solutions of WW88 that also show the interactions to be soliton-like when the vortices have the same latitudinal (Hermite) order and to be quasi-soliton-like when they have differing orders. Rossby solitons occupy a wider parameter range than that given by the theoretical coefficients and are easily generated in the SW model by the action of vortices lying in low latitudes.

Although stable SW vortices of different form exist at the equator and elsewhere, it is not obvious how relevant they are for a continuously stratified fluid. It is generally accepted that *linear* SW processes have meaningful equivalents in continuous systems because only a single vertical and horizontal mode is involved (Gill 1982). Usually, the reduced-gravity SW model represents flows with a single vertical mode such as the first baroclinic eigenmode. But the representation is not so simple when vertically nonlinear phenomena such as the Rossby vortex and soliton are involved because multiple vertical modes in the continuous system can exist that are nonlinearly coupled and capable of leaking significant energy downward from the upper layer into the abyss. Anderson and Killworth (1979) and Greatbatch (1985) discuss this issue for midlatitudes and the equator, respectively, and note that it is the thermocline form of $B(z)$, confining modes aloft, that gives the SW theories some relevance.

b. The SW–PE connection in midlatitudes

A connection between the shallow-water and primitive equation systems has been established for certain classes of nonlinear motion, in midlatitudes by Anderson and Killworth (1979) and at the equator by MB87. Both studies show that for nonlinear Rossby waves the SW system closely corresponds to a PE system with an exponential stratification of the form $B_e(z) = B_0 \exp(Nz')$ when N is large.

A limited PE equivalent of the nonlinear long-wave part of (20) is derived by Anderson and Killworth (1979) using the Welander (1959) mass function $M_z = p/\rho_0$ and the Needler (1967) similarity solution

$$M = A + \frac{Ez}{H} + Ce^{z/h}, \tag{21}$$

where A, E, and C are functions of x, y, and t on a β-plane and h is the thermocline thickness. Substituting (21) into the planetary geostrophic equations, applying the w boundary conditions, and assuming that $h \ll H$ produces the governing equation

$$C_t + \left(\tilde{u} - \frac{\beta}{hf^2} C\right) C_x + \tilde{v} C_y = 0, \tag{22}$$

where $\tilde{(\ )}$ denotes the barotropic flow component. Contributions from the E term are negligible and only the exponential part of M contributes to the Brunt stability, $B \sim M_{zzz}$. Thus the nonlinear term CC_x in (22) defines the primary baroclinic self-interactions, where $C \sim gh^2\Delta\rho/\rho_0$ and $\Delta\rho$ is the density difference between the thermocline and the abyss.

The PE nonlinear wave equation (22) differs from the SW version in that the thermocline thickness h is constant and the density differential $\Delta\rho$ varies, whereas in the SW case h varies and $\Delta\rho$ is constant. Thus the SW system provides at best a simple analog of the PE system, not an approximation. Furthermore, the PE long-wave speed, $c_\beta = \tilde{u} - \beta g' h f^{-2}$, can be Doppler shifted by the barotropic flow and altered by the thermocline thickness, whereas the SW form $c_\beta = -\beta g' H f^{-2}$ cannot, where $g' = g\Delta\rho/\rho$ is the reduced gravity. These modifiers, however, are small and the nonlinear term dominates when the scales are large. The two-layer version of (22) has nonlinear wave terms of the form

$$h_{1t} - \beta \frac{g'}{f} h_1 h_{1x} = 0 \tag{23}$$

for the upper layer and a longwave drift rate given by $c_\beta = -\beta g' h_1 f^{-2}$, provided that $h_1 \ll H$. Thus, overall, the analysis suggests that a limited SW–PE connection exists in analog form for nonlinear Rossby waves with stratifications of the $\exp(Nz')$ or confined layer form. Further limitations of the SW model, with its single vertical mode, in representing planetary flows are discussed by Rhines (1989).

c. *The SW–PE connection at the equator*

The exponential stratification also connects the PE and SW systems at the equator in the remarkable MB87 analysis, thus attaining a global status. The connection, however, is complex and defined for only one phenomenon, the Rossby soliton, and for only one stratification, B_e with $N = 8$. To show what terms are involved, we outline the MB87 derivation of the soliton solution that is used to initialize the calculations in section 4.

In the theory, disturbances on an equatorial β plane are measured relative to a reference frame moving at the linear Rossby long-wave speed c and are described by quantities nondimensioned with respect to c_g, L_E, and H, so that $c = -1/(2n + 1)$, where $c_g = (gH)^{1/2}$ and $L_E = (c_g/\beta)^{1/2}$ are the gravity wave speed and the equatorial Rossby radius. Introducing the slow variables $x' = \varepsilon^{1/2}(x - ct)$ and $t' = \varepsilon^{3/2}t$, and then dropping the primes, allows u, v, and p to be expanded in powers of the ordering parameter ε.

The resulting zero-order variables obey the classic linear equations and their eigenmodal solutions (Matsuno 1966):

$$u^0 = A(x, t)\left[\frac{H_{n+1}(y)}{2(1-c)} - \frac{nH_{n-1}(y)}{(1+c)}\right] e^{-y^2/2} \Phi_l(z) \tag{24}$$

$$T^0 = A(x, t)\left[\frac{H_{n+1}(y)}{2(1-c)} + \frac{nH_{n-1}(y)}{(1+c)}\right] e^{-y^2/2} \frac{d\Phi_l}{dz}(z) \tag{25}$$

$$v^0 = \frac{\partial A(x, t)}{\partial x} H_n(y) e^{-y^2/2} \Phi_l(z), \tag{26}$$

where $H_n(y)$ is the Hermite polynomial of order n, and $\Phi_l(z)$ is the vertical eigenvector of order l as given by the structure equation $(B^{-1}\Phi_{lz})_z = -\lambda_l \Phi_l$ for the eigenvalue λ_l. Solutions may be expressed as the double sum $\Sigma_n \Sigma_l$ of such modes.

At this order the amplitude $A(x, t)$ is arbitrary but can be defined by vertically integrating the first-order equations for the velocity and divergence of a particular vertical mode l. Although some of the terms involved vanish for long waves, the integrals still involve cubic products of Φ, Φ_z, and Φ_{zz} when the variables are eliminated to give the single equation

$$v^1_{yy} - \left(\frac{1}{c^2} + y^2\right) v^1 = Q_3, \tag{27}$$

where Q_3 is a complex function of first-order terms from three equations. Then, on substituting the zero-order solutions (24)–(26) into the Q_3 expressions and applying the orthogonality condition $\int Q_3 H_n(y) e^{-y^2/2} dy = 0$ to eliminate the secular term, the Hermite-weighted integrals regroup into tendency, nonlinear, and dispersion terms to form the KdV amplitude equation

$$A_t - \alpha_n A A_x - \beta_n A_{xxx} = 0, \tag{28}$$

where α_n, β_n involve complicated cubic terms based on integrals of Φ_l and H_n (see Table A1 of MB87 for details).

Solutions to (28) of the form

$$A(x, t) = A_0 \operatorname{sech}^2\left[\left(\frac{\alpha_n}{\beta_n}\frac{A_0}{12}\right)^{1/2}\left(x - ct + \frac{\alpha_n}{3} A_0 t\right)\right] \tag{29}$$

TABLE 1. Vortex stability cases at the equator and in midlatitudes. Constant parameter values are resolution: $66 \times 42 \times 20$ in λ, ϕ, z; $\Delta\phi = 1°$, $\Delta z \sim e^{3z'}$, and $\lambda_0 = \Lambda/2$. The $\Delta\lambda$ grids are actually 60/64 of the values shown, as 64 internal points are specified for FFT efficiency. Cases marked (a) are for the ocean's physical parameters. Case marked (b) defines the vortex using the streamfunction ψ. The abbreviations BC1 and BTR denote the first baroclinic eigenmodal and barotropic vertical structures. Computational parameter: $\nu_4 = -10^{16}$ m^4 s^{-1} except $\nu_4 = -0.5 \times 10^{11}$ m^4 s^{-1} for E2–E4.

Case	Domain length Λ	Grid $\Delta\lambda$	Depth H (km)	Structure rate N	Static stability T_s	Vortex form
						$(\alpha_1, \beta_1, A_0)\ \hat{T}(z)$
E1	120°	2°	100	8	$4 + 20\,e^{Nz'}$	(0.46, 0.099, 0.25) BC1
E2[(a)]	120°	2°	4	8	$4 + 20\,e^{Nz'}$	(0.46, 0.099, 0.25) BC1
E3[(a)]	120°	2°	4	8	$4 + 20\,e^{Nz'}$	(0.23, 0.099, 0.25) BC1
E4[(a)]	120°	2°	4	8	$4 + 20\,e^{Nz'}$	(0.92, 0.099, 0.25) BC1
						$T_v\,(\delta\lambda \times \delta\phi)\ \phi_0 \cdot \hat{T}(z)$
M1	60°	1°	600	20	$1 + 10\,e^{Nz'}$	0.6 (6 × 4) 40°·BC1
M2	30°	0.5°	600	20	$1 + 10e^{Nz'}$	0.3 (2 × 1.5) 40°·BC1
M3	15°	0.25°	600	20	$1 + 10\,e^{Nz'}$	0.1 (1 × 0.75) 40°·BC1
M4	60°	1°	600	20	$1 + 10\,e^{Nz'}$	0.6 (6 × 4) 40°·BC1
M5[(b)]	15°	0.25°	600	20	$1 + 10\,e^{Nz'}$	10^{13} (1 × 0.75) 40°·BTR

are combined with (24)–(26) to define the Rossby soliton for the initial states in section 4. The finite amplitude effect boosts the linear easterly phase speed by $\alpha_n A_0/3$ and gives an effective longitudinal wavenumber of $[(\alpha_n/\beta_n)(A_0/12)]^{1/2}$.

The PE solitons have the same horizontal form as their SW counterparts in Boyd (1980) but differ in the vertical by having a normal mode structure. They also have new or modified contributions to the α_n coefficients, particularly from the vertical derivatives, advections, and structure. The vertical density variations are the main cause of changes in the size of the nonlinear coefficients α_n from their SW values. The dispersion coefficients β_n remain the same as their SW counterparts, being unaffected by the coupling of multiple vertical modes.

4. Stability of equatorial solitons

We begin our numerical calculations by examining the existence and stability of the MB87 stratified Rossby soliton solutions in the PE model. The solutions confirm that the exponential $B_e(z)$ structure favors stable vortices at the equator and thus provides a preliminary system for Jovian exploration.

a. Parameter selection

The initial parameters and flows are limited by the MB87 analysis to the first-order latitudinal and vertical eigenmodes and to an exponential stratification with $N = 8$. To initialize the calculations with the expressions in (24)–(26) and (29), the value of nonlinear α_1 coefficient given by MB87 must be modified to allow for differences in normalization procedures. The linear coefficient, however, remains unaffected at $\beta_1 = 8/81$. We chose to normalize the Hermite polynomials by factors of $(2^n n!\pi^{1/2})^{1/2}$ and thus require values of $\alpha_1 = 0.460$ for the PE soliton and $\alpha_1 = 0.816$ for the SW soliton of WW88. These values correspond to the PE $\alpha_1 = 0.258$ in MB87 and the SW $\alpha_1 = 0.444$ in Boyd (1983), where energy normalization factors are used.

The nonlinear coefficient is significantly smaller for the exponential stratification than for the SW system and vanishes completely for a constant stratification. Although no attempt is made to isolate the contributions from the different terms due to their complexity, we note that the SW α_1 is mainly determined by the advection of u and thus expect that the PE α_1 is similarly influenced. Neither do we try to re-solve the MB87 equations for other conditions, and so our initial choice for the Jovian structure and parameters is limited to that given by mapping from the ocean to Jupiter in such a way that the known α_1, β_1 coefficients may be used.

We also use ocean parameters, in section 4c, to examine some basic properties of the Rossby solitons. For those calculations, the domain constants are

$$a = 6.37 \times 10^6 \text{ m}, \quad g = 9.8 \text{ m s}^{-1},$$

$$\Omega = 7.29 \times 10^{-5} \text{ s}^{-1}, \quad H = 4000 \text{ m}$$

$$\alpha = 0.00025 \text{ K}^{-1}, \quad \nu_4 = -5 \times 10^{10} \text{ m}^4 \text{ s}^{-1},$$

$$\nu_2 = 5 \times 10^{-7} \text{ m}^2 \text{ s}^{-1}, \quad \alpha_R = 0.005$$

$$\phi = -20°{:}20°, \quad \lambda = 0°{:}120°,$$

$$\Delta z \sim e^{3z'}, \quad \Delta t = 0.1 \text{ day},$$

and

$$\text{resolution } (\lambda, \phi, z) = 66 \times 42 \times 20,$$

and the soliton constants are $A_0 = 0.25$, $\alpha_1 = 0.46$, $\beta_1 = 0.099$, $T_s = 4 + 20e^{8z'}$, and $n = l = 1$. The value of α_1 is also halved and doubled in two later cases to examine the robustness of the MB87 solution (Table 1).

Selecting Jovian parameters for the MB87 soliton is so restricted that only the depth H needs to be derived. To

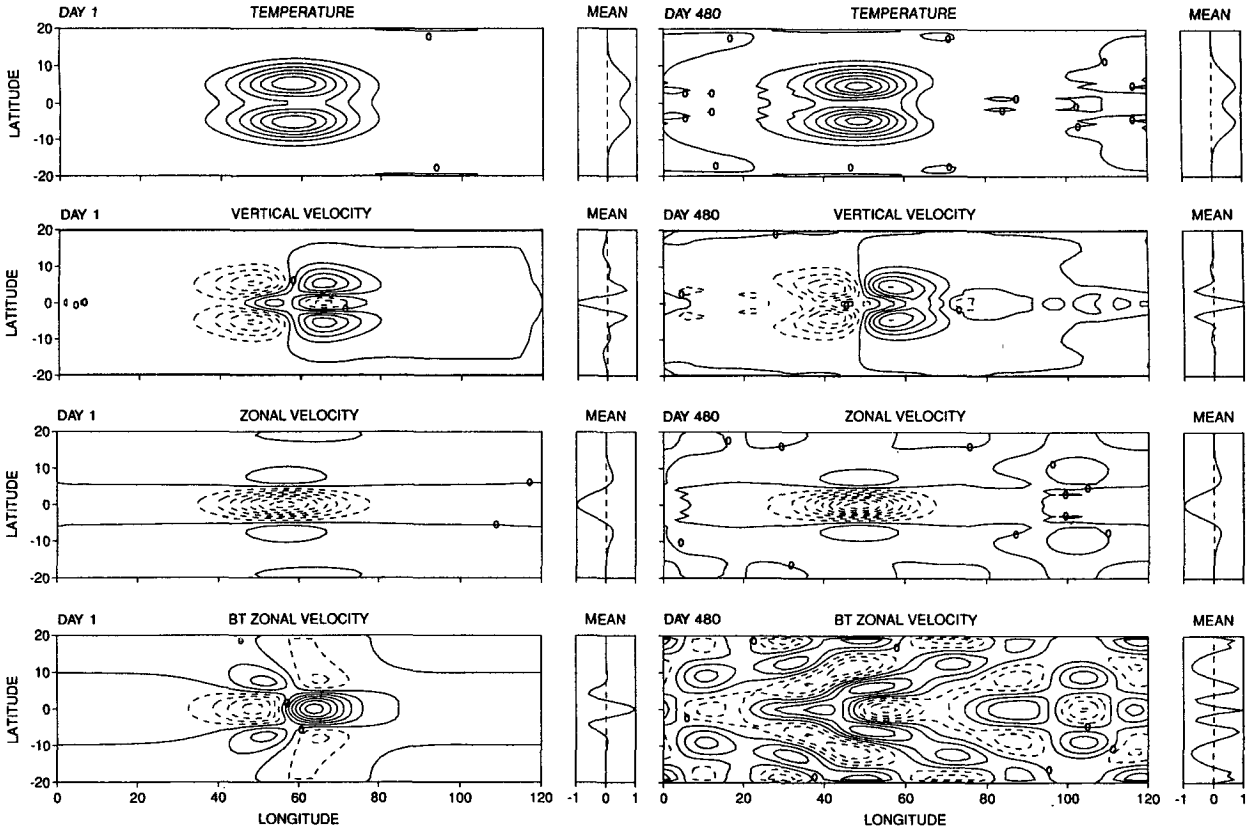

FIG. 1. Equatorial solution E1, stability of the Marshall and Boyd (1987) soliton. For Jovian $P_0(N8)$ parameters and soliton coefficients, as in Table 1. Properties are $c = -47$ m s^{-1}, $U = 43$ m s^{-1}, $T = 0.9$ K, $B = 2 \times 10^{-4}$ s^{-2}; Contour intervals and scales are Day 1: (a) $\Delta T = 0.05$ K, $T^* = 0.1$ K, $Z = 1$ km; (b) $\Delta w = 0.02$ cm s^{-1}, $w^* = 0.0013$ cm s^{-1}, $Z = 2$ km; (c) $\Delta u = 5$ m s^{-1}, $u^* = 8$ m s^{-1}, $Z = 1$ km; (d) $\Delta u_{BT} = 0.05$ m s^{-1}, $u^*_{BT} = 0.004$ m s^{-1} and Day 480: (e) $\Delta T = 0.05$ K, $T^* = 0.1$ K, $Z = 1$ km; (f) $\Delta w = 0.02$ cm s^{-1}, $w^* = 0.002$ cm s^{-1}, $Z = 2$ km; (g) $\Delta u = 5$ m s^{-1}, $u^* = 8.1$ m s^{-1}, $Z = 1$ km; (h) $\Delta u_{BT} = 0.2$ m s^{-1}, $u^*_{BT} = 0.008$ m s^{-1}.

map the theoretical ocean conditions to Jupiter requires that the Lamb parameter $\hat{e} = (L_E/a)^2 = c_g/2\Omega a$ be kept unaltered (see Gill 1982 for definitions). This requires that the gravity wave speed c_g and hence $(\alpha g H)^{1/2}$ be 30 times larger to match the Ωa increase. Given that $(\alpha g)^{1/2}$ is 7 times larger, this implies that H be 20 times deeper. We settle on $H = 100$ km as an initial estimate. Alternatively, we could take $N = 80$ and $H = 1000$ km if the α_1 coefficient were known for such a steep static stability.

Consequently, the Jovian parameters for the soliton calculation in section 4b use the planetary constants discussed in section 2c, together with the following domain constants:

$$H = 100 \text{ km}, \quad \alpha = 0.005 \text{ K}^{-1},$$
$$\nu_4 = -10^{16} \text{ m}^4 \text{ s}^{-1}, \quad \nu_2 = 10^{-5} \text{ m}^2 \text{ s}^{-1}$$
$$\phi = -20°{:}20°, \quad \lambda = 0°{:}120°,$$
$$\Delta z \sim e^{3z'}, \quad \Delta t = (1/50) \text{ day},$$

and

$$\text{resolution } (\lambda, \phi, z) = 66 \times 42 \times 20.$$

The soliton amplitude A_0 is set to a small value to keep velocities within the preferred theoretical limits and the observed range, so that the phase speed $c_g/(2n + 1)$ approaches 50 m s^{-1} for Jupiter and 1 m s^{-1} for the oceans. For convenience, we refer to the above Jovian parameters and structure as the P_0 system or regime.

b. *Equatorial vortices in the Jovian P_0 regime*

When an equatorial anticyclone based on the MB87 solitary wave described in section 3c is inserted into the PE model with the Jovian P_0 parameters listed above, it behaves as the case E1 shown in Figs. 1 and 2. The basic T, u, and w fields alter little from start to finish, so the progression over 480 days suffices to confirm the existence, stability, and longevity of these singular modes. The soliton nature of their interactions is established in the next section.

The horizontal temperature fields in Fig. 1 confirm the theoretical view that the two vortex halves interact across the equator to form a coherent whole. Deviations from the theory are seen in the occasional

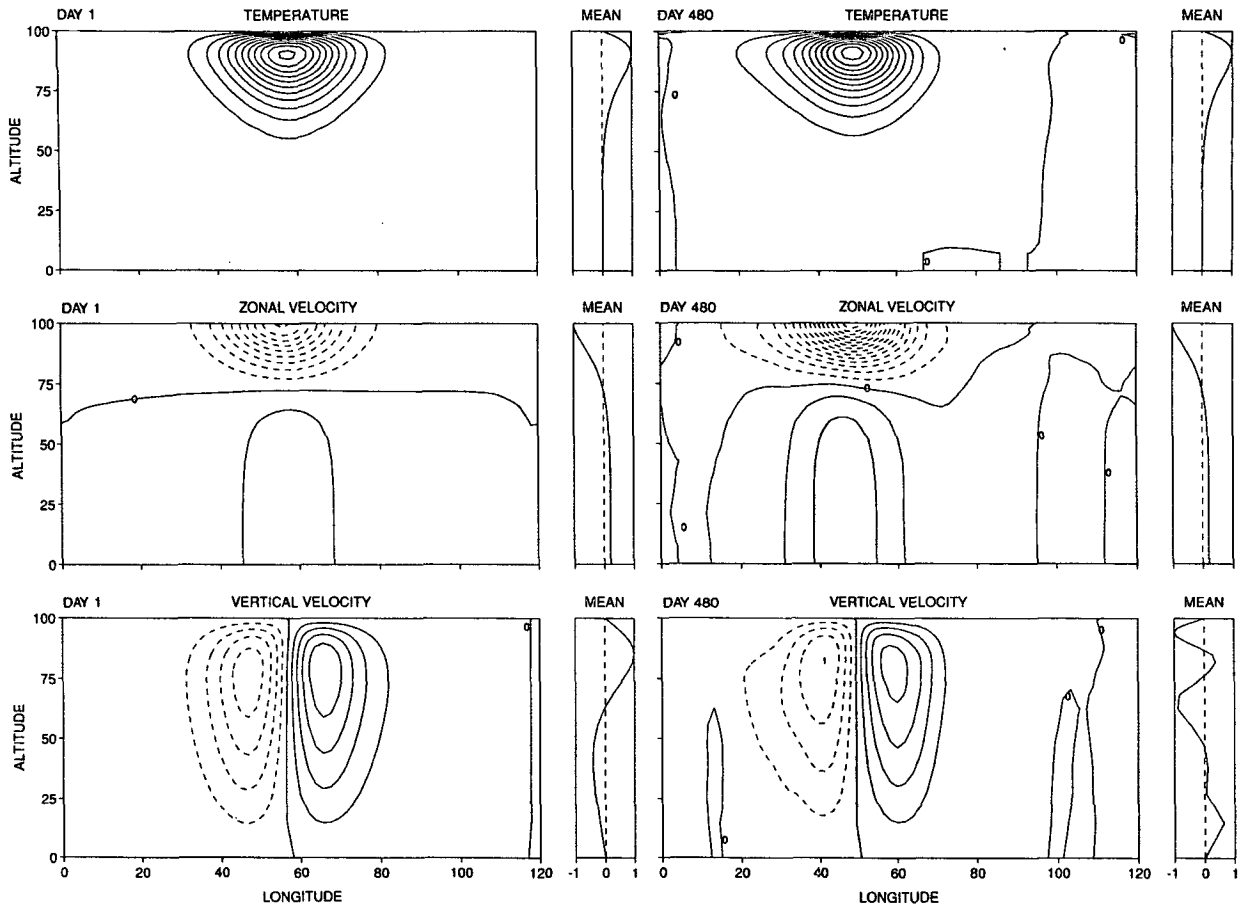

FIG. 2. Vertical sections for the equatorial solution E1. Altitude measured in kilometers. Contour intervals and scales are Day 1: (a) $\Delta T = 0.1$ K, $T^* = 0.25$ K, $\phi = -6°$; (b) $\Delta u = 2$ m s^{-1}, $u^* = 3.9$ m s^{-1}, $\phi = -3°$; (c) $\Delta w = 0.1$ cm s^{-1}, $w^* = 0.002$ cm s^{-1}, $\phi = -6°$ and Day 480: (d) $\Delta T = 0.1$ K, $T^* = 0.25$ K, $\phi = -4°$; (e) $\Delta u = 2$ m s^{-1}, $u^* = -6.3$ m s^{-1}, $\phi = -2°$; (c) $\Delta w = 0.1$ cm s^{-1}, $w^* = -0.002$ cm s^{-1}, $\phi = -4°$.

formation of a distinctive, but weak, third temperature peak right on the equator and in the existence of transient wavelike tails behind the main peaks. In the vertical, however, the first baroclinic mode prevails throughout (Fig. 2). The 0.9-K temperature amplitude, chosen to give a soliton with a 30° longitudinal scale, is much smaller than the value needed to produce a vortex of comparable size and strength in midlatitudes. The maximum value of the Brunt–Väisälä stability field, $B = 2 \times 10^{-4}$ s^{-2}, matches some observational estimates (Gierasch and Conrath 1993) and produces a small Rossby radius.

The motion within the vortex is mainly easterly aloft, reaching -43 m s^{-1} at the equator, a value just below the propagation speed of -47 m s^{-1}, in line with the theory (Fig. 1). Most of the action is confined to an upper layer with $h/H < 0.25$, while in the abyss the motion forms a weak but uniform westerly of 5 m s^{-1} in keeping with the eigenvector distribution (Fig. 2). The associated vertical motions form a downwelling in the leading western half and an upwelling in the east, as expected from the connection $w \sim -\beta T_\lambda$ discussed in section 5a. Although peaking aloft at 0.1 cm s^{-1}, the vertical motion extends strongly into the abyss and implies that vortex formation requires an impermeable lower boundary to support the $w = 0$ constraint.

The vortex does vary slightly in time, with a regular 100-day oscillation recorded in the energy integrals. Some adjustment occurs at the start due to the generation of a barotropic flow by the inertia gravity waves created by the stirring action of the baroclinic vortex. The barotropic zonal flow develops a 2 m s^{-1} amplitude and a 10° scale but, being disorganized, has no strong feedback on the vortex. Clearly, the Rossby soliton is highly stable in the preliminary Jupiter P_0 regime. The MB87 theory almost completely defines its dynamics, although the development of the barotropic component lacks an explanation.

c. *Equatorial vortices in the oceanic P_0 regime*

We now consider a PE model with ocean parameters and insert the MB87 solitary wave, first with the standard coefficients and then with the nonlinear coefficient altered to create an imbalance and thereby test the robustness of the form. One case incidently confirms that the vortex interactions are soliton-like.

The first case, E2 in Fig. 3, uses the standard ocean and soliton parameters listed in section 4a and Table 1. The flow exhibits a strong stability and a permanence out to 2000 days, but it has less variation in its energy integrals than case E1 did, even though the barotropic energy component now equals half the baroclinic value. The two cases E1 and E2 do not correspond exactly, despite mapping the parameters closely and keeping the amplitude factor the same at $A_0 = 0.25$. Other amplitudes were examined: a lower value, 0.15, gives a steadier soliton, whereas a higher value, 0.40, gives a strongly fluctuating vortex with an energy oscillation resembling that for the E1 case.

In the second ocean case, E3 in Fig. 4, an MB87 solitary wave, unbalanced by halving its nonlinear coefficient to $\alpha_1 = 0.23$, adjusts its size, strength, and shape to achieve a new stable configuration. It begins by forming a *positive* tail by 100 days that is shed by 400 days to create a weak second vortex of the same order. This differs from the SW solutions of WW88, where an overly strong soliton tends to shed a vortex of a higher latitudinal order.

The two vortices go through a series of *exchange* phases, where they overlie each other to temporarily form a larger vortex at 800 and 1600 days, and of *recurrence* phases, where their individual identities are restored at 1300 and 2000 days. The total baroclinic kinetic energy decreases during exchanges and increases at recurrences. The gradual dispersion or absorption of the secondary vortex in Fig. 4 suggests that

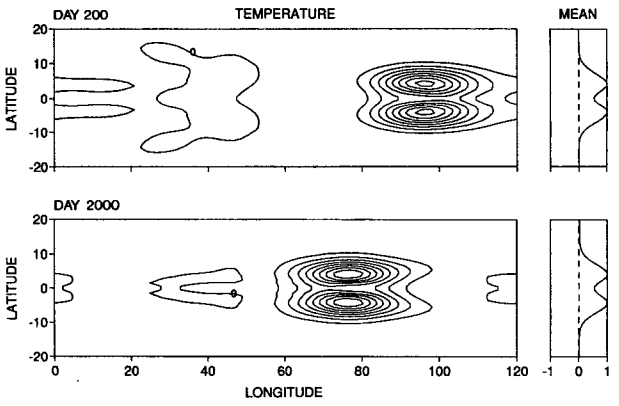

FIG. 3. Equatorial solution E2, stability of the Marshall and Boyd (1987) soliton. For ocean parameters and soliton coefficients, as in Table 1. Properties: $c = -1.3$ m s^{-1}, $U = 1.0$ m s^{-1}, $T = 0.9$ K, $B = 10^{-4}$ s^{-2}; contours: $\Delta T = 0.1$ K, $T^* = 0.19$ K, $Z = 0.2$ km.

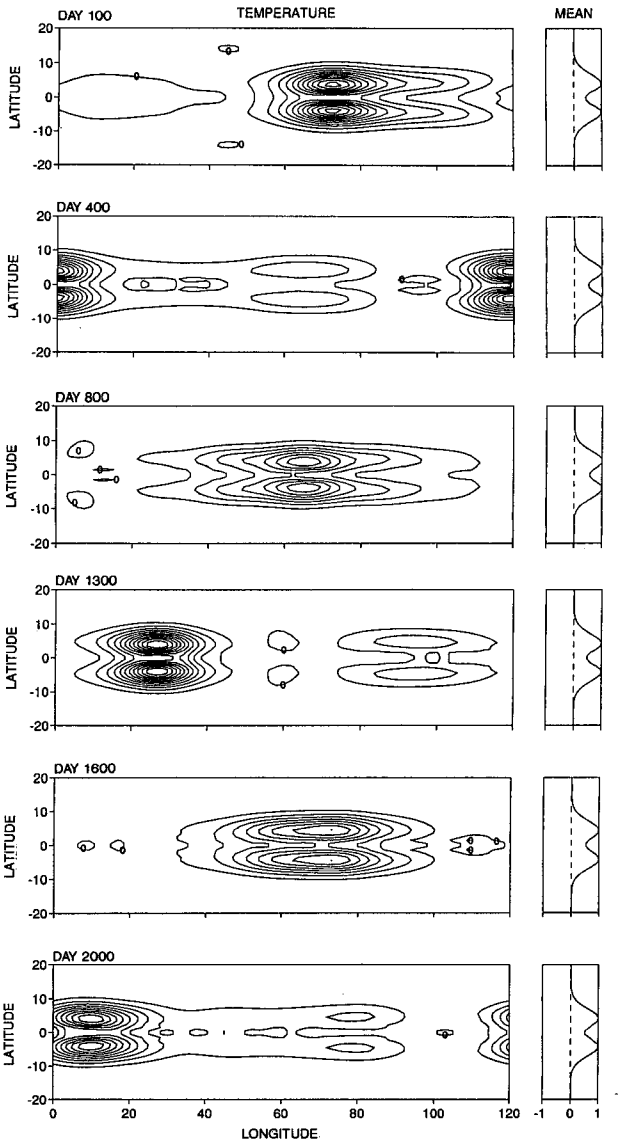

FIG. 4. Equatorial solution E3. Variation of the Marshall and Boyd (1987) soliton. For ocean parameters and soliton coefficients with a reduced nonlinear term, as in Table 1. Properties: $c = -1.34$ m s^{-1}, $U = 1.3$ m s^{-1}, $T = 0.8$ K. Contours: $\Delta T = 0.1$ K, $T^* = 0.26 - 0.28$ K, $Z = 0.2$ km.

the interactions are not fully soliton-like. Pure soliton interactions may require the existence of two strong solitary waves that are properly balanced from the beginning. Here, however, the interactions do result in the E3 vortex approaching the E2 soliton in size, strength, and shape to restore the preferred theoretical balance.

In the third ocean case, E4 (not shown), where the nonlinear coefficient is doubled to $\alpha_1 = 0.92$, the solitary wave adjusts more simply by elongating and by lowering its amplitude. This involves shedding a weak *negative* cyclonic tail that it later reabsorbs. Thus, the

equatorial vortices based on the MB87 solitary wave and the $e^{8z'}$ structure appear to be more robust than the theory suggests and so, perhaps, more readily realized. Furthermore, the existence of similar modes within zonal currents in the numerical solutions suggests that the solitons may be relevant to Jupiter's plumes. Resolving the MB87 equations with eigenfunctions modified by zonal jets, however, presents a daunting task.

5. Stability of shallow ($N = 20$) vortices in midlatitudes

We now examine whether exponential stratifications also favor the existence of stable vortices in midlatitudes. The more hostile, more dispersive regime that occurs in low latitudes, where the GRS lies, is dealt with later. For generality, we consider generic Gaussian forms rather than specific solitary wave solutions. This gives us the freedom to choose the values of N, H, and T_s such that certain observational constraints are met. After selecting representative values, we show how the size of a vortex affects its stability and then proceed to isolate the main destabilizing process.

a. The N, H, T_s parameter selection

Global observations of dynamic value are limited to Jupiter's upper-cloud level[4] but, nevertheless, are sufficient to constrain some of the parameters. To begin with, we note that Jovian vortices propagate[5] at about -5 m s^{-1}, which implies from the longwave phase speed relationship $c_\beta = -\beta L_R^2$ that the deformation radius is about 1000 km. This in turn implies that the internal gravity wave speed, $c_g = f_0 L_R$, is about 150 m s^{-1}. Then, given the estimated stability value of $B = 0.3 \times 10^{-4}$ s^{-2} near the cloud tops (L. E. Branscome 1982, personal communication), we derive a thickness, $h = c_g/B^{1/2}$, of about 40 km for the upper layer. Unfortunately, there is no observational constraint on the abyssal depth but theory suggests that h/H must be small, of order 10^{-1}, for vertical nonlinearity to prevail (Anderson and Killworth 1979).

To meet these constraints, we select values that are not too far removed from the initial P_0 set: $T_s = 1 + 10e^{Nz'}$, $N = 20$, and $H = 600$ km. The thermal wind relation $u \sim (\alpha g h \Delta T)/(f_0 L)$ then gives velocities of about 60 m s^{-1} for horizontal temperature differentials of about $\Delta T = 3$ K over distances of about $L = 5000$ km and depths of $h = 100$ km. We refer to these parameters as the $P_1(N20)$ system. Vortices in the P_1 system are shallower than those in the P_0 regime and should be typical of all shallow, vertically confined storms, but they are not; thinner vortices behave differently. Nevertheless, it is useful to examine their behavior to reveal the processes involved and see why even thinner structures must be invoked for Jupiter.

It is important to realize that this initial set of parameter values is based on limited observational estimates and on arbitrary theoretical arguments. Fortunately, we are dealing with generic modes, so all solutions can be simply rescaled in the vertical to apply to systems with other values of h and H, provided the relative scale factor h/H is maintained, as in section 9. But the main problem for planetary application remains the lack of an absolute vertical scale.

The Gaussian vortices inserted into the PE model all have temperature fields of the form

$$T' = T_v \exp\left[-\frac{1}{2}\left\{\left[\frac{\phi - \phi_0}{\delta\phi}\right]^2 + \left[\frac{\lambda - \lambda_0}{\delta\lambda}\right]^2\right\}\right]\hat{T}(z), \quad (30)$$

where T_v is the amplitude, $(\delta\phi, \delta\lambda)$ are the half widths, (ϕ_0, λ_0) define the center, and the vertical form $\hat{T}(z)$ is normally the first baroclinic eigenvector. The values used in the calculations are documented in Tables 1 and 2. The vortex velocities are set geostrophically.

b. Large anticyclone at $\phi_0 = 40°$

Our calculations show that midlatitude anticyclones with P_1 structures are "quasi-stable" if they are sufficiently large and strong. The designation quasi-stable refers to the fact that all P_1 vortices tend to migrate, at rates that depend on their size, into low latitudes, where they rapidly disperse. We must determine the cause of this migration and discover how to eliminate or control it, if possible.

The first midlatitude solution, M1, illustrates the behavior of a large strong vortex that initially has the elliptic and first-baroclinic forms of (30). According to the temperature field in Fig. 5, the vortex continuously adjusts its size and shape while losing strength as it propagates steadily westward and migrates slowly equatorward over 1000 days. The cause of the migration lies in the asymmetry of the u field and in the elongation of the easterly flow produced by the growing barotropic component, as comparison with case M4 later reveals in section 5e. The first baroclinic modal structure resembles that seen in many later cases (cf. Fig. 12) and prevails in the vertical because there is no apparent downward transport of heat and no generation of higher baroclinic modes. It confines motion to an upper layer of thickness 100–150 km.

The vertical flow remains constant in form and parallels that of the equatorial solitons, with western downwelling and eastern upwelling, peaking aloft with a value of 0.4 cm s^{-1} and extending strongly into the abyss (cf Fig. 35). This pattern follows from the basic geostrophic relations, written as

[4] Most of this study preceded the *Galileo* data (see section 9).

[5] For issues concerning variations in propagation rates and ambiguities about the rotational reference frame, see WW88.

TABLE 2. Vortex stability and jet coexistence cases in low latitudes. Constant parameters are H = 600 km, except H = 1200 km for L8–L10; $\Lambda = 60°$; resolution in (λ, ϕ, z) $R = 66 \times 42 \times 20$; $\Delta\lambda \sim 1°$, $\Delta\phi = 1°$; $\Delta z \sim e^{3z'}$ for L1–L4, $\Delta z \sim e^{5z'}$ for L5–L7 and L10, Δz = [0.05, 0.95] $H/10$ for L8 and L9; vortex centered at $\lambda_0 = \Lambda/2$. Easterly jets have slower exponential rates where marked (a) $e^{Nz'/1.5}$ and (b) $e^{Nz'/2}$. The abbreviations BC1 and BTR denote the first baroclinic eigenmodal and barotropic vertical distributions. Jet profiles are given by $\Phi_J = \Phi_{8,9,10}$, where the subscripts refer to the central jet width in degrees, such that Φ_8 = [0, −8, −16, −24, −32, −40]°, Φ_9 = [0, −7, −14, −23, −33, −40]°, and Φ_{10} = [0, −6, −15, −25, −35, −40]° denote the latitudes at which the sinusoidal jets vanish, except for the first two values that denote the extent of the W_1 jet maximum. Computational parameters are: Δt = (1/50) day, $\nu_4 = -(4 \text{ to } 10)\ 10^{16}$ m^4 s^{-1}, $\nu_2 = 10^{-6}$ m^2 s^{-1} for L1–L5, $\nu_2 = 10^{-8}$ m^2 s^{-1} for L6–L10.

Case	Structure N or h_c (km)	Static stability $T_S - 1$	Vortex form $T_v\,(\delta\lambda \times \delta\phi)\,\phi_0\,\bar{T}(z)$	Jet amplitudes $W_1 + E_1 + W_2 + E_2$	Jet form $U_J(z)$, $\Phi_J(y)$
L1	$N = 20$	$10\ e^{Nz'}$	1 (6 × 4)(−25°) BC1	—	—
L2	$N = 20$	$10\ e^{Nz'}$	1 (6 × 4.5)(−25°) BC1	50 − 20 + 20 − 0	BC1, Φ_8
L3	$N = 20$	$10\ e^{Nz'}$	1 (6 × 4.5)(−30°) BC1	0 − 20 + 0 − 0	BTR, Φ_8
L4	$N = 20$	$10\ e^{Nz'}$	—	50 − 25 + 25 − 5	BC1 + BTR, Φ_8
L5	$N = 60$	$10\ e^{Nz'}$	3 (4 × 4)(−25°) BC1	—	—
L6	$N = 60$	$10\ e^{Nz'}$	3 (4 × 4)(−25°) BC1	0 − 5 + 0 − 0	BC1 + BTR, Φ_9
L7	$N = 90$	$10\ e^{Nz'}$	3 (4 × 4)(−25°) BC1	—	—
L8 (LIN)	$h_c = 40$	$10\ C\,[z_c^2, 0]$	8 (6 × 4)(−23°) C [1, 0]	—	—
L9 (LIN)	$h_c = 40$	$20\ C\,[z_c^2, 0]$	6 (6 × 4)(−23°) C [1, 0]	100 − 40 + 30 − 15	$C\,[z_c, 0]$, Φ_9
L10	$N = 180$	$45\ e^{Nz'}$	36 (6 × 4)(−23°) $e^{Nz'}$	100 − 30[(a)] + 30 − 12[(b)]	$e^{Nz'}$, Φ_9

$$v = \frac{1}{f\rho_0} p_x, \quad u = \frac{-1}{f\rho_0} p_y, \quad w_z = -u_x - v_y, \qquad (31)$$

which reduce to

$$w_{zz} = \frac{\alpha\beta}{f^2} T_x \qquad (32)$$

and then to

$$\hat{w} = \frac{-\alpha\beta}{l^2 f^2} \cdot T_x \qquad (33)$$

for the simplest vertical form $w = \hat{w}\cos(lz)$ that satisfies the boundary conditions.

The M1 vortex differs from its shallow-water counterpart (M1 of WW88) to the extent that it migrates, generates barotropic motion, and is only quasi-stable. Nevertheless, similarities suggest that the PE vortex evolution is mainly brought about by the advection and twisting processes, as is evident from the elongation and tilt of the temperature field at 250 days in Fig. 5. Unfortunately, no three-dimensional equivalent of the geostrophic potential vorticity equation (20) exists to define the vortices in terms of basic processes. Because of its size, the M1 vortex probably lies in the planetary geostrophic regime and probably obeys some sort of Rossby–KdV balance, as do the large SW vortices of WW88. Generally, vortices such as M1 exist over a narrower range than their shallow-water counterparts, with only modest changes of amplitude or shape allowed. Clearly, the P_1 system is not very accurately described by the shallow-water analog.

c. *Medium anticyclone at $\phi_0 = 40°$*

The medium vortex M2 in Fig. 6 has less than half the amplitude and size of the M1 storm but remains coherent while propagating westward at −1.9 m s^{-1} and rapidly migrating 3° equatorward in 200 days. The tight core, 5° scale, and wave dispersion, when compared with their shallow-water counterparts (cf. M6 of WW88), all suggest that the M2 vortex lies in the complex intermediate-geostrophic regime. Therefore, we expect the dispersion to force the dynamics and be balanced by the vorticity advection and by the steepening and twisting produced by the $c(\phi)$ phase speed variation.

The zonal velocity field (not shown) reveals that the main barotropic component takes the form of a westerly current centered at 40° latitude. Although the vortex develops some asymmetry between its easterly and westerly parts, the barotropic flow is not involved and is not the cause of the migration in this case. This suggests that barotropy only influences the large P_1 vortices.

d. *Small anticyclone at $\phi_0 = 40°$*

Halving the vortex size once more then leads to the M3 case with standard quasigeostrophic characteristics (Fig. 7). At this scale, both cyclones and anticyclones are considered to be quasi-stable as they remain temporarily coherent and do not collapse immediately into waves. They do, however, migrate rapidly to latitudes where the ambient potential vorticity f/T matches their initial potential vorticity, whereas large vortices tend to determine their own local potential vorticity gradient. In this instance, the M3 vortex propagates 7° westward at −1.0 m s^{-1} and migrates 3° equatorward in just 75 days, while losing amplitude and developing a strong core and trailing wave envelope through the action of dispersion just as in its shallow-water counterpart (M7 of WW88). Migrating vortices such as this have been studied in

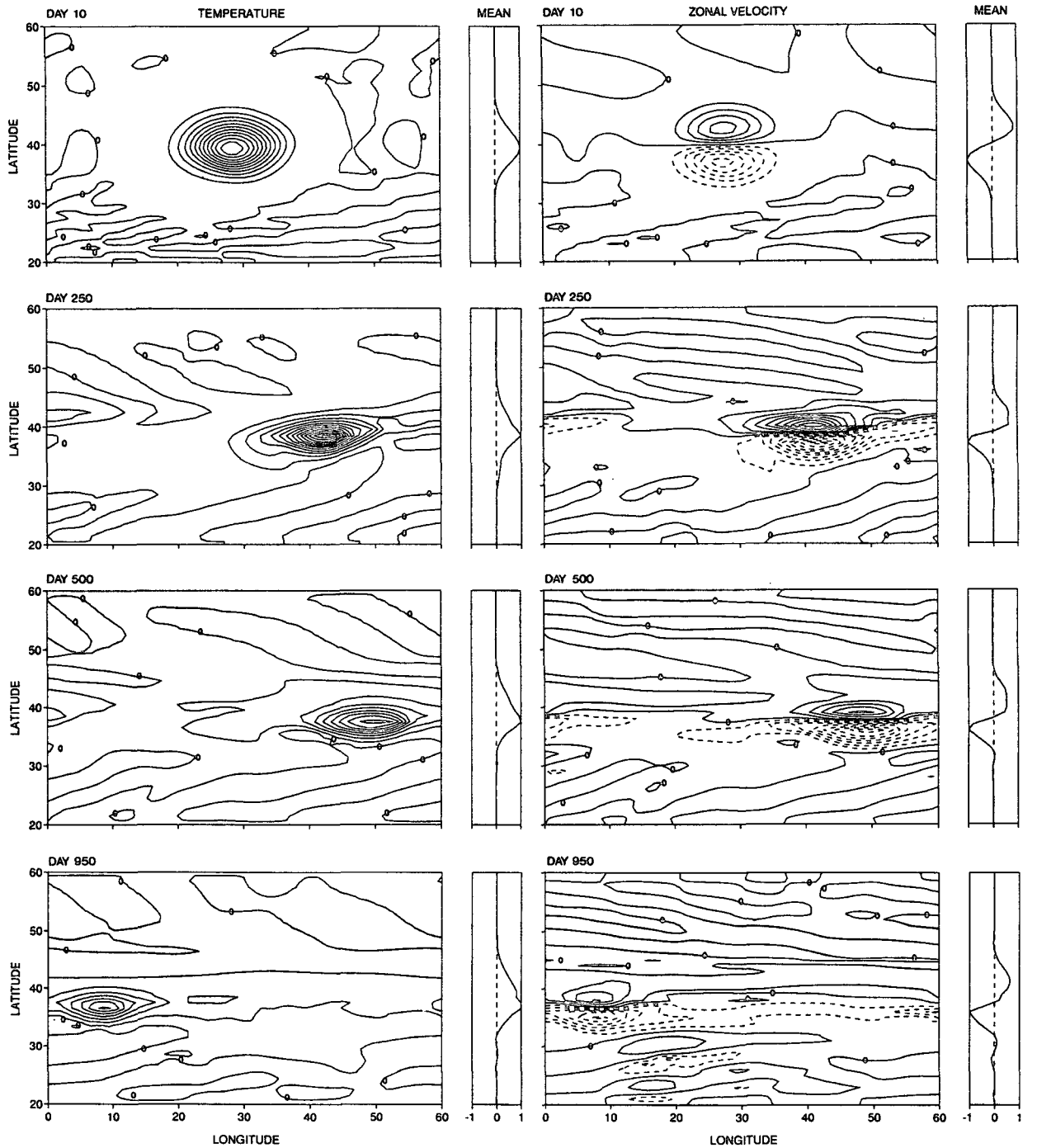

FIG. 5. Midlatitude solution M1, quasi-stability of a large P_1 anticyclone. For Jovian $P_1(N20)$ parameters and a geostrophic Gaussian vortex, as in Table 1. Properties: $c = -2.5$ m s^{-1}, $U = 20$ m s^{-1}, $T = 1.5$ K, $B = 0.4 \times 10^{-4}$ s^{-2}; contours: (a) $\Delta T = 0.1$ K, $T^* = 0.21 - 0.26$ K, $Z = 8$ km and (b) $\Delta u = 2$ m s^{-1}, $u^* = (-1.9, -4.1, -5.1, -4.7)$ m s^{-1}, $Z = 8$ km.

great detail, usually with the quasigeostrophic equations, for Earth's oceans [see the reviews by Flierl (1987) and McWilliams (1991)]. Overall, the dependence of vortex behavior on size in the P_1 regime parallels that seen for the shallow-water system.

e. Large anticyclone without barotropy at $\phi_0 = 40°$

To examine the role of barotropy in large vortices, case M1 is rerun with the external mode suppressed. This produces the M4 anticyclone in Fig. 8, which

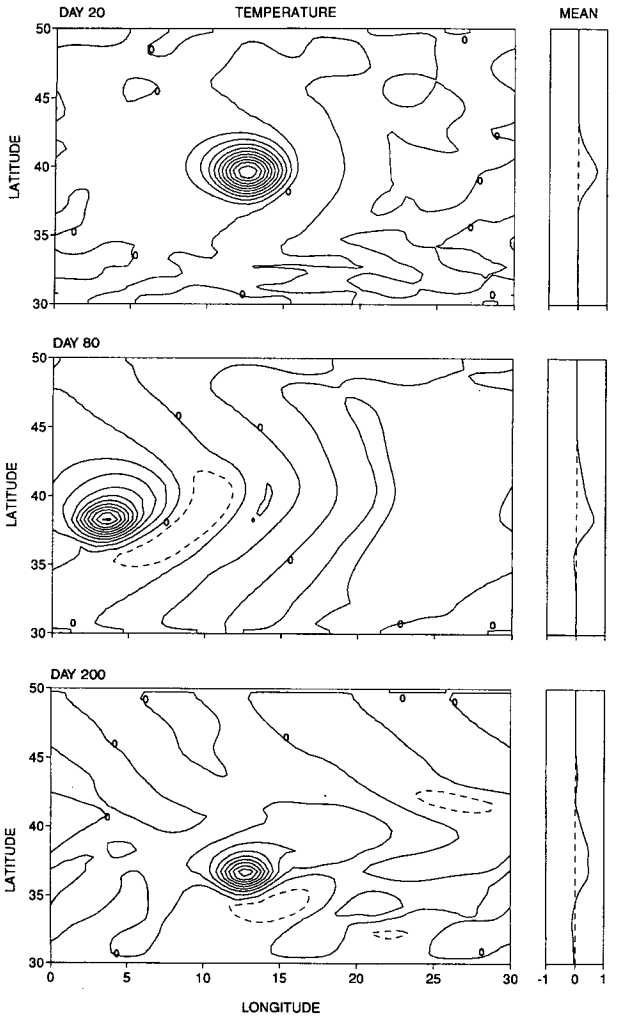

FIG. 6. Midlatitude solution M2, quasi-stability of a midsize P_1 anticyclone. For Jovian $P_1(N20)$ parameters and a geostrophic Gaussian vortex, as in Table 1. Properties: $c = -2.0$ m s^{-1}, $U = 10$ m s^{-1}, $T = 0.5$ K, $B = 0.4 \times 10^{-4}$ s^{-2}. Contours: $\Delta T = 0.05$ K, $T^* = 0.1$ K, $Z = 8$ km.

barely changes once it has adjusted and only migrates 0.5° in 1000 days while propagating 188° westward at -2.1 m s^{-1}. The vortex appears destined for longevity. Moreover, the zonal flow remains symmetrical, although some dispersion is evident toward the equator at 1000 days.

Comparing the M1 and M4 solutions clearly suggests that, for large vortices, the main cause of the migration and deviation from shallow-water behavior lies in the development of a barotropic component. Thus the basic problem in deriving the conditions for stability reduces to finding out how to control or eliminate the projection of the baroclinic mode onto the barotropic. In the equatorial soliton, this projection is small because the baroclinic mode is more self-interacting and consequently the baroclinic kinetic energy greatly exceeds the barotropic, whereas in midlatitudes the opposite holds true. Reducing the projection by putting the vortex in a larger domain is not enough; rather, the projection must be fully controlled or eliminated.

f. Small barotropic anticyclone at $\phi_0 = 40°$

To reinforce the result that a vortex must be vertically confined for longevity, an example is given that describes the behavior of a completely barotropic anticyclone in a stratified fluid, case M5 in Fig. 9. Only small barotropic vortices remain coherent but, compared to baroclinic storms, even they collapse quickly through wave dispersion. In the M5 case, the equatorward migration actually exceeds the westward propagation, and the vortex soon approaches the southern boundary, where energy is reflected to create a new vortex to the north.

6. Stability of shallow ($N = 20$) vortices in low latitudes

As we saw in the previous section, vortices can exist for about 1000 days in midlatitudes in the P_1 system provided they lie within a rather narrow range of sizes and strengths. These vortices all tend to migrate slowly equatorward and eventually collapse in the highly dispersive low latitudes. The cause of the migration is seen to lie in the projection of energy from the baroclinic mode onto the barotropic and the consequent feedback. Given the lack of a simple regime with absolute stability in midlatitudes, we now move to low latitudes—where all problems and processes are more acute but must be dealt with for application to the Great Red Spot—and consider the possibility that zonal jets can block migration and make vortices long-lived the way they do in the shallow-water system (WW88).

In the shallow-water calculations, the low-latitude anticyclones are stable only when zonal currents exist to eliminate the generation and propagation of the highly dispersive equatorial modes. Specifically, the westerly currents $W_1 + W_0$ limit the wave propagation by modifying the eigenfunctions so that only the largest modes occur at the equator. The generation of these large equatorial modes, however, is reduced by the easterly jet E_1 through its modification of the internal vortex dynamics by eliminating twisting (see WW88). To see if such mechanisms are effective in stabilizing vortices in the P_1 system, we examine how anticyclones behave in the presence of one or more of these currents.

The following solutions, L1–L5 in Table 2, reveal that the vortices cannot be stabilized by the jets in low latitudes, so the shallow-water analogy is yet further limited for the P_1 system. All of the remaining calculations are set in the Southern Hemisphere so that the symmetry boundary condition in (13) may be applied at the equator.

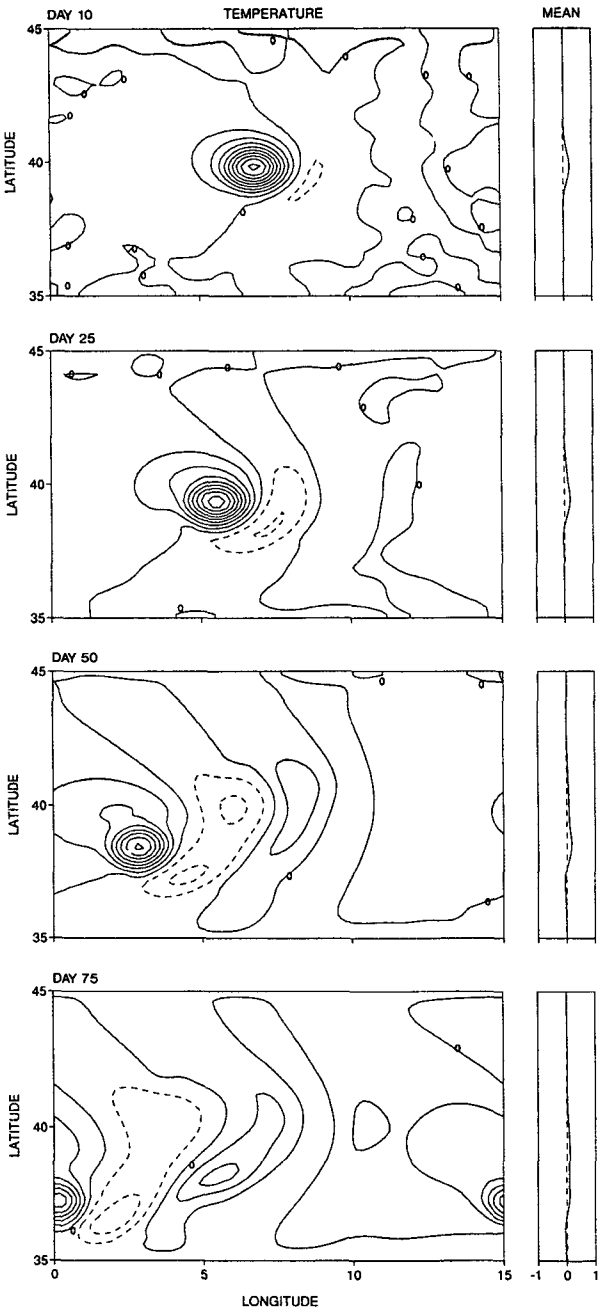

FIG. 7. Midlatitude solution M3, quasi-stability of a small P_1 anticyclone. For Jovian P_1 ($N20$) parameters and a geostrophic Gaussian vortex, as in Table 1. Properties: $c = -1.0$ m s^{-1}, $U = 9$ m s^{-1}, $T = 0.2$ K; contours: $\Delta T = 0.02$ K, $T^* = 0.1$ K, $Z = 8$ km.

a. *Large anticyclone at $\phi_0 = -25°$*

For reference, we first examine the behavior of a vortex in low latitudes in the absence of jets. Typically, when a large anticyclone such as L1 in Fig. 10 is placed at $\phi = -25°$, it remains coherent and persistent for about 600 days. After quickly adjusting to a narrower shape by 100 days, it continues to propagate westward, migrate equatorward, and generate highly dispersive equatorial Rossby waves.

During its 600-day existence, the vortex propagates 340° westward at a phase speed that increases from -6.2 m s^{-1} to -10.7 m s^{-1} as it migrates 7° into lower latitudes, where a larger β and a smaller f_0 both boost $c_\beta = -\beta\bar{B}/f_0^2$. The anticyclone also becomes smaller and weaker as it progresses, especially after it reaches $\phi = -18°$ and the dispersion intensifies, and it vanishes completely by 650 days. The elongation of the easterly component again implies that the baroclinic kinetic energy is projecting onto the barotropic mode. Compared to its M1 midlatitude counterpart, the L1 storm has a shorter timescale, adjusting more quickly, dispersing more rapidly, moving faster, and vanishing sooner.

b. *Large anticyclone in westerly and easterly jets at $\phi_0 = -25°$*

Consider now what happens when Jupiter-style, alternating zonal currents, U_J, are introduced and the large vortex is embedded within the anticyclonic zone formed by the W_2 westerly and E_1 easterly jets, as for case L2 in Figs. 11 and 12. To set their amplitudes individually, the jets are made up of a series of half-sine functions that are joined together at their zero values, at latitudes spaced at 8° intervals in this particular case (Table 2). In the equatorial zone, $\phi = 0°$ to $-8°$, the W_0 westerly is made uniform and set equal to the W_1 amplitude (Fig. 12). The amplitudes chosen for the jets are smaller than the observed to keep them in scale with the vortex. More realistic values are used later in sections 7–9. Vertically, the jets have the same first baroclinic eigenmodal structure as the vortex.

The temperature field T_J associated with the jets is formed by integrating geostrophically over latitude and is arbitrarily normalized over the domain so as to have a zero net value, $\langle T_J \rangle = 0$. Note that the temperature in Fig. 12 and in all other vertical plots excludes the hydrostatic component T_s that stabilizes the cool cyclonic zones. Comparing the fields in Fig. 12 with the eigenfunctions shows that the flow retains the first baroclinic eigenmodal structure and is accurately resolved by the gridpoint distribution, $\Delta z \sim e^{3z'}$, used for the $P_1(N20)$ system throughout section 6 (cf. Fig. 20).

The imposed U_J and T_J fields produce a very orderly flow when the vortex starts to propagate and come into coexistence with the jets (Fig. 11). The vortex steepens by 250 days, forming a front on its northwest frontier, and temporarily resembles some *Voyager* spacecraft views of the GRS. This suggests that the GRS may be defined, to first order, as a nonlinear baroclinic Rossby wave embedded in jets with the same vertical structure. The flow ahead (west) of the vortex resembles the GRS wash (not wake) and persists longer when more appropriate parameter values are used, as in sections 7–

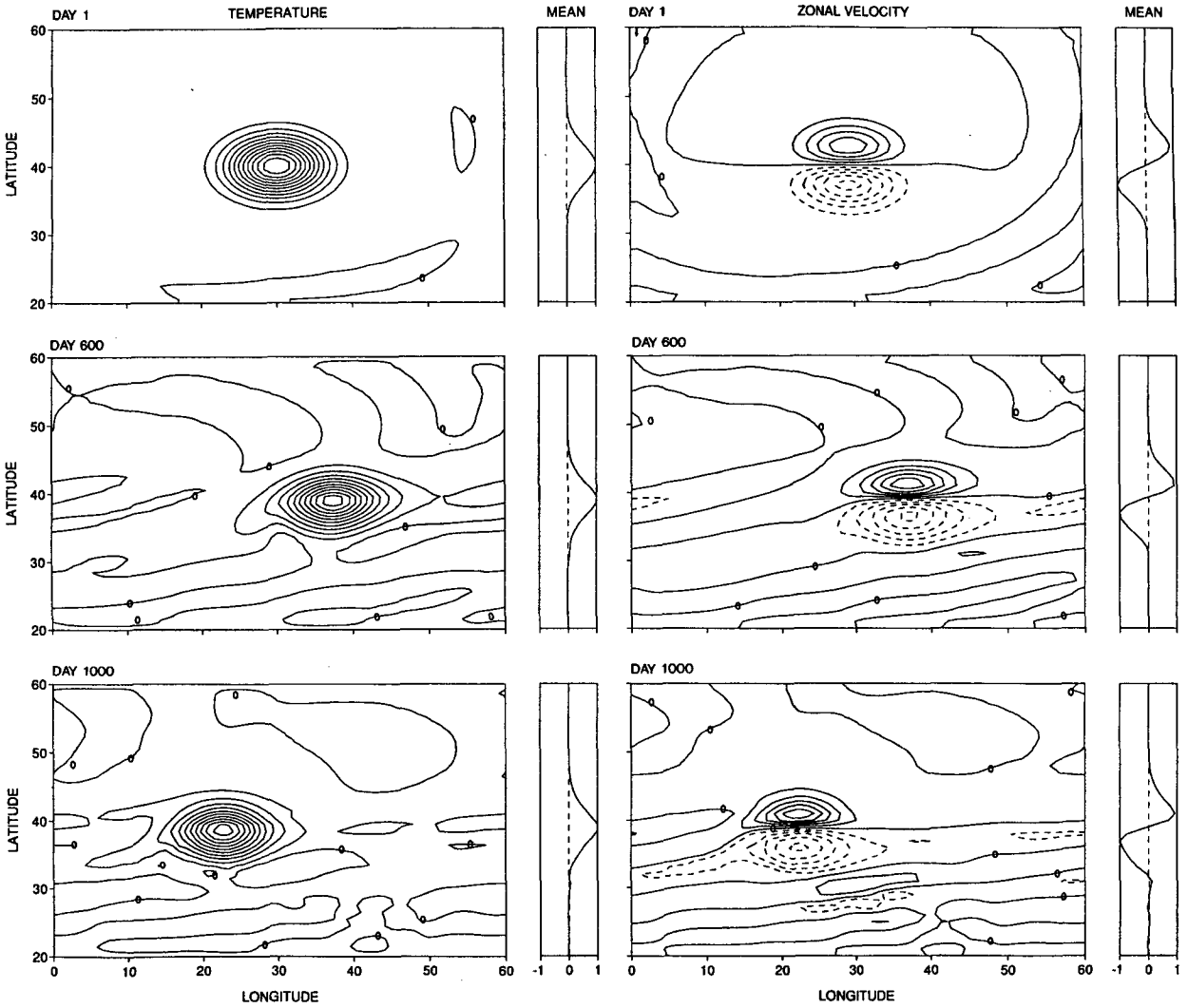

FIG. 8. Midlatitude solution M4, stability of a large P_1 anticyclone with a suppressed barotropic mode. For Jovian $P_1(N20)$ parameters and a geostrophic Gaussian vortex, as in Table 1. Contours: (a) $\Delta T = 0.1$ K, $T^* = 0.21 - 0.24$ K, $Z = 8$ km; (b) $\Delta u = 2$ m s^{-1}, $u^* = -1.9$ to -2.5 m s^{-1}, $Z = 8$ km.

9. This flow pattern is caused by the impact of the vortex on the easterly jet, in part due to its tendency to migrate.

The easterly jet blocks the migration for the first 400 days, holding the vortex at $\phi = -25°$. The anticyclone, however, becomes smaller and rounder over this period, while the easterly jet becomes broader and weaker due to instability, wave action, and the generation of a barotropic westerly current of 6 m s^{-1} at $\phi = -20°$. Consequently, the vortex manages to migrate equatorward to $\phi = -20°$ by 600 days and to $\phi = -15°$ by 750 days, gradually shrinking to 6° in diameter before vanishing at 800 days. Comparing the L2 and L1 solutions shows that the easterly current merely slows the migration, extending vortex existence by only a 100 days.

Calculations with just an easterly jet resemble the multijet case L2, confirming that only that current has any real effect on vortex stability in the P_1 system. How the T_J temperature field associated with the easterly jet actually influences the vortex is not known. In the simpler shallow-water system, the easterly jet acts through the latitudinal variation of the height field h_J to match the f_0 variation and make $c_\beta = -\beta g h_J / f_0^2$ more uniform, thereby reducing the twisting and the vortex collapse. In the PE model, however, long waves can be Doppler shifted, as (22) shows, and may also be influenced by the turning and critical latitudes produced by the $U_J(\phi)$ field.

Although an easterly jet can, in principle, block migration completely if it is strong enough, we were unable to verify this because we could not find any form

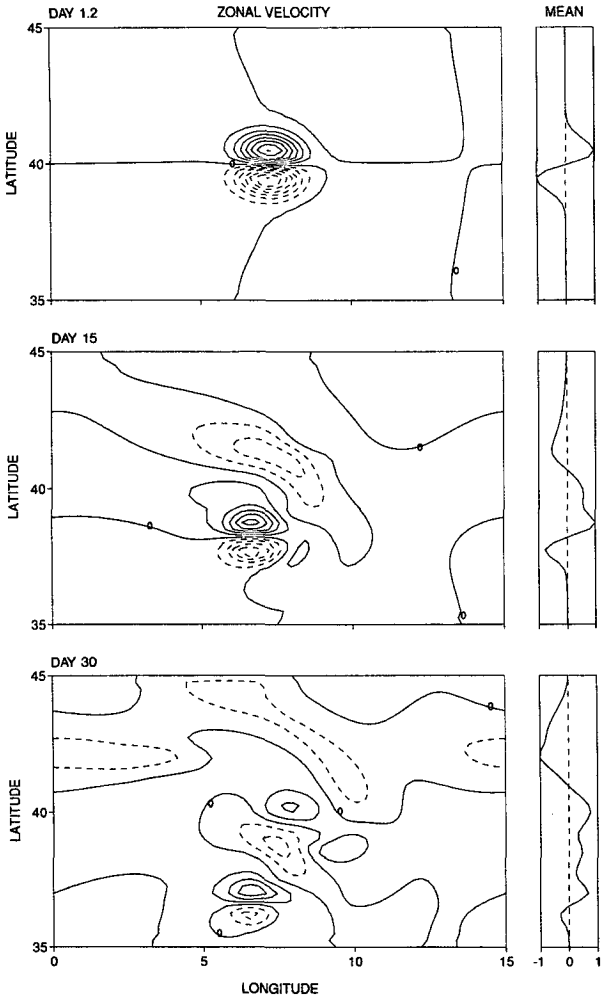

FIG. 9. Midlatitude solution M5, stability of a small barotropic anticyclone. For Jovian $P_1(N20)$ parameters and a geostrophic Gaussian vortex with no vertical variation, as in Table 1. Contours: $\Delta u = 2$ m s^{-1}, $u^* = -1.3$ to -1.7 m s^{-1}, $Z = 8$ km.

of easterly jet with an amplitude above 20 m s^{-1} that remains baroclinically stable in the P_1 regime. A variety of vertical forms of $U_J(z)$ and $B_J(z)$, with a vanishing shear at the surface and a vanishing QG potential vorticity gradient internally, did not give stable jets because, as we shall see in Part II, these quasigeostrophic constraints are not relevant in these regimes.

c. *Anticyclone and barotropic easterly jet*

One way to make easterly jets stronger without making them more unstable is by adding a barotropic component. To see what flow strength is needed to block migration, we consider a fully barotropic easterly jet first, case L3 in Fig. 13. Placing the vortex at $\phi = -30°$ allows it to adjust gradually to the -20 m s^{-1} jet at $\phi = -20°$.

The vortex starts to interact with the easterly jet when it reaches $\phi = -28°$ at 200 days, according to the u field in Fig. 13. The jet holds the vortex at $\phi = -26°$ and causes it to become longer and narrower by 500 days. The length doubles to 50° by 800 days, so the storm becomes self-interacting in its final stage. This collapse also widens the jet by 4° of latitude. This interaction is consistent with the well-known fact that baroclinic waves are absorbed by the critical layer associated with barotropic easterly jets (Killworth 1979).

Clearly, a barotropic jet of -20 m s^{-1} stops the migration completely, as does a jet of -10 m s^{-1}, but a -5 m s^{-1} current fails to block the vortex. This implies that we can add, at most, only a -5 m s^{-1} barotropic component to the basic baroclinic easterly, and this may not even be enough to counter the westerly barotropic current generated by the vortex, let alone block the vortex. Fortunately, as we see in section 7, the role of the easterlies becomes simpler for other vertical structures.

d. *Baroclinic instability of an easterly jet*

As we have seen, the coexistence between a vortex and the zonal currents is complicated by the tendency of easterly jets to become baroclinically unstable. Such instabilities generate waves in the P_1 regime, but in the more nonlinear P_3 regime examined later in section 8, they generate vortices. Case L4 in Fig. 14 illustrates the conventional instability for jets that are totally confined to the upper layer by adding a small barotropic component to counter the first baroclinic mode in the abyss.

The instability starts at 220 days in an easterly of -25 m s^{-1} that is centered at $\phi = -20°$ and abutted by stable westerly jets. Because the jet barely exceeds the critical value, the instability produces regular waves and only lasts about 20 days. According to the vertical velocity, the instability arises at the easterly jet axis at $\phi = -20°$ and evolves into waves trapped by the critical latitude at $\phi = -12°$. These features bear some similarity to those of the classic terrestrial easterly instabilities (Feldstein 1991).

Complete eddy mixing of the u and T fields in the easterly jet eliminates most of the zonal flow and baroclinicity in that zone. Vertical plots (not shown) reveal that the eddy T', v' fields are confined to the upper layer, while w' extends into the abyss. The u' eddies become deeper as the cascade to barotropy grows. The northwest–southeast orientation of the initial eddies in the barotropic zonal flow reflects the equatorward transport of barotropic vorticity and the formation of the barotropic westerly and easterly jets, seen later at $\phi = -20°$ and $-15°$.

7. Stability of thin ($N = 60$–180) vortices

From the above cases, we conclude that the P_1 system, unlike the shallow-water model, does not support

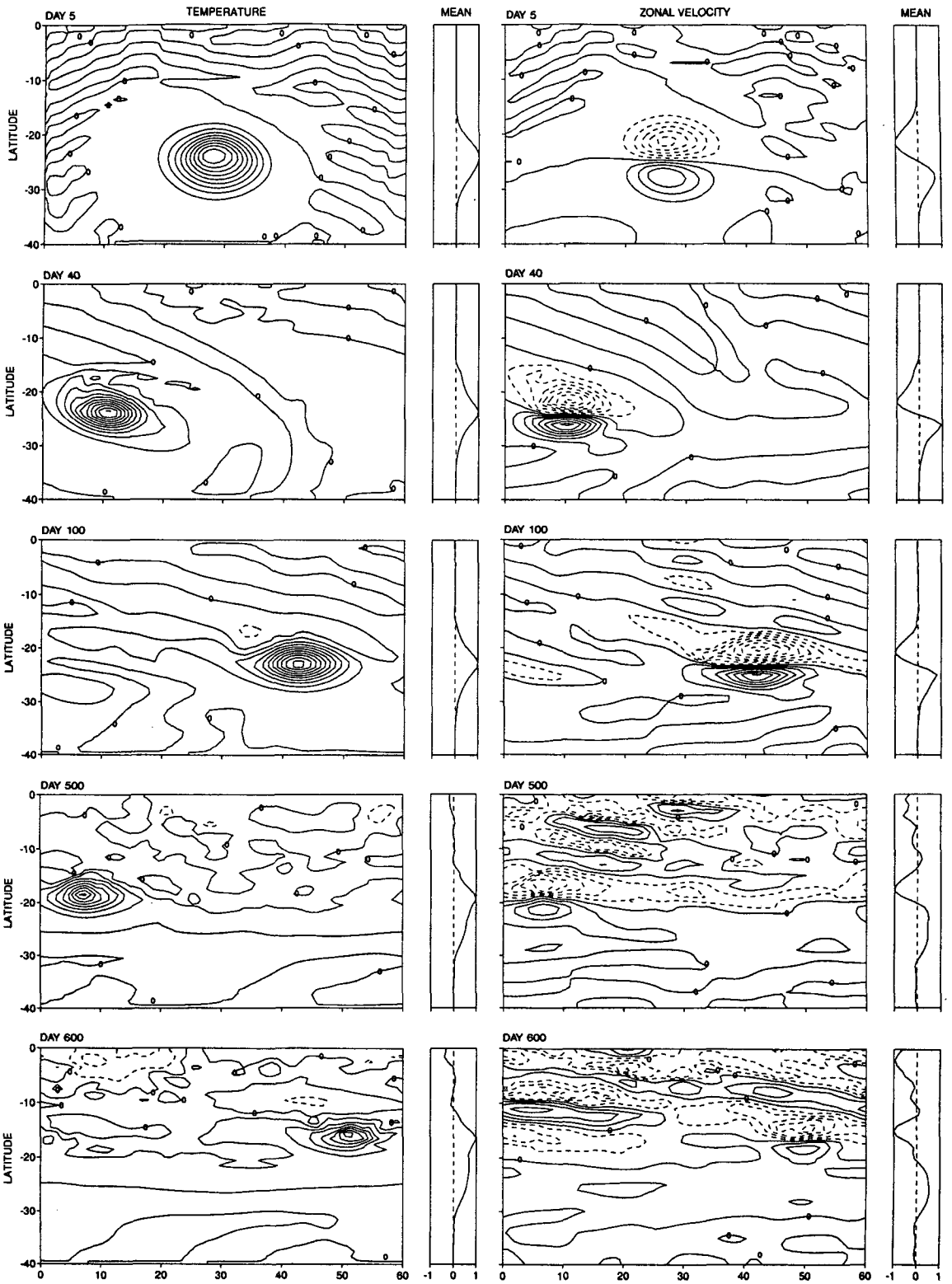

FIG. 10. Low-latitude solution L1, quasi-stability of a large P1 anticyclone. For Jovian $P_1(N20)$ parameters and a geostrophic Gaussian vortex, as in Table 2. Properties: $c = -6.2$ to -10.7 m s^{-1}, $U = 30$ m s^{-1}, $T = 1.2$ K, $B = 0.4 \times 10^{-4}$ s^{-2}. Contours: (a) $\Delta T = 0.2$ K, $T^* = 0.35 - 0.43$ K, $Z = 8$ km; (b) $\Delta u = 5$ m s^{-1}, $u^* = (-4.7, -6.2, -8.6, -9.2, -7.8)$ m s^{-1}, $Z = 8$ km.

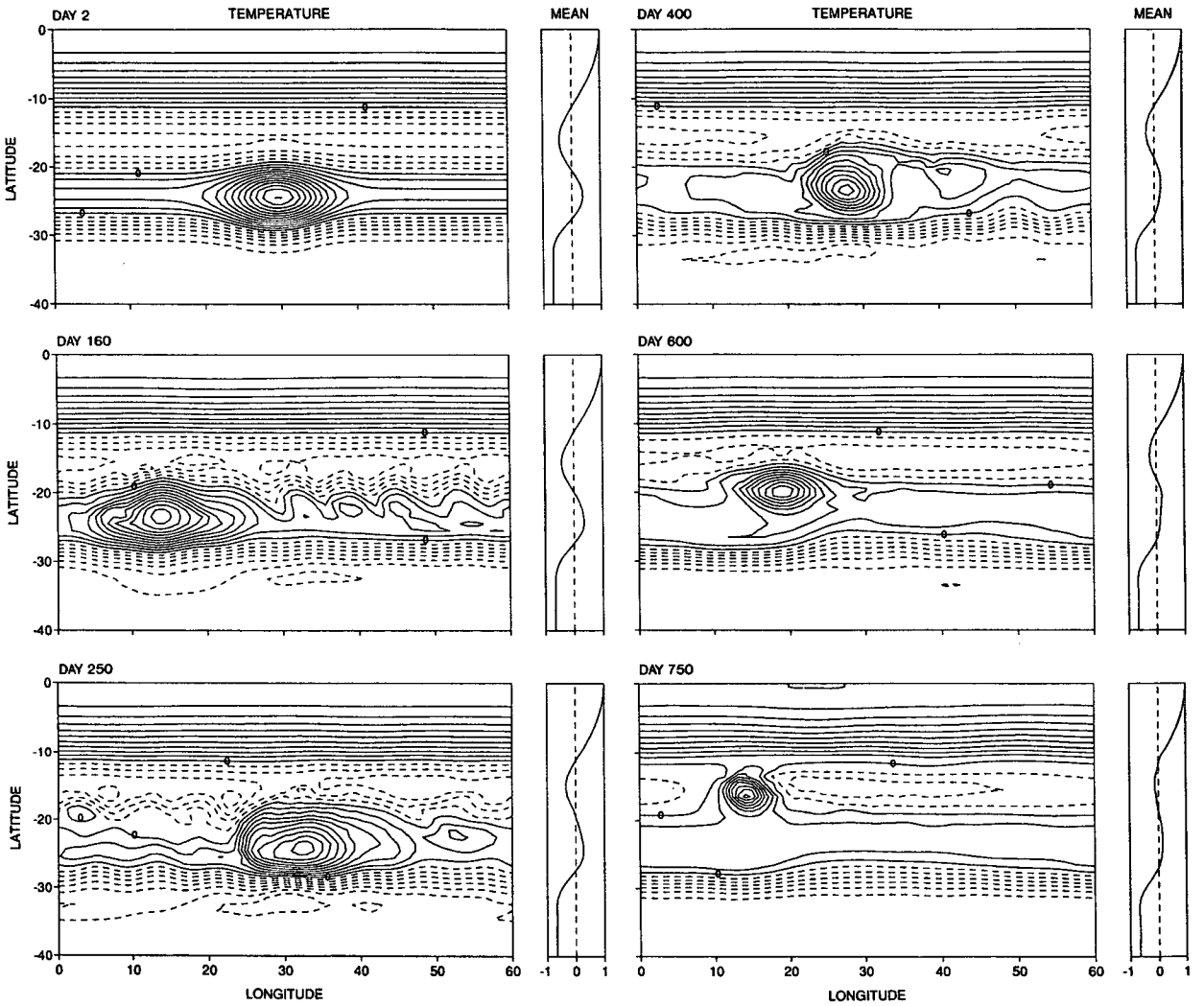

FIG. 11. Low-latitude solution L2, quasi-stability of a large P1 anticyclone in alternating jet streams. For Jovian $P_1(N20)$ parameters and a geostrophic Gaussian vortex embedded in geostrophic sinusoidal jet streams, as in Table 2. Contours: $\Delta T = 0.2$ K, $T^* = 1.98$ K, $Z = 8$ km.

long-lived stable vortices. Although strong easterly jets slow the tendency for vortices to collapse by migration, such jets also tend to collapse from baroclinic instability, while the vortices tend to shrink and tunnel through regardlessly. Other factors, such as the westerly jets, help shape and guide the vortex and may also help the easterly jet survive longer, but none alter the basic character of the regime.

Given the difficulties in stabilizing the $P_1(N20)$ vortices, we now vary the parameters in a more extreme way and thus depart further from our MB87 theoretical roots. We stay in low latitudes but move from shallow to thin vortices, first by increasing the exponential structural rate N to 60 to define a P_2 regime, and then by increasing N to 90–180 to define a P_3 regime and its alternative confined linear representation L_3. The corresponding calculations, L5–L10 in Table 2, reveal that the above P_1 cases are not fully representative of confined vortices because their basic character alters as the rate N increases: migration does not just diminish, it stops completely; baroclinically unstable waves do not become smaller, they become solitary.

Indeed, the basic problem alters in the P_3 regime because vortices can exist without jets and for a wide range of amplitudes, scales, and shapes. We no longer need to see if jets can block vortices but rather need to see if they can coexist with them. Neither need we apply the P_1 solutions to the planets because the P_2 and P_3 regimes are more relevant. But the best solutions remain difficult to isolate because of the long timescales (10^3 days) and the degree of nonlinearity involved.

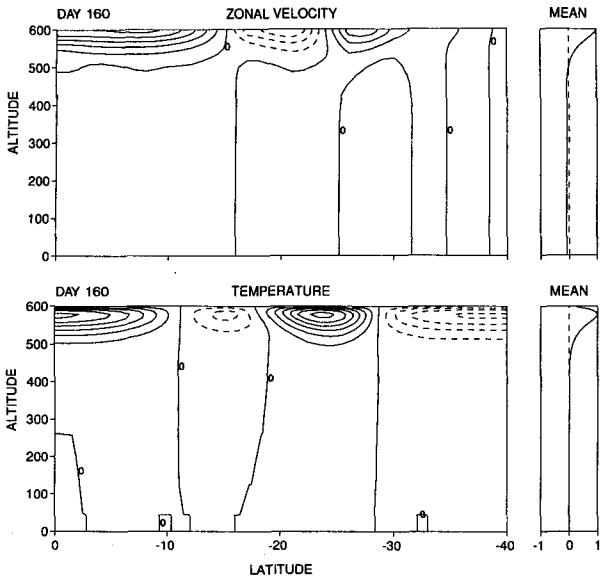

FIG. 12. Vertical sections for the low-latitude solution L2, sampled at the longitude of the vortex center. Contours: (a) $\Delta u = 10$ m s^{-1}, $u^* = 15.4$ m s^{-1}, $\lambda = 15°$; (b) $\Delta T = 0.5$ K, $T^* = 0.48$ K, $\lambda = 14°$.

a. *Thin anticyclone in the $P_2(N60)$ system*

Calculations that vary the rate N of the exponential structure show that the large anticyclones become more stable when they are made thinner. The first solution with $N = 60$, case L5 in Fig. 15, illustrates this development. After the initial adjustment, the vortex migrates only 2° in latitude over 1000 days, far less than in the L1 case with $N = 20$ in Fig. 10. Migration still occurs, however, so the storm is still only quasi-stable although jets can now make it conditionally stable, as we shall see.

The L5 vortex propagates 230° westward at a realistic speed of -3 m s^{-1} but has scales that are on the low side. If H is increased to 1200 km while T_v is doubled in amplitude and T_s halved, the vortex has more realistic scales, but a greater migration of 4° over 1000 days. Vertically, the storm extends about 50 km, supporting the idea that a small thickness factor $h/H \leqslant 0.1$ is needed for stability. For thin flows such as L5 the barotropic kinetic energy remains weaker than the baroclinic, which adds to the stability. The vortex also retains the first baroclinic modal form and is well resolved by the $\Delta z \sim e^{5z'}$ grid distribution (cf. Fig. 20).

Varying the vortex amplitude reveals that the propagation rate, in flows such as L5, depends as much on the vortex T_v field as on the background $T_s(z)$ profile. The T_s contribution is essential, however, for coherence and cannot be made too small in trying to minimize the phase speed. When jets are present, their static stability contribution, B_J, can exceed B_s and add a latitudinal variation, making it difficult to define a basic state. Because the phase speed depends on B_s, B_v, and B_J, the first baroclinic eigenmode based on B_s alone may not be the most meaningful structure. Moreover, when the jets are free to generate the vortex structure, they select their own $e^{Nz'}$ form rather than an eigenmode, as in section 8.

b. *Thin anticyclone with easterly jet in the $P_2(N60)$ system*

Given that the thin P_2 vortices migrate so much more slowly than the P_1 storms, we now reconsider the issue of whether easterly jets can block them completely and thereby produce conditionally long-lived flows. The example, L6 in Fig. 16, shows that a weak easterly jet of -5 m s^{-1} can indeed stop the migration of a P_2 vortex indefinitely. Consequently, this parameter range could be relevant to the planets.

The easterly jet is centered at $\phi = -20°$ and has the same vertical structure as the vortex but with a small barotropic component added to remove the abyssal flow. After some initial adjustment, the jet and vortex enter into a balance in which the jet remains stable and the vortex remains at $\phi = -25°$ with the relevant scales $U = 40$ m s^{-1}, $T = 6$ K, and $c = -3$ m s^{-1}. The conditional longevity found in L6 is oversimplified, however, because if the jet is strengthened to -15 m s^{-1}, it not only stops the migration, it actually reverses it, gradually pushing the vortex 3° poleward over 800 days.

c. *Thin anticyclone in the $P_3(N90)$ system*

Although the large P_2 vortices are coherent and can be made conditionally long-lived by easterly jets, they suffer from a complex dependence on jet amplitude and from reverse migration. This leads us to consider even thinner systems, P_3, with $N \geqslant 90$. Consequently, we find that somewhere between $N = 60$ and $N = 90$ we enter the realm of absolute stability for large vortices. Behavior for $N > 90$ remains constant in character, so there is no need to distinguish regimes beyond P_3. In this parameter region the large vortices no longer migrate and can exist indefinitely, with or without jets. The issue of jets then simplifies to one of establishing coexistence and later of genesis.

The existence of absolute stability in the P_3 regime is illustrated by the L7 case detailed in Figs. 17–19. Because its initial circular shape is not optimal, the L7 anticyclone undergoes a major adjustment toward the preferred elliptic form in the first 100 days (Fig. 17). This adjustment reduces the temperature amplitude from 8 K to 6 K and produces some residual zonally aligned isotherms equatorward of the vortex in the zone between $\phi = -10°$ and $-20°$. Such residual isotherms or "background radiation" are not produced by elliptic vortices and so may be regarded as containing historical information about the original storm.

The vertical cross sections in Fig. 18 reveal both the residual temperature zone and the persistent first baro-

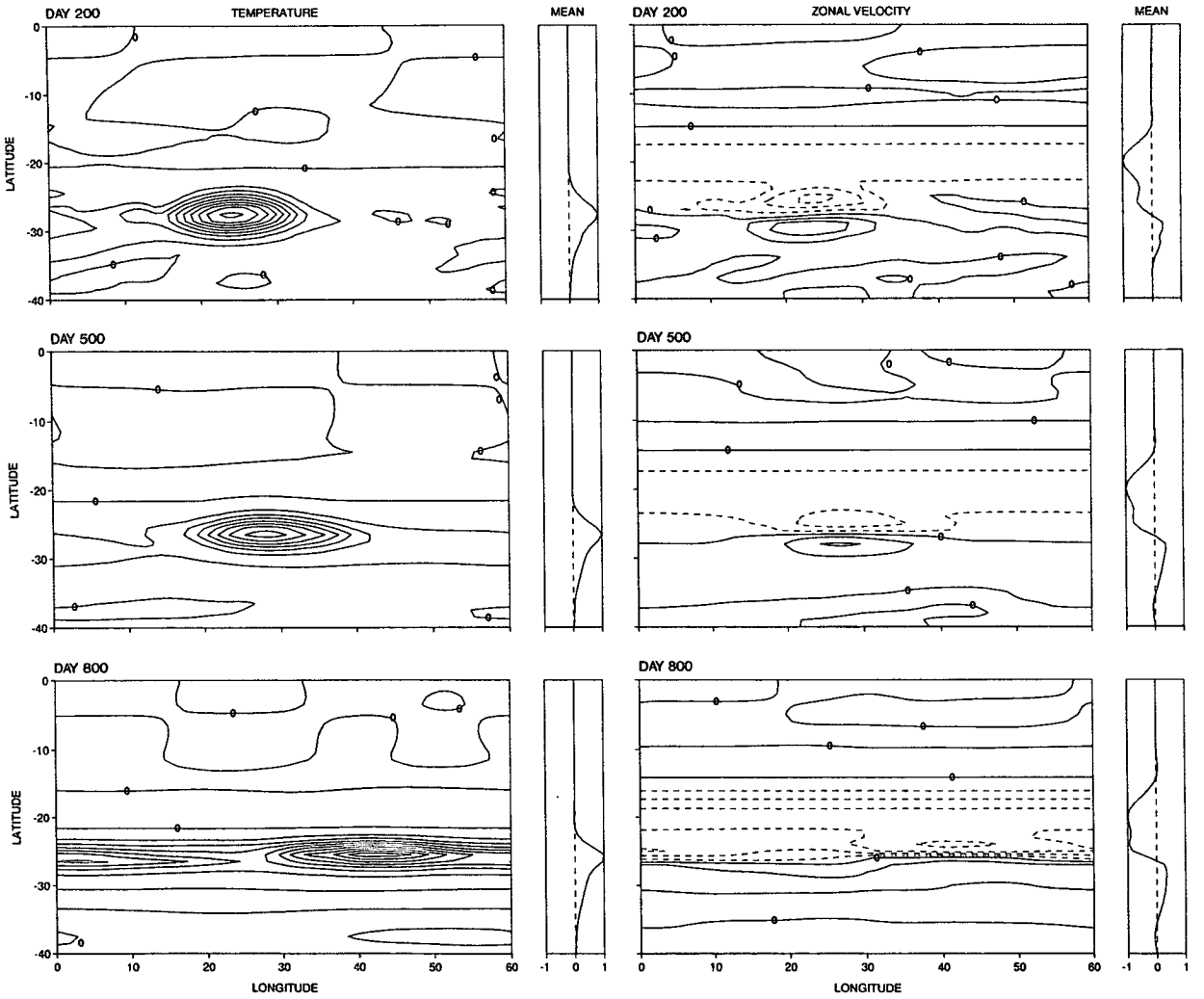

FIG. 13. Low-latitude solution L3, effect of a barotropic easterly jet on the stability of a large P_1 anticyclone. For Jovian $P_1(N20)$ parameters and a geostrophic Gaussian vortex bordered by a barotropic sinusoidal easterly jet, $E_1 = -20$ m s^{-1}, over $\phi = -16°$ to $-24°$, as in Table 2. Contour intervals and scales all at $Z = 8$ km. Day 200 and 500: (a) $\Delta T = 0.2$ K, $T^* = 0.52 - 0.56$ K; (b) $\Delta u = 10$ m s^{-1}, $u^* = 19.5 - 17.7$ m s^{-1}. Day 800: (c) $\Delta T = 0.1$ K, $T^* = 0.59$ K; (d) $\Delta u = 5$ m s^{-1}, $u^* = 16.7$ m s^{-1}.

clinic modal structure. The thickness factor for the active layer h/H now drops to about $^{25}/_{600}$ or $^{1}/_{24}$, a measure of the small value needed for absolute stability. Furthermore, the Brunt–Väisälä stability field $B(\phi, z)$ indicates that the storm's negative B_v contribution aloft matches the hydrostatic B_s component to the extent that convection will occur if the vortex is made stronger. The form of the first baroclinic mode, with $T_z < 0$ near the top, limits vortex strength, but the simpler $e^{Nz'}$ profile used later does not. Nevertheless, with scales of $U = 30$ m s^{-1}, $T = 6$ K, $B = 1.7 \times 10^{-4}$ s^{-2}, and $c = -2$ m s^{-1}, the vortex is relevant.

The orderly evolution is summarized by a histogram that displays the much sought after flat latitudinal track that signifies zero migration (Fig. 19). Of course, migration may still be occurring on a time-scale exceeding 1000 days, but for present purposes the P_3 vortices are deemed to be absolutely stable within the computational limits set by the resolution and dissipation. The gridpoint arrangement, $\Delta z \sim e^{5z'}$ in Fig. 20, guarantees accuracy in the vertical by providing a close spacing near the top, where the temperature eigenmode drops rapidly, and an adequate spacing in the abyss. The vertical resolution is never a major issue, even for the thin P_3 system, and the $e^{5z'}$ spacing is used for most of the remaining calculations in Parts I and II.

The vertical grid arrangement does, however, affect the sampling of the flow and can be a factor in trying to compare the solutions with observations. This leads us next to devise an alternative structure that is less sensitive.

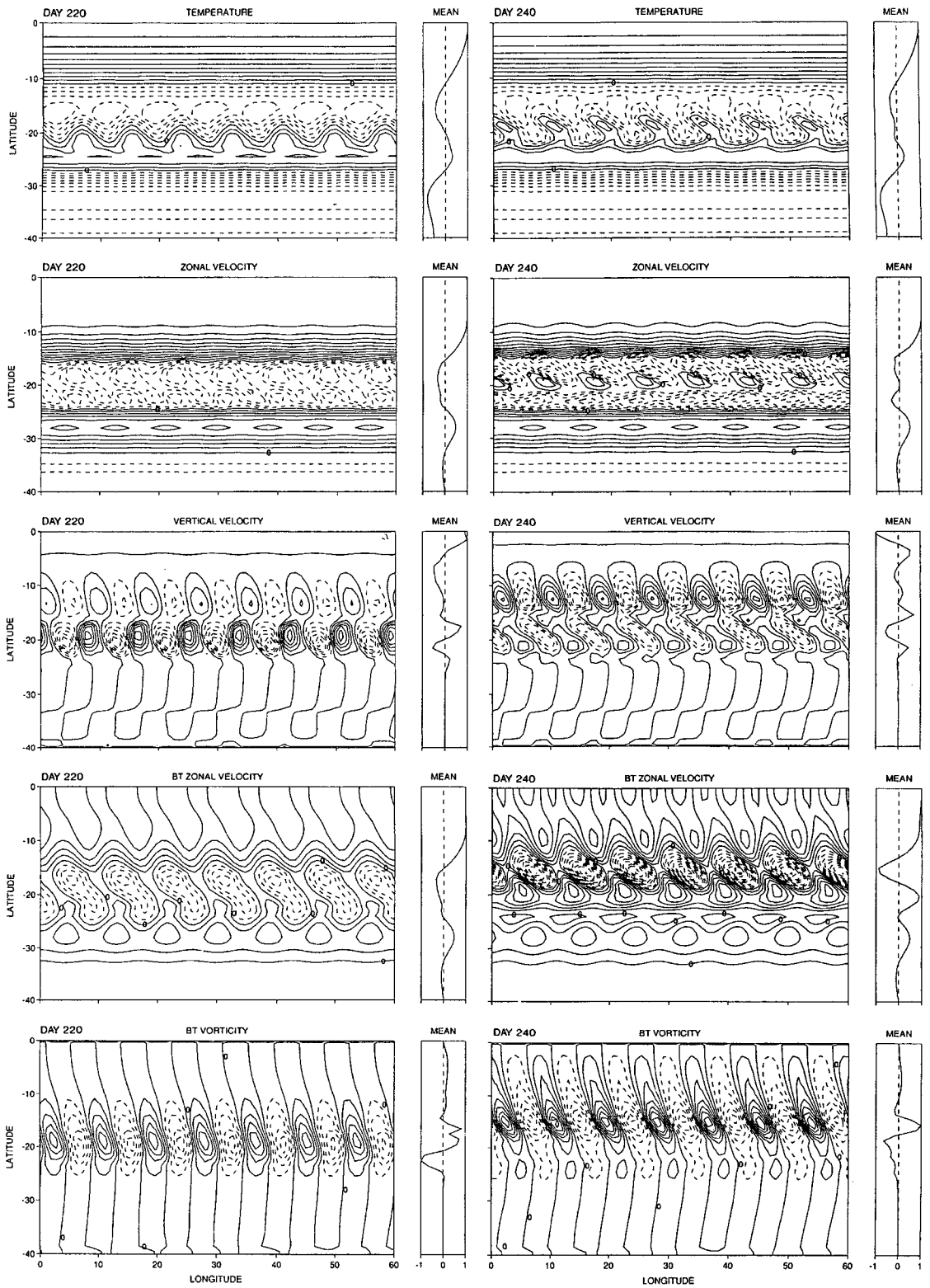

FIG. 14. Low-latitude solution L4, baroclinic instability of a P_1 easterly jet. For Jovian $P_1(N20)$ parameters and geostrophic sinusoidal jet streams, as in Table 2. Contour intervals and scales: (a) $\Delta T = 0.2$ K, $T^* = 1.9$ K, $Z = 8$ km; (b) $\Delta u = 5$ m s^{-1}, $u^* = 52$ m s^{-1}, $Z = 8$ km; (c) $\Delta w = 0.2$ cm s^{-1}, $w^* = 0.15 - 0.19$ cm s^{-1}, $Z = 11$ km; (d) $\Delta u_{BT} = 1$ m s^{-1}, $u^*_{BT} = 4.2$ m s^{-1}; (e) $\Delta\zeta_{BT} = 10^{-11}$ s^{-1}, $\zeta^*_{BT} = (0.06 - 0.22)\ 10^{-11}$ s^{-1}.

d. Alternative linear-z structures

The pressure eigenmode in Fig. 20 indicates that velocities are almost linear in z over the upper layer for exponential systems with $N \geqslant 90$. This leads us to develop an alternative structure where some fields are initialized with simple linear-z forms over a confined upper layer, $|z| \leqslant h_c$, and with zero or constant values below. We refer to this setup as the LIN system and to its being in the L_3 regime when layers remain as thin as those in the associated P_3 regime, now also designated as the EXP system for comparative purposes. Because it may easily be improved upon, the LIN system should not be thought of as an approximation to the EXP system, but rather as an *alternative* form with some similar characteristics—it favors stable vortices—and some useful dissimilar characteristics; for example, it allows westerly and easterly jet instability, whereas the EXP system only allows easterly instability.

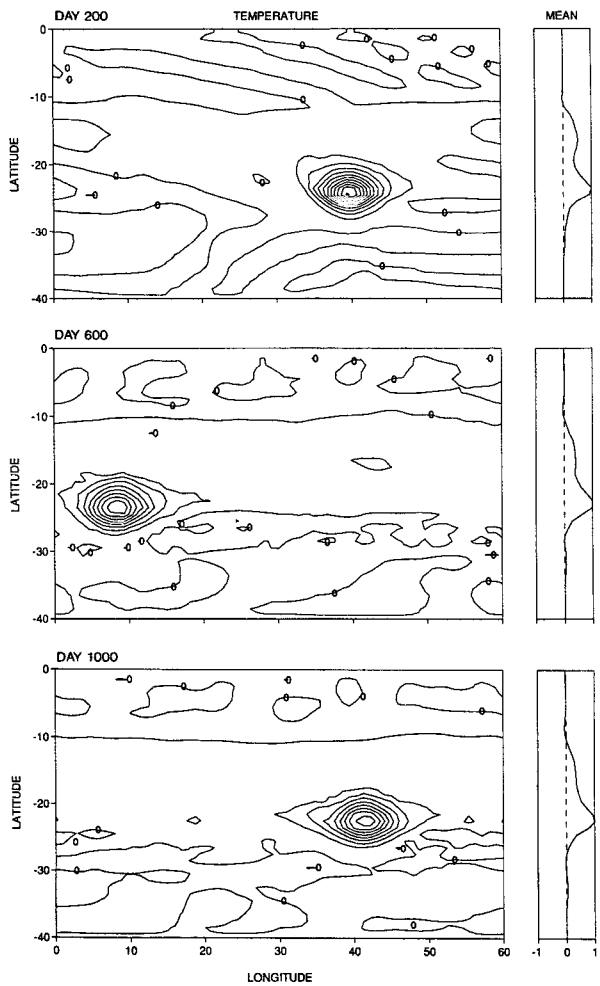

FIG. 15. Low-latitude solution L5, quasi-stability of a large P_2 anticyclone. For Jovian $P_2(N60)$ parameters and a geostrophic Gaussian vortex, as in Table 2. Properties: $c = -3.0$ m s^{-1}, $U = 35$ m s^{-1}, $T = 4.3$ K, $B = 1.2 \times 10^{-4}$ s^{-2}. Contours: $\Delta T = 0.5$ K; $T^* = 0.69, 0.79, 0.90$ K; $Z = 1.9$ km.

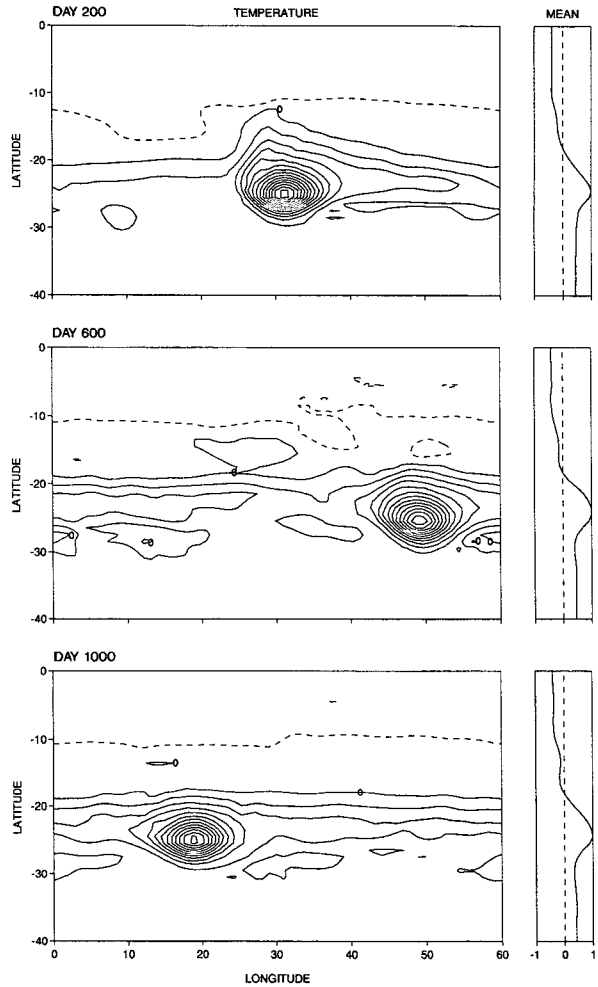

FIG. 16. Low-latitude solution L6, effect of a weak easterly jet on the stability of a large P_2 anticyclone. For Jovian $P_2(N60)$ parameters and a geostrophic Gaussian vortex bordered by a sinusoidal easterly jet, $E_1 = -5$ m s^{-1}, over $\phi = -15°$ to $-25°$, as in Table 2. Properties: $c = -3.2$ m s^{-1}, $U = 38$ m s^{-1}. Contours: $\Delta T = 0.5$ K, $T^* = 1.6 - 1.7$ K, $Z = 3.6$ km.

It is not obvious which items should be represented by the linear-z functions, but the two main options[6] are (a) LIN (v, B_s), with linear velocities and static stability, and (b) LIN(B_v, B_s), with linear stability for the vortex, jet, and static components. Both systems allow stable vortices but option (a) gives lower phase speeds. On the other hand, option (b) provides a better approximation to the EXP form but as such fails to pro-

[6] A third option with linear T_s (constant B_s) aloft is possible but does not allow stable vortices.

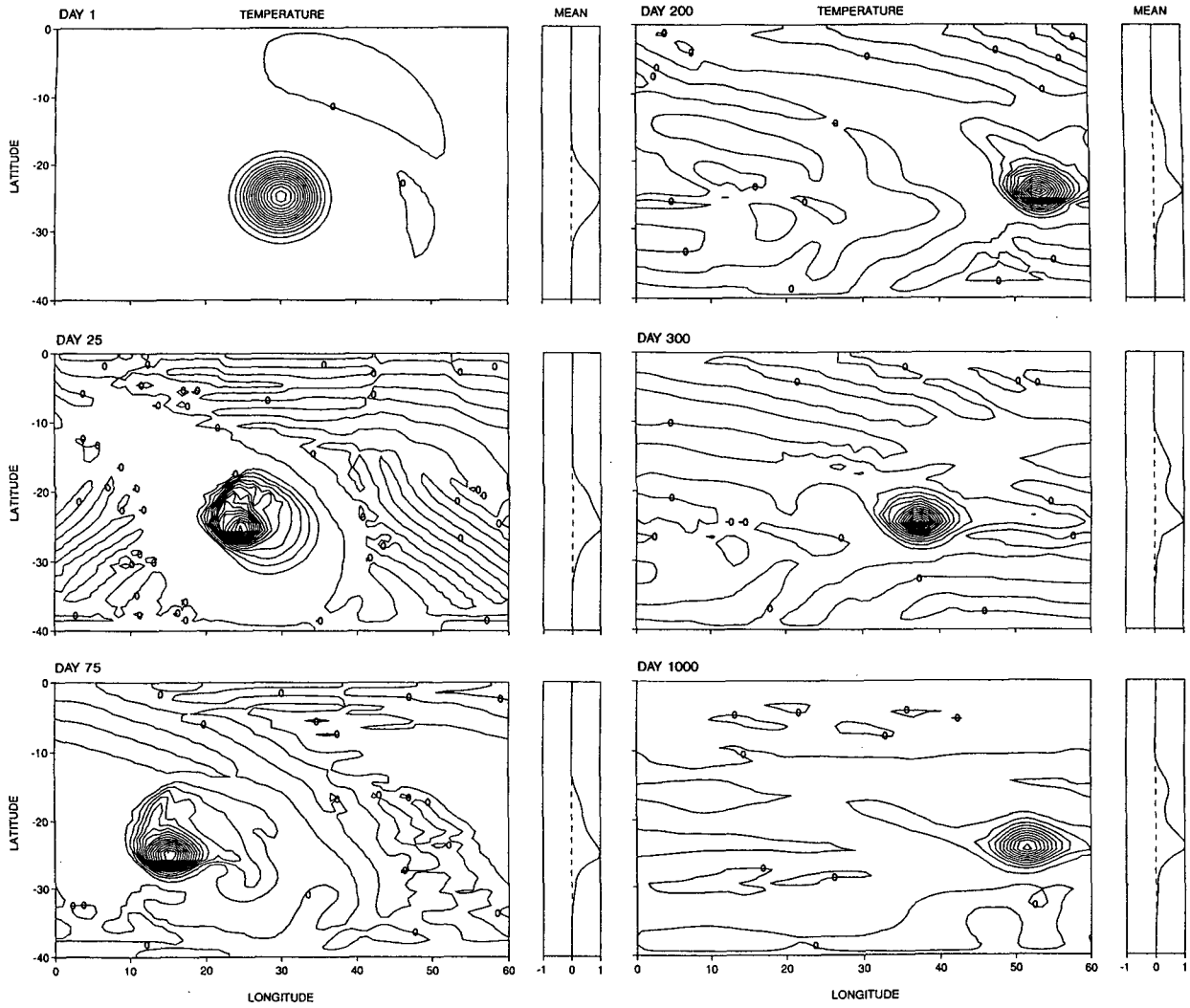

FIG. 17. Low-latitude solution L7, absolute stability of a large P_3 anticyclone. For Jovian $P_3(N90)$ parameters and a geostrophic Gaussian vortex, as in Table 2. Properties: $c = -2.0$ m s^{-1}, $U = 25$ m s^{-1}, $T = 6$ K. Contours: $\Delta T = 0.5$ K, $T^* = 0.9 - 1.1$ K, $Z = 3.6$ km.

vide a real alternative.[7] So we select the LIN($\mathbf{v}$, B_s) option, which requires that T_s vary quadratically aloft and that T_v and T_J be constant aloft, thus forming a sharp interface with the abyss. The physical significance of this difference between the T_v and T_s forms is unclear, as is the process by which such distributions could be created in an atmosphere.

The LIN structure is implemented with a split vertical grid, denoted as $\Delta z = [\Delta z_1, \Delta z_2] = [0.05, 0.95]$ $2H/K$, where half the K grid points have the thin Δz_1 spacing and half have the thick Δz_2. The upper grid thus resolves a layer of depth $H/20$. The initial fields are defined by the split functions $T_s \sim C[z_c^2, 0]$, $T_v \sim C[1, 0]$, and $U_J \sim C[z_c, 0]$ in the upper and lower regions, where $z_c = 1 - |z|/h_c$ for $|z| \leq h_c$. The motions extend over the first 6–8 grid points when $K = 20$, so they always lie within the high resolution layer and create no computational problems at the Δz_1:Δz_2 interface.

e. *Anticyclone in the linear L_3 system*

We now introduce the LIN($\mathbf{v}$, B_s) structure into our calculations and also make the fluid deeper, setting $H = 1200$ km, so as to get more flow for less baroclinicity. Furthermore, we stay with elliptic vortex shapes to reduce the horizontal adjustment and place them at $\phi = -23°$ as they no longer migrate. Selecting a linear-z velocity profile also means that the vortex no longer has an initial eigenmodal structure. Calculations with this setup confirm that stable vortices can exist indefinitely in the LIN system provided that the thickness

[7] Option (b) requires that T_s vary quadratically, and v cubically.

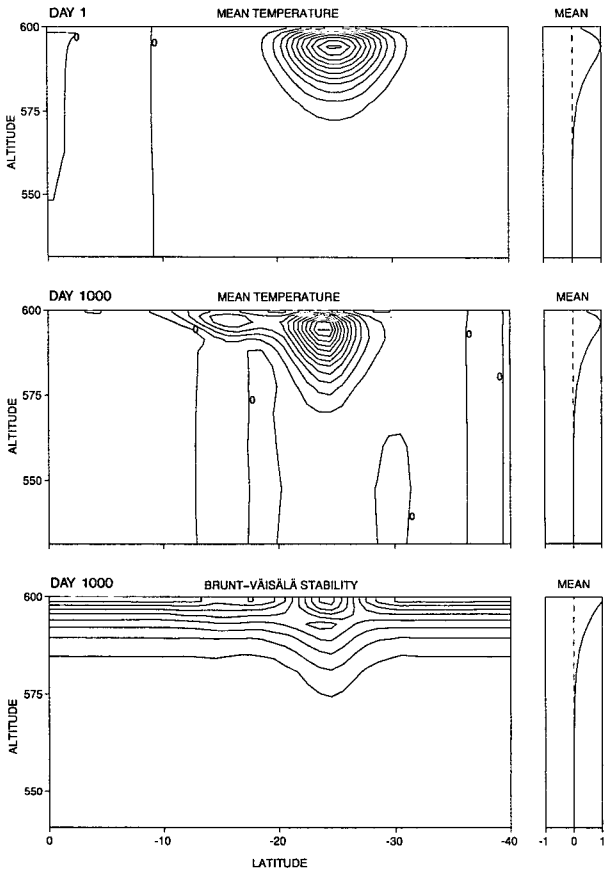

FIG. 18. Vertical sections for the low-latitude solution L7, sampled at the start and finish and, for $B(\phi, z)$, at the longitude of the vortex center. For an upper-level subdomain. Contours: (a) $\Delta T = 0.1$ K, $T^* = 0.19, 0.21$ K; (b) $\Delta B = 0.2 \times 10^{-4}$ s^{-2}, $B^* = 1.4 \times 10^{-4}$ s^{-2}, $\lambda = 52°$.

factor remains low. The solution L8, in Fig. 21, is typical of large vortices in the L_3 regime and has a thickness factor $h/H = {}^{50}/_{1200}$, equaling that of L7 in the P_3 regime.

The evolution of the L8 vortex differs from its EXP counterpart because it must adjust both horizontally and vertically in the first 100 days (Fig. 21). It adjusts horizontally by forming a smaller core and creating a frontal layer that breaks off to produce a weak storm. This new disturbance is eventually absorbed so that, unlike the L7 case, there is no residual background temperature field. The L8 vortex propagates 428° westward at a rapid -6 m s^{-1} rate that may be large because $c(L_R)$ depends on the vertical integral of a bulkier $B(z)$ distribution.

The vertical adjustment mainly involves the vortex relaxing its interface until the temperature takes on a smoother profile and the velocity softens its cutoff (as for the L9 vortex in Fig. 23). Both the temperature and the velocity remain unaltered aloft, so the vortex does not revert to the first baroclinic eigenmode. Nevertheless, being a longwave phenomenon, it may be adjusting toward some normal mode structure. Jets, on the other hand, are not wave related and do not relax vertically but instead maintain their steep thermal interface and linear velocity. Furthermore, as we shall see in section 8, the LIN jets tend to generate vortices of eigenmodal baroclinic form, while the EXP jets generate vortices of exponential form.

f. Vortex and jet coexistence in the L_3 system

Given that absolutely stable vortices can exist in a resting fluid, we now show that they can also coexist with jet streams. Having increased the depth to 1200 km for all remaining calculations, we try to realize flows with realistic scales $U \sim 80$ m s^{-1}, $T \sim 6$ K, and $c \sim -5$ m s^{-1}. But given the limitations of the model, scales such as $U \sim 50$ m s^{-1}, $T \sim 20$ K, and $c \sim -10$ m s^{-1} are deemed acceptable. The LIN system is considered first.

The mutual adjustment—horizontal and vertical—of the vortex and jets toward a stable coexistence in

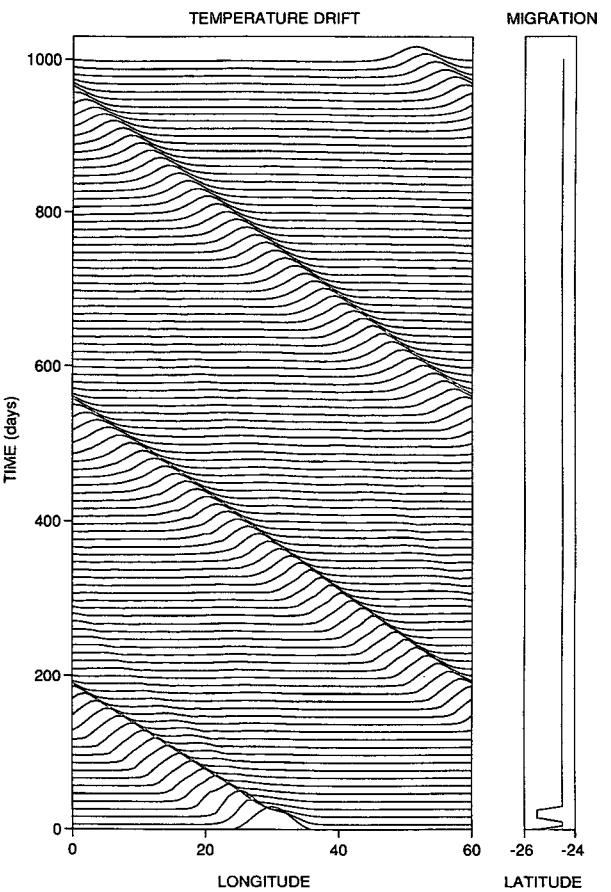

FIG. 19. Time sections for the low-latitude solution L7. Temperature is sampled at the latitude, shown on the right-hand side, where the vortex maximum occurs. Scale: maximum $T = 7.9$ K $\equiv 3\times$ vertical increment.

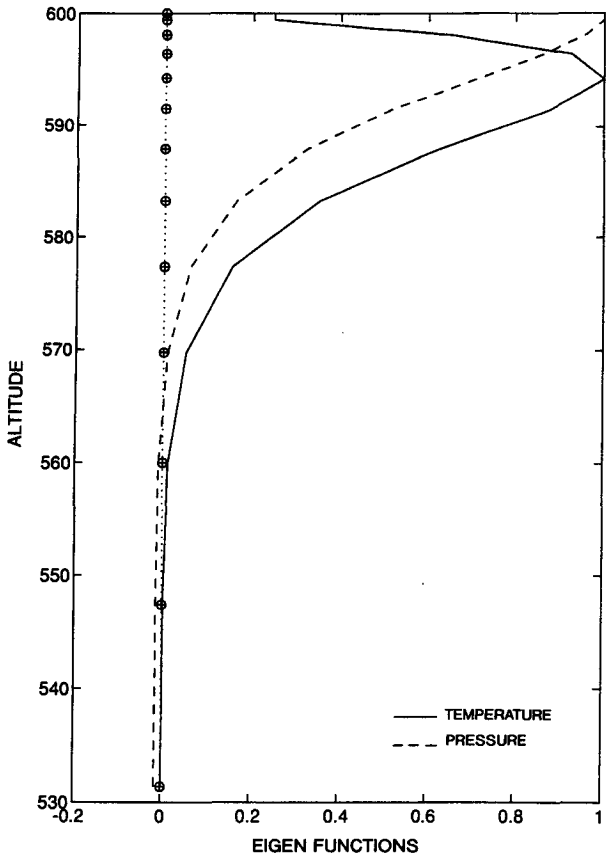

FIG. 20. Structure of the first baroclinic eigenvectors for the low-latitude solution L7 in the $P_3(N90)$ system, for an upper-level subdomain. Crosses mark the gridpoint distribution for the $\Delta z \sim e^{5z'}$ spacing.

the L_3 regime is exemplified by the case L9 in Figs. 22 and 23. The vortex becomes smaller and rounder but remains strong and stable, with its peak temperature dropping from 10 K to 9 K, and its peak velocity remaining near 60 m s^{-1}. Barotropic zonal flows with a 5 m s^{-1} amplitude are generated but do not form systematic currents. Over 1000 days the anticyclone propagates 794° westward at a rather rapid speed of -10.6 m s^{-1}.

During the adjustment phase, between 100 and 120 days, the vortex gets a boost from instabilities centered at $\phi = -12°$ and $-30°$. But repeating the calculation without a vortex shows that the jets are basically stable. Thus, the instabilities are local and produced by the combined vortex and jet flows. The instabilities also cause the easterly jet to weaken gradually from -40 m s^{-1} to -32 m s^{-1} by 300 days, then to drop down and equilibrate at -20 m s^{-1} by 600 days.

Vertically, the vortex relaxes its thermal interface by 100 days (Fig. 23). The jets, however, maintain their thermal interface and linear velocities indefinitely. The undulating form of the stability $B(\phi, z)$ section suggests that the anticyclone lies in a warm potential well and reveals just how vertically nonlinear the system is—and has to be for vortex formation—when the local stability variations match the background component.

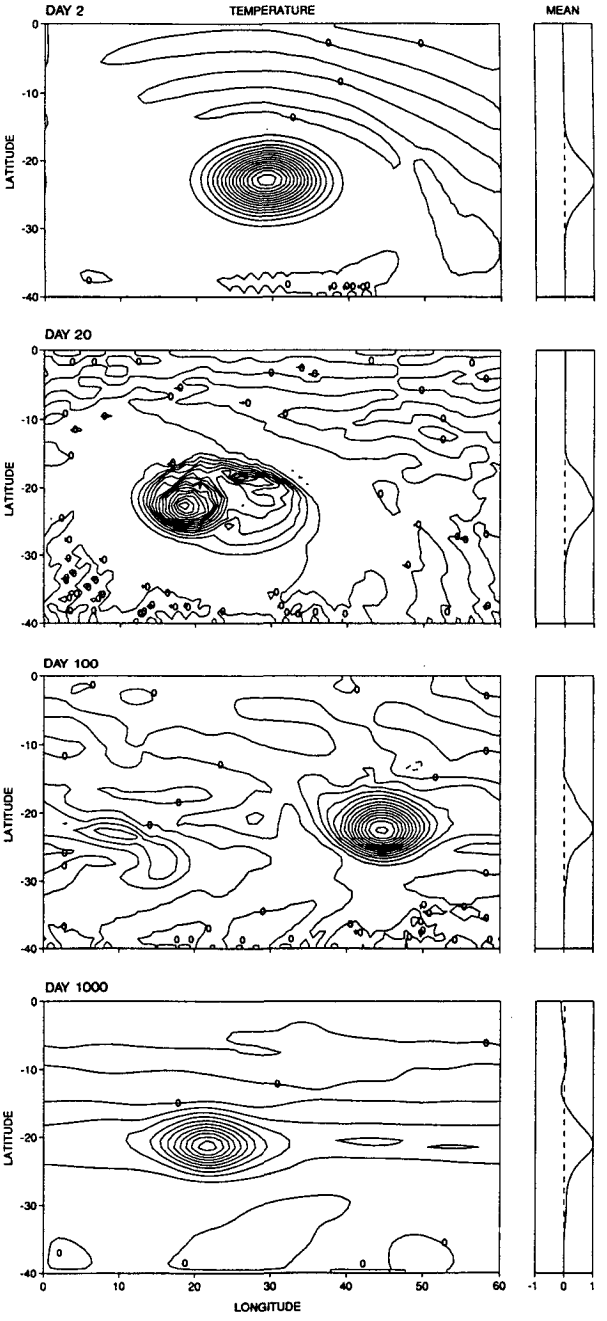

FIG. 21. Low-latitude solution L8, absolute stability of a large LIN anticyclone in the confined linear v, B_s system. For Jovian $L_3(H/h = 24)$ parameters and a geostrophic Gaussian vortex, as in Table 2. Properties: $c = -5.7$ m s^{-1}, $U = 38$ m s^{-1}, $T = 4.3$ K, $B = 0.9 \times 10^{-4}$ s^{-2}. Contours: $\Delta T = 0.5$ K, $T^* = 1.4 - 1.6$ K, $Z = 9$ km.

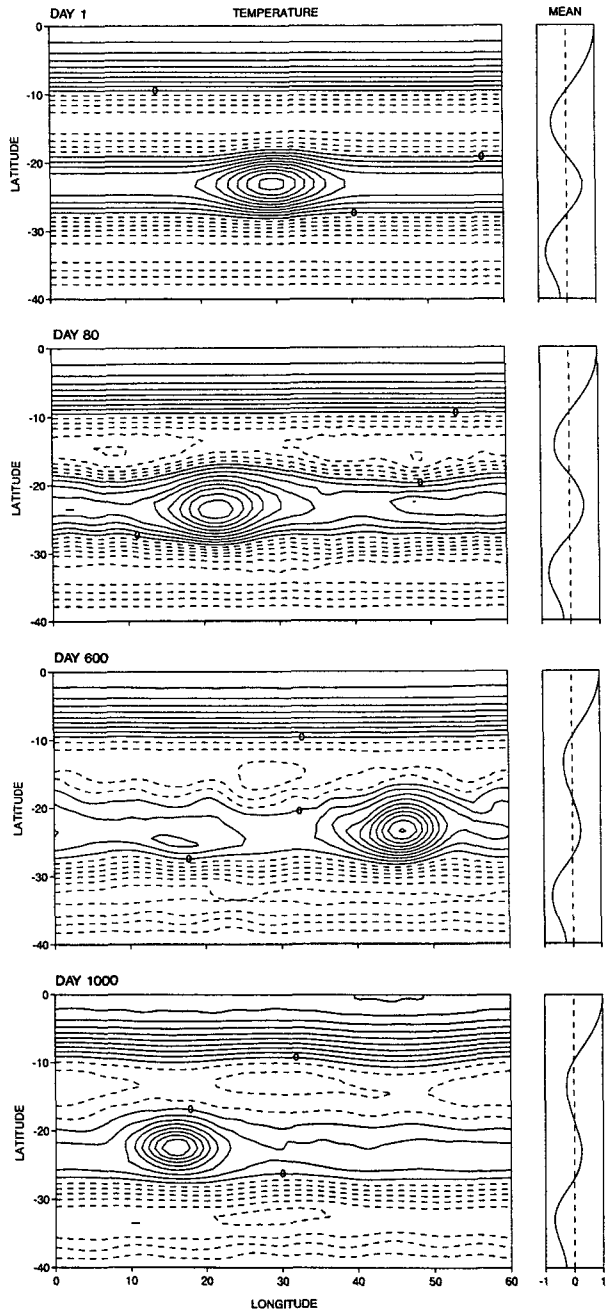

FIG. 22. Low-latitude solution L9, coexistence of a large LIN anticyclone and alternating jet streams in the confined linear **v**, B_s system, for Jovian $L_3(H/h = 24)$ parameters and a geostrophic Gaussian vortex embedded in geostrophic sinusoidal jet streams, as in Table 2. Properties: $c = -10.6$ m s^{-1}, $T = 8.8$ K, $B = 1.7 \times 10^{-4}$ s^{-2}. Contours: $\Delta T = 1$ K, $T^* = 8.5 - 8.7$ K, $Z = 9$ km.

g. Vortex and jet coexistence in the P_3 system

Naturally, if vortices and jets can coexist for the rough L_3 structure, they can do so much more cleanly in the smooth P_3 system, as the case L10 in Figs. 24 and 25 shows. This flow needs to adjust only in the horizontal and does so with little change in the vortex shape, size, or strength over 1030 days. This suggests that we may be approaching the optimal parametric conditions here.

The initial conditions differ slightly from earlier cases (see Table 2). In particular, the jets and vortices are given the same exponential structure as B_s, rather than an eigenmodal form, and the system is made even thinner by setting $N = 180$, so the thickness factor $h/H = {}^{30}/_{1200} = {}^{1}/_{40}$ reaches a new low. In addition, the easterlies are given a slower exponential rate than the other fields, $E_1 = -30\, e^{Nz'/1.5}$ and $E_2 = -12\, e^{Nz'/2}$, so that they can remain stable for larger amplitudes. In the solution, the E_1 jet drops from -30 m s^{-1} to -20 m s^{-1}, while the E_2 jet goes from -12 m s^{-1} to -8 m s^{-1} after the instability at 550 days (Fig. 24). Coexistence does not depend on these rate variants, which are not used in the EXP cases with weaker easterlies nor in any LIN cases, but they do allow greater control and do represent a feasible state.

The jets and vortex retain their original structures throughout, and the vortex, in particular, does not revert to the first baroclinic form (Fig. 25). Because of its exponential form, the temperature reaches much higher values aloft than its LIN counterpart in L9, but the vertically averaged temperature remains similar and leads to a similar phase speed, with the vortex propagating 755° westward at $c = -10$ m s^{-1}. The vortex velocities reach relevant (66 and -54 m s^{-1}) values near the top surface but are very sensitive to the choice of sampling height.

The stability field $B(\phi, z)$ in Fig. 25 almost disappears in the highest latitudes, and convective adjustment is very active there. This situation occurs when the static temperature T_s is not strong enough to match the negative temperatures associated with the jets when the $\langle T_J \rangle$ constraint is imposed. This problem is typical of atmospheric or oceanic layers that are cooled aloft in high latitudes and is discussed further in Part II. The T_s amplitude cannot be increased arbitrarily because that leads to unrealistic phase speeds. For our calculations we try to maintain the smallest T_s consistent with vortex coherence and with convective stability.

8. Genesis of thin vortices

Having shown that thin anticyclones can exist with absolute stability in a resting fluid or within alternating jets, we can now proceed to examine the origin of such vortices. We know from quasigeostrophic linear theory (Gill et al. 1974) that easterly jets readily become baroclinically unstable for exponential systems. Numerical tests reveal that the periodic waves produced by such instabilities in the thicker $P_{1,2}$ regimes (cf. Fig. 14) give way to solitary wave vortices in the thinner P_3 regime as motions become more nonlinear in the vertical. This section describes the variety of paths that the generated vortices can take in the P_3 and L_3 regimes.

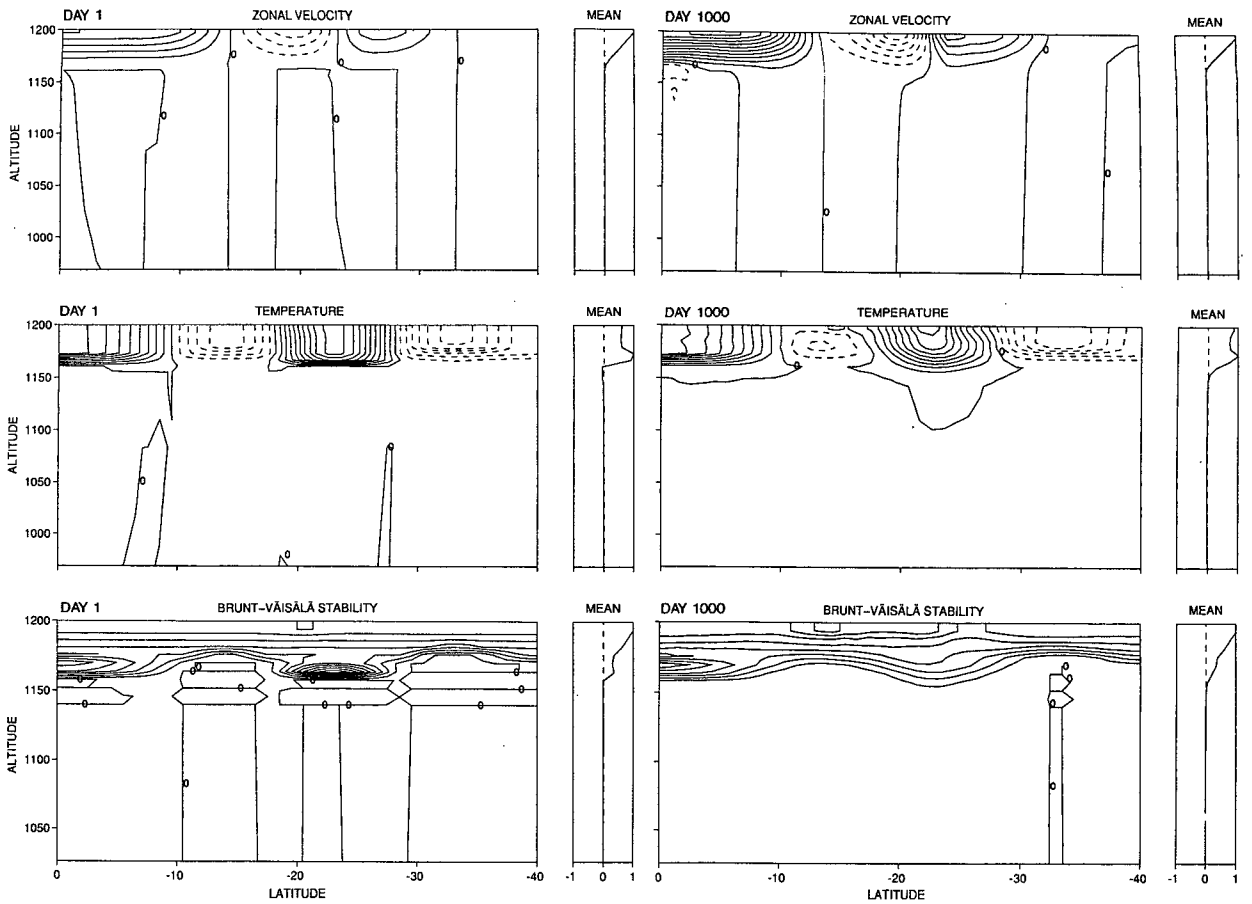

FIG. 23. Vertical sections for the low-latitude solution L9, sampled at the start and finish, and at the longitude of the vortex center. For an upper-level subdomain. Contour intervals and scales for Day 1 at $\lambda = 30°$: (a) $\Delta u = 20$ m s^{-1}, $u^* = 25$ m s^{-1}; (b) $\Delta T = 1$ K, $T^* = 1.7$ K; (c) $\Delta B = 0.2 \times 10^{-4}$ s^{-2}, $B^* = 1.3 \times 10^{-4}$ s^{-2} and Day 1000 at $\lambda = 16°$: (d) $\Delta u = 10$ m s^{-1}, $u^* = 26$ m s^{-1}; (e) $\Delta T = 1$ K, $T^* = 1.5$ K; (f) $\Delta B = 0.2 \times 10^{-4}$ s^{-2}, $B^* = 1.4 \times 10^{-4}$ s^{-2}.

We are particularly interested in determining the conditions that favor the formation of single and multiple vortex states and in defining how they evolve along various paths. To help understand the origin and uniqueness of Jupiter's Great Red Spot, we continue to confine our calculations to low latitudes and try to find the simplest, most general conditions under which single vortex states occur. The more general problem of the simultaneous formation of vortex families in the three anticyclonic zones centered near $\phi = -21°, -33°$, and $-41°$, relating to Jupiter's Ovals, is reserved for Part II.

From a variety of calculations, we find that while factors such as the strength of the easterly, the width of the anticyclonic zone, and the magnitude of the static stability determine the *initial* development, the *final* vortex state depends primarily on the interaction history. But, predicting exactly how an instability will evolve is difficult in these nonlinear regimes. The main tendency, however, is toward a final single vortex.

The following genesis examples, listed in Table 3, illustrate the range of vortex states and the paths that can occur. The first two cases, G1 and G2, give examples of a single vortex created ab initio; then cases G3–G6 give examples of a single vortex emerging after a series of mergers from various initial states, and finally, case G7 describes a possible two-vortex end state. We work with both the EXP ($N = 90–180$) and LIN structures, and try to achieve the realistic c, U, and T levels in most of the cases. Furthermore, the initial perturbation to the easterly jet is always localized so as to favor the emergence of a dominant vortex.

A major variant in the calculations is the longitudinal extent of the domain; it varies from 60° to 120° to 180°. The smaller domains are used to study smaller vortices, or larger vortices in greater detail, and to avoid plotting monotonous regions. The use of smaller domains, while extremely useful, also distorts some aspects of the flows, particularly the interaction history, and requires careful interpretation—hence the need for so-

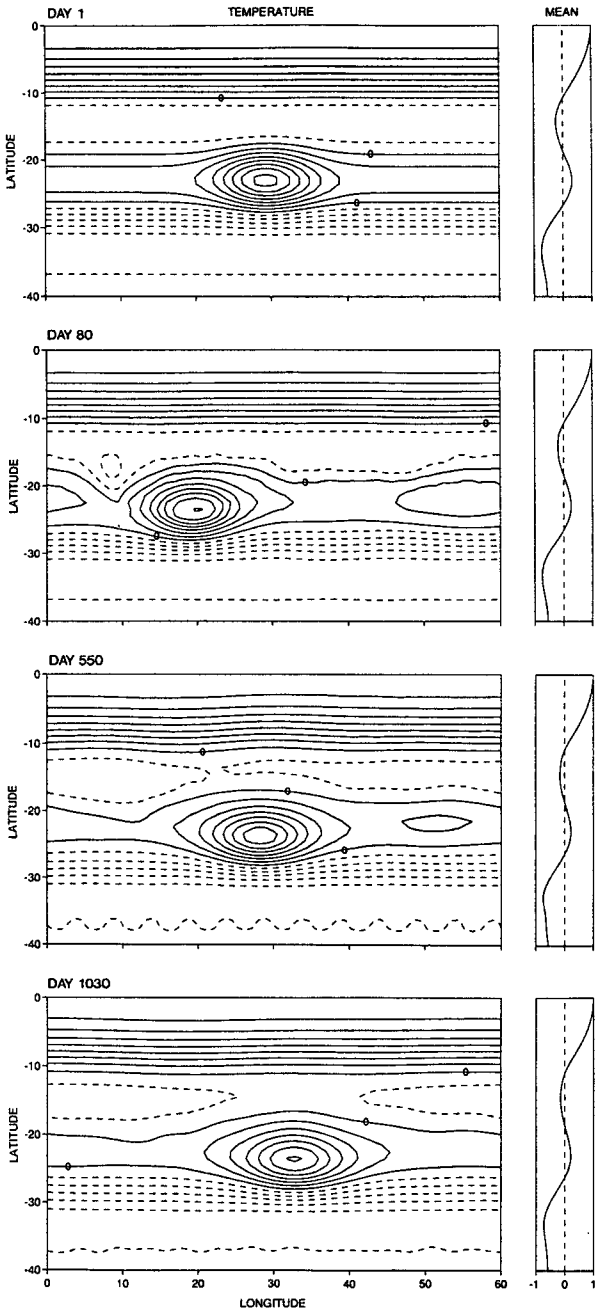

FIG. 24. Low-latitude solution L10, coexistence of a large P_3 anticyclone and alternating jet streams. For Jovian $P_3(N180)$ parameters and a geostrophic Gaussian vortex embedded in geostrophic sinusoidal jet streams, where the easterlies have modified structures, as in Table 2. Properties: $c = -10$ m s^{-1}, $T = 34$ K, $B = 10^{-3}$ s^{-2}. Contours: $\Delta T = 4$ K, $T^* = 31.7 - 31.2$ K, $Z = 3.8$ km.

lutions with a variety of domain sizes. Small domains, provided they remain representative, also help overcome the practical problem of mergers taking a long time in large domains. In drawing conclusions from small domains, a useful hypothesis to make and test involves that of "merger extrapolation." With it, for example, we may assume that if two vortices merge into one in a 120° domain, then six will merge into one in a 360° domain. We see some justification for the merger extrapolation hypothesis from the solutions in the general tendency for all vortices to merge into one.

Overall, vortex genesis in the PE model resembles that in the simpler SW model in that easterly shears provide the preferred source and a single dominant vortex remains the preferred end state (cf. Fig. 27 in WW88). Mergers, however, are more complex in the PE model and exhibit two possible modes: strong vortices can, in classic SW fashion, catch and absorb weaker ones ahead of them, or can, in unique fashion, reel in weaker ones from behind.

a. Single vortex ab initio in a 60° domain

The basic vortex formation process is shown close-up in Fig. 26. The G1 anticyclone develops from a very long wave that starts to grow at 200 days and reaches maturity at 350 days. At the start the leading edge forms

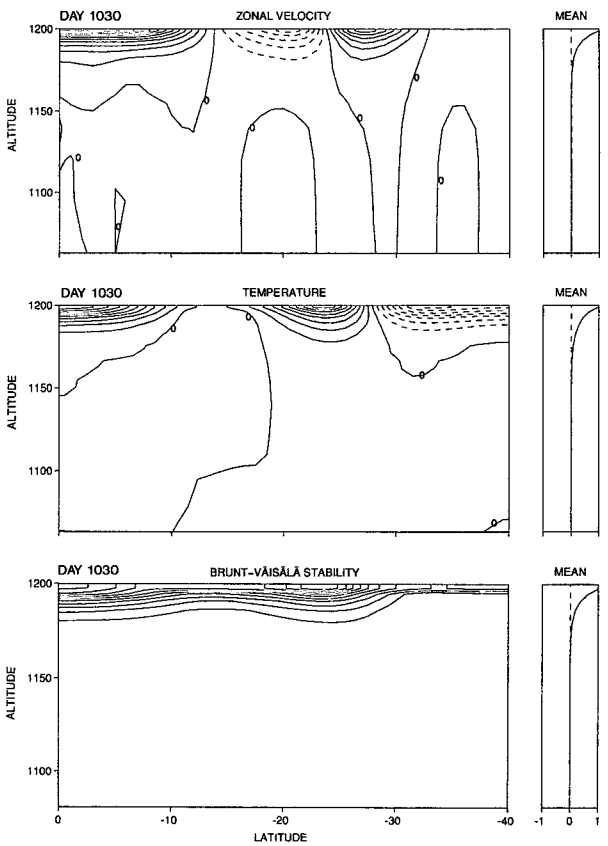

FIG. 25. Vertical sections for the low-latitude solution L10, sampled at the longitude of the vortex center. For an upper-level subdomain. Contours: (a) $\Delta u = 10$ m s^{-1}, $u^* = 26$ m s^{-1}; (b) $\Delta T = 4$ K, $T^* = 5.4$ K; (c) $\Delta B = 10^{-4}$ s^{-2}, $B^* = 7 \times 10^{-4}$ s^{-2}; all fields at $\lambda = 33°$.

TABLE 3. Vortex genesis cases in low latitudes. Constant parameter values are $H = 1200$ km, $\phi = -40$: 0°; resolution in (λ, ϕ, z) $R = 66 \times 42 \times 20$, except $R = 194 \times 42 \times 20$ for G7; $\Delta\phi = 1°$, $\Delta\lambda \sim 1°$, except $\Delta\lambda \sim 2°$ for G4 and $\Delta\lambda \sim 3°$ for G2, G5, and G6; $\Delta z \sim e^{5z'}$ for EXP cases, $\Delta z = [.05, .95]H/10$ for LIN cases; $\Delta t = (1/50)$ day, $\nu_4 = -10^{17}$ m^4 s^{-1}, $\nu_2 = 10^{-8}$ m^2 s^{-1}. Jet profiles are given by $\Phi_J = \Phi_9$, except $\Phi_J = \Phi_8$ for G3, where $\Phi_{8,9}$ are defined in Table 2. Easterly jets have slower exponential rates where marked (a) $e^{Nz'/1.3}$ and (b) $e^{Nz'/1.5}$. The superscript (e) indicates that the W_1 jet goes to zero at the equator in this special case.

Case	Domain length	Structure N or h_c (km)	Static stability $T_s - 1$	Jet amplitudes W_1	$+ E_1$	$+ W_2 + E_2$	Jet structure $U_J(z)$
G1 (LIN)	60°	$h_c = 40$	25 C [z_c^2, 0]	100	− 50	+ 30 − 15	C [z_c, 0]
G2 (LIN)	180°	$h_c = 40$	25 C [z_c^2, 0]	100	− 40	+ 30 − 15	C [z_c, 0]
G3	60°	$N = 180$	40 $e^{Nz'}$	50	− 30	+ 50 − 5	$e^{Nz'}$
G4 (LIN)	120°	$h_c = 40$	25 C [z_c^2, 0]	100$^{(e)}$	− 50	+ 30 − 15	C [z_c, 0]
G5	180°	$N = 90$	40 $e^{Nz'}$	100	− 60$^{(a)}$	+ 30 − 12$^{(b)}$	$e^{Nz'}$
G6	180°	$N = 90$	40 $e^{Nz'}$	100	− 60$^{(b)}$	+ 30 − 12$^{(b)}$	$e^{Nz'}$
G7	180°	$N = 180$	25 $e^{Nz'}$	50	− 20	+ 20 − 5	$e^{Nz'}$

a steep kink at $\phi = -20°$ in the warm isotherms associated with the easterlies of the anticyclonic zone. These isotherms close off by connecting with those at $\phi = -28°$, while the disturbance propagates westward and creates a secondary cold spot ahead at $\phi = -15°$. Once the leading edge has occluded, the anticyclone relaxes the sharp front and pulls up the rear to give a sech^2-like profile over 40° of longitude.

The mechanism by which the instability in the E_1 jet forms a three-dimensional frontal surface is not known but probably involves a KdV-related, nonlinear vertical steepening of the isotherms, as discussed in section 3b. Although the E_1 and W_2 jets are reduced by the flow along the north–south isotherms in the front, they remain zonally continuous but with the mean easterly flow dropping from −50 to −25 m s^{-1} over the 500 days. The anticyclonic zone remains centered at $\phi = -23°$ but the final vortex is centered at $\phi = -28°$ and has a strong latitudinal asymmetry resembling that seen in the very large SW vortices (cf Fig. 9 of WW88). In the vertical, the flow resembles that of the basic LIN case in Fig. 23 but with the vortex temperature peaking more toward the middle of the active layer like the first baroclinic eigenmode (cf Fig. 30).

The G1 solution is compromised by having such a large vortex in a small domain but is still meaningful as the self-interaction is not serious. Similar calculations with a larger domain indicate that the G1 solution gives a reasonable representation of the final vortex, although it does not tell us that in a larger domain no other vortex would occur.

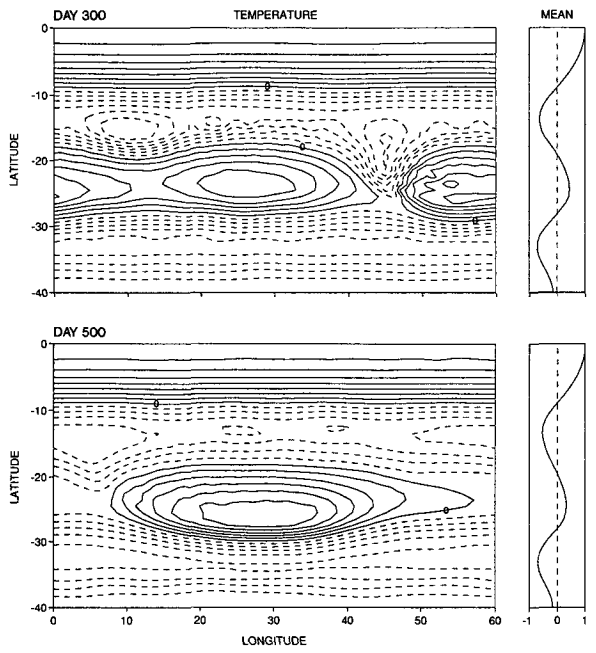

FIG. 26. Vortex genesis solution G1, generation of a single long-lived LIN anticyclone ab initio in a 60° domain from baroclinically unstable currents. For Jovian $L_3(H/h = 24)$ parameters and geostrophic sinusoidal jet streams, as in Table 3. Properties: $c = -11$ m s^{-1}, $T = 7$ K, $B = 1.9 \times 10^{-4}$ s^{-2}. Contours: $\Delta T = 1$ K, $T^* = 7.5$ K, $Z = 9$ km.

b. *Single vortex ab initio in a 180° domain*

A more realistic genesis requires that the domain be much larger than the vortex and this is so for case G2 in Fig. 27. The structure and parameters remain those of case G1 but with the easterly jet reduced to −40 m s^{-1} to minimize the instability and the energy available for vortex growth (Table 3). Consequently, the instability produces from the beginning a single, large, dominant vortex together with a lengthy complex tail that the vortex gradually assimilates. Presumably, a similar scenario would occur if the domain extended to a full 360°, with the single vortex possessing perhaps a longer tail.

Initially, the U_J and T_J fields remain geostrophically balanced and constant for 200 days, while the weak localized perturbation slowly grows. The vortex emerges over the 300–400-day period when the leading edge forms a closed front that continues to strengthen until 500 days (Fig. 27). At this stage, the anticyclone is trailed by three weak cores. The G2 vortex continues to grow and becomes dominant by absorbing the cores by reeling them in from behind, rather than catching and sweeping them up at the front in the classic SW way. By 1200 days,

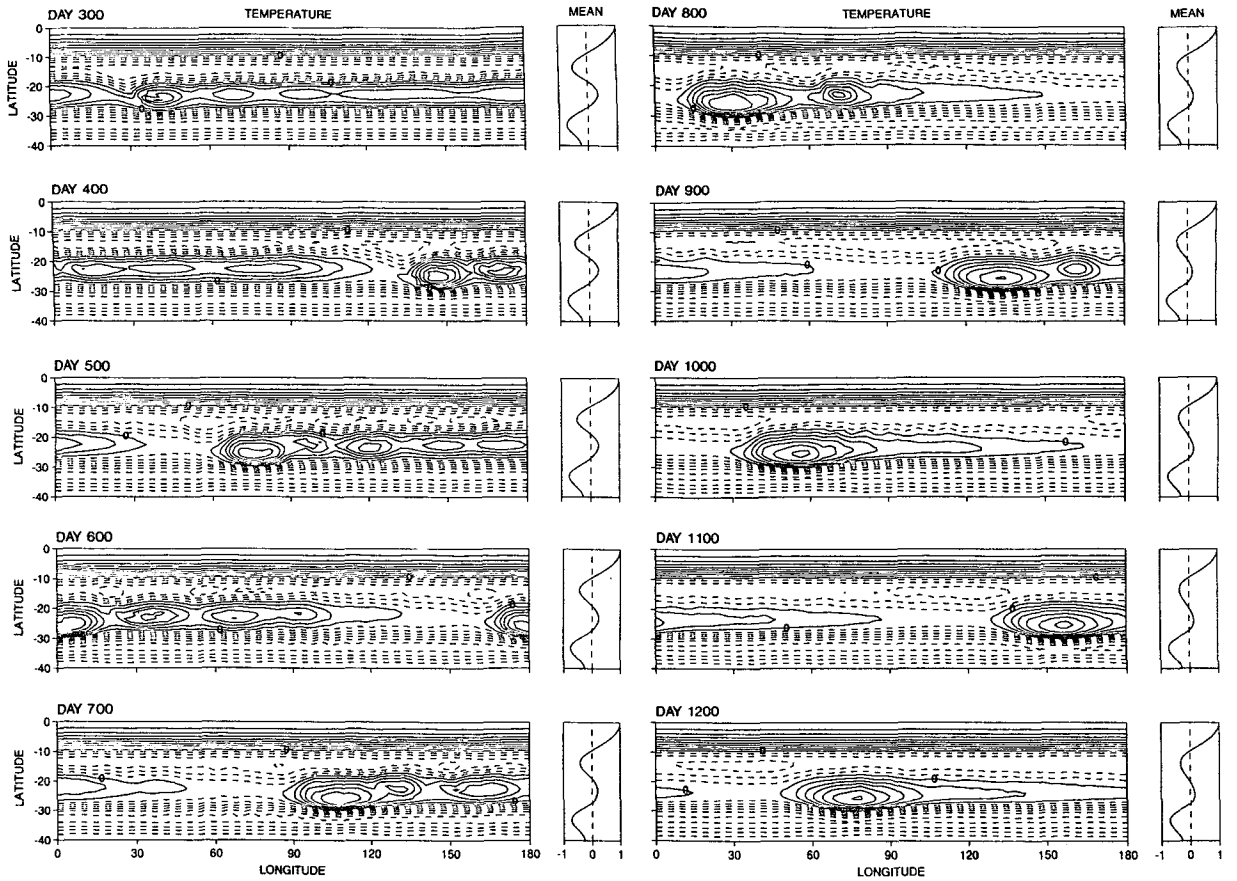

FIG. 27. Vortex genesis solution G2, generation of a single long-lived LIN anticyclone ab initio in a 180° domain from baroclinically unstable currents. For $L_3(H/h = 24)$ parameters and geostrophic sinusoidal jet streams, as in Table 3. Properties: $c = -10$ m s^{-1}, $T = 8.1$ K, $B = 1.8 \times 10^{-4}$ s^{-2}. Contours: $\Delta T = 1$ K, $T^* = 8.5 - 8.6$ K, $Z = 9$ km.

all cores have been absorbed and the vortex has relaxed to the standard sech^2-like profile in longitude, with the same 40° length as the G1 case. As in the other LIN cases, the vortex also relaxes in the vertical toward the first baroclinic eigenmode, with the temperature peaking in midlayer (cf. Fig. 30).

c. *Vortex genesis at the equator*

We now make a brief detour to present an example of the vortices that are sometimes generated at the equator, such as for case G3 in Fig. 28. These equatorial vortices display many of the characteristics of the analytical Rossby soliton discussed in section 3c, even though they are now embedded in strong equatorial jets. They occur more often in the EXP system than the LIN, but the general conditions for their genesis remain obscure.

Initially the unstable easterly generates four vortices that proceed to merge at 150, 300, and 400 days (Fig. 28). The final vortex almost fills the domain and is kept at $\phi = -23°$ by the strong W_2 jet. The u field shows that the waves generated by the vortices create localized disturbances at the equator, one of which contains a small westerly flow of 33 m s^{-1} at 200 days. Later, the larger waves create an equatorial vortex with the Hermitian soliton form seen earlier in Fig. 1: easterlies at the equator, with amplitudes of -30 and -15 m s^{-1} at 500 and 800 days, and westerlies at $\phi = -6°$.

d. *Single vortex by mergers for the LIN system in a 120° domain*

To assess the effect of parameters on genesis in the LIN systems, we consider case G4 in Figs. 29 and 30, which is equivalent to the G1 case with a larger domain and to the G2 case with a stronger easterly jet. The initial development is similar to G2 with a large vortex and three weak cores forming, but these all evolve further. Compared to G1, the same processes are at work at similar scales and produce a similar final vortex, but we also see that the G1 state is not periodic and that doubling the domain does not double the vortex number.

Initially, the instability produces a strong leading frontal vortex plus three weak trailing cores by 300–

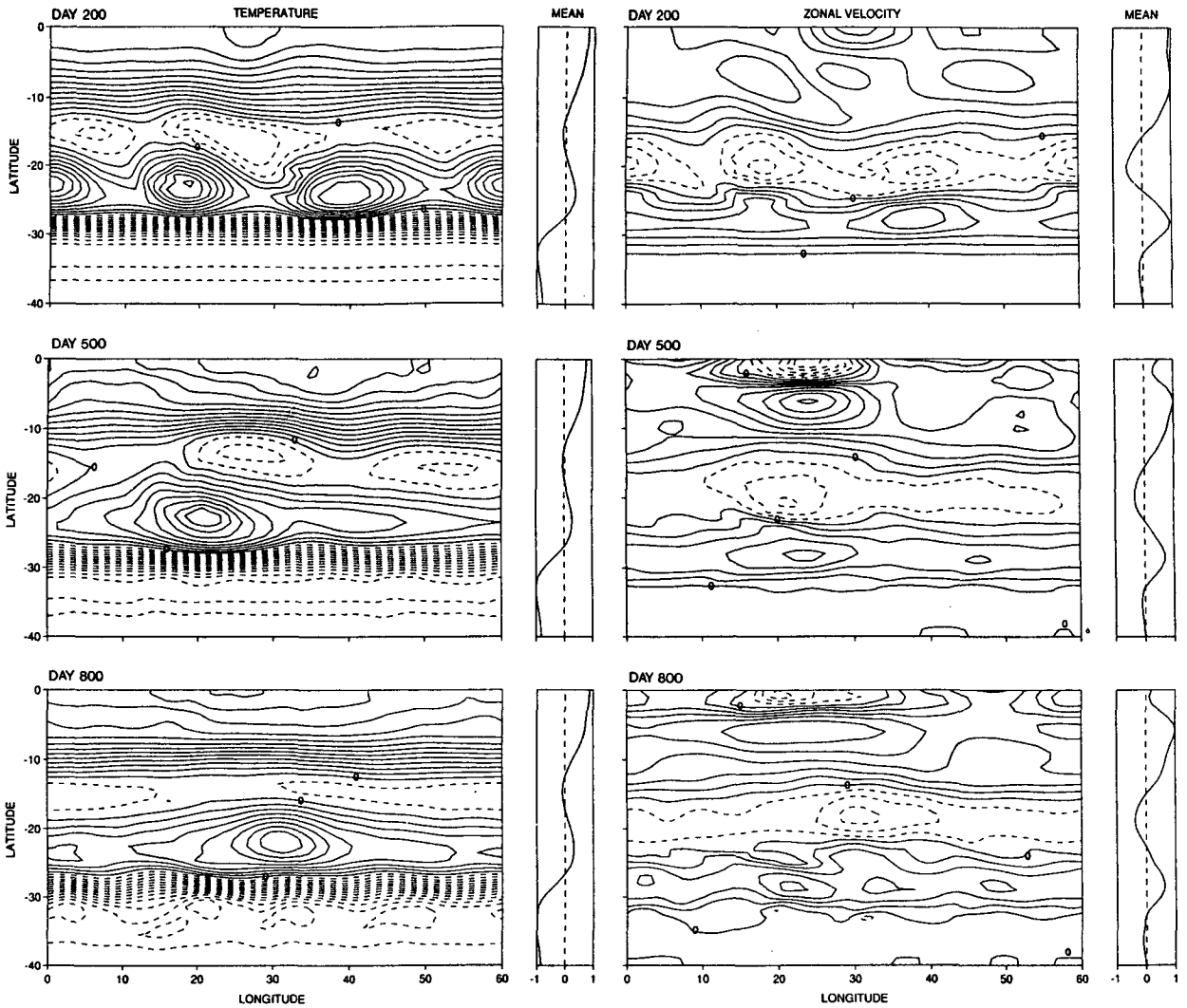

FIG. 28. Vortex genesis solution G3, generation of an equatorial anticyclone by the action of vortices produced in low latitudes by baroclinically unstable currents. For Jovian $P_3(N180)$ parameters and geostrophic sinusoidal jet streams, as in Table 3. Contours: (a) ΔT = 1 K, T^* = 13.6 − 12.8 K; (b) Δu = 5 m s^{-1}, u^* = 18, 21, 23 m s^{-1}. All fields at Z = 7.2 km.

350 days (Fig. 29). The lead vortex reels in the nearest core by 380 days, and the remaining cores then merge to form a second vortex over 400–500 days. Despite their proximity, the two vortices merge very slowly but they do so in the classic manner with the rear one rotating anticyclonically about the lead one to give a single 30° long anticyclone with relevant scales at 900 days. The instability reduces the easterly jet from −50 m s^{-1} to −19 m s^{-1}.

In the vertical, the final vortex adopts the first baroclinic eigenmodal form and the same depth as the jets (Fig. 30) unlike when the vortex is imposed as in Fig. 23. Not only does the vortex relax its own structure, it also forces the mean flow to relax in the vortex zone, though elsewhere the interface remains sharp. Consequently, the temperature peaks at the layer's midheight in the ϕ = −10° to −30° region.

One other change made in this calculation involves altering the latitudinal profile of the W_1 westerly jet so that it vanishes at the equator. This is done to see if the waves generated by the instability and by the vortices can drive an equatorial flow. Although a westerly flow of 24 m s^{-1} does develop, mostly during the first 200 days, other cases that selectively omit the vortices, instabilities, and computational diffusion show that this flow can be attributed to the ν_4 diffusion. To get a realistic 100 m s^{-1} equatorial current requires a real physical source, as we see in Part II.

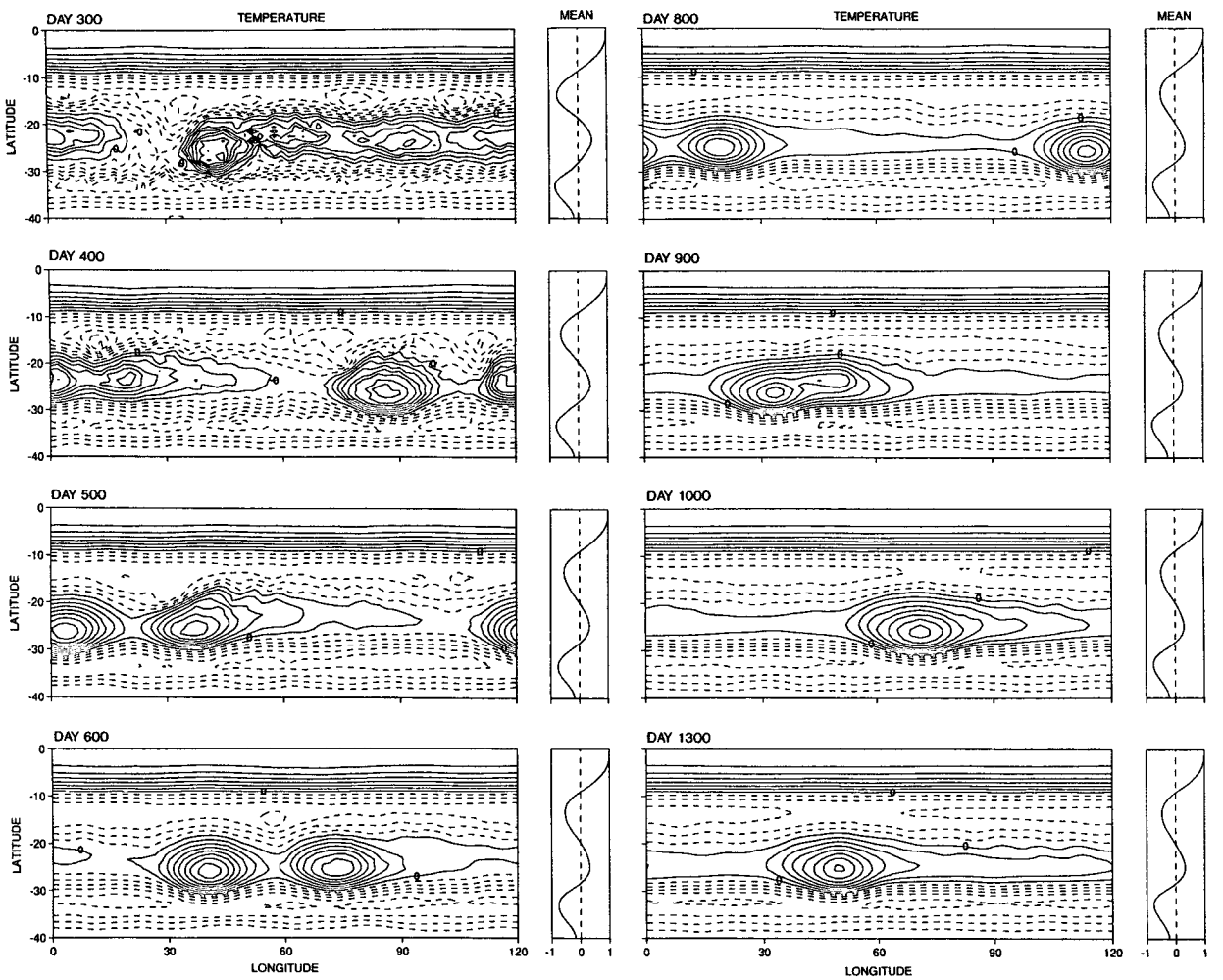

FIG. 29. Vortex genesis solution G4, generation of a single long-lived LIN anticyclone by mergers in a 120° domain. For Jovian $L_3(H/h = 24)$ parameters and geostrophic sinusoidal jet streams, as in Table 3. Properties: $c = -11$ m s^{-1}, $U = 62$ m s^{-1}, $T = 9$ K, $B = 1.9 \times 10^{-4}$ s^{-2}. Contours: $\Delta T = 1$ K, $T^* = 6.6$ K, $Z = 9$ km.

e. Single vortex by four mergers in a 180° domain

In this and the next section, two closely related EXP cases—G5 and G6—illustrate the variety of merger paths and the sensitivity of the vortex formation to the initial conditions in a realistic 180° domain (Table 3). While in the earlier cases the lead frontal vortex usually forms the nucleus of the final vortex, here in the G5 case the second vortex becomes the dominant one. Mergers of both types occur and proximity seems to be more important than strength or speed in determining which type prevails. The V and C labels in Fig. 31 are used to track storms from their origins as frontal vortices or trailing core disturbances.

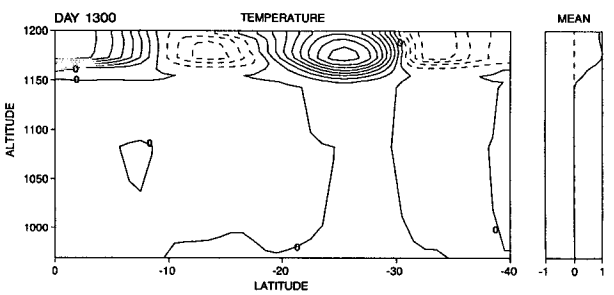

FIG. 30. Vertical section for the genesis solution G4, sampled at a longitude near the vortex center. Contours: $\Delta T = 1$ K, $T^* = 1.5$ K, $\lambda = 51°$.

Initially, two vortices, rather than the usual one, form out of the instability by 200 days (Fig. 31). They are trailed by three cores that grow into full vortices by 300 days, at which time the second vortex, V_2, starts to reel in the adjacent C_1 storm to become the strongest by 400 days. The V_2 storm catches the lead vortex V_1 at 500 days and absorbs it to become dominant by 600 days. Then the C_2 and C_3 storms, while being chased by the V_2 anticyclone, merge over 800–900 days to produce a stronger C_2

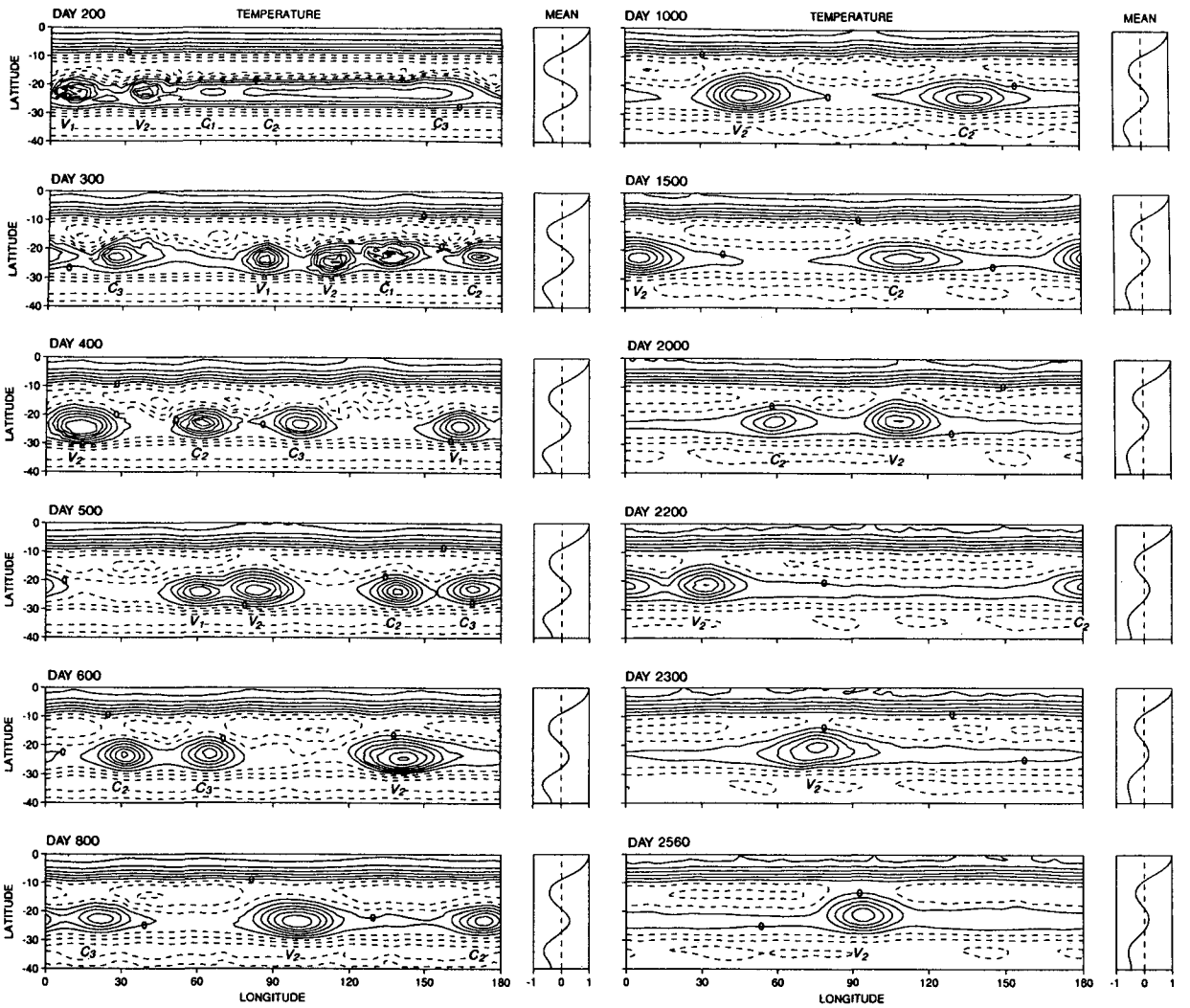

FIG. 31. Vortex genesis solution G5, generation of a single long-lived anticyclone by four mergers in a 180° domain. For Jovian $P_3(N90)$ parameters and geostrophic sinusoidal jet streams, as in Table 3. Labels $V_{1,2}$ and $C_{1,2,3}$ refer to the vortex and core origins. Properties: $c = -15$ m s^{-1}, $U = 45$ m s^{-1}, $T = 12$ K, $B = 4.7 \times 10^{-4}$ s^{-2}. Contours: $\Delta T = 2$ K, $T^* = 10.7 - 10.5$ K, $Z = 7.2$ km.

storm. By 1000 days, the resulting V_2 and C_2 storms have a similar size but a different strength. The stronger, faster V_2 storm then proceeds to close the 90° gap with C_2, making contact at 2150 days and merging fully by 2300 days. The final vortex in Fig. 31 is strong enough and centered at a low enough latitude, $\phi = -20°$, to disrupt the zonality of the equatorward cool zone and induce a secondary disturbance there. In the vertical, the vortex extends to a greater depth (50 km) than the jets but retains an exponential form with a slower rate.

f. Single vortex by three mergers in a 180° domain

If we repeat the previous case with just the exponential rate of the easterly jet reduced from $N/1.3$ to $N/1.5$ for the basic $P_3(N90)$ system, then the instability is substantially reduced and only generates two major vortices compared to the previous five (Table 3). This G6 case in Fig. 32 also shows how difficult it is to control and minimize the instability so as to get only a single vortex ab initio. Compared to G5, the G6 vortices take longer to develop from the stabler easterly jet but, being fewer in number, lead to a single vortex state more quickly, in 1500 days rather than 2500 days.

Initially, the long perturbation becomes more wavelike before becoming frontal and forming the lead vortex and the three trailing cores at 400 days (Fig. 32). The vortex V_1 then absorbs the adjacent core C_1 at 460 days, so that by 700 days it is trailed by an equally large C_2 vortex and by a distinct C_3

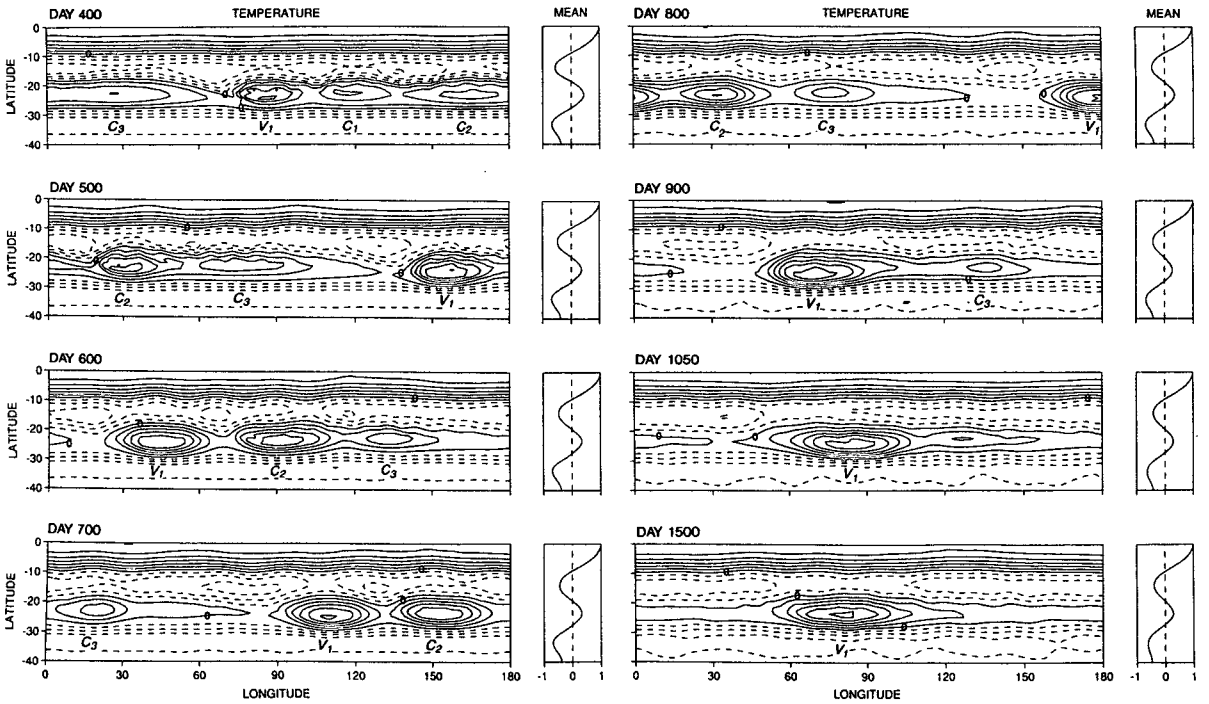

FIG. 32. Vortex genesis solution G6, generation of a single long-lived anticyclone by three mergers in a 180° domain. For Jovian $P_3(N90)$ parameters and geostrophic sinusoidal jet streams, as in Table 3. Labels V_1 and $C_{1,2,3}$ refer to the vortex and core origins. Properties: $c = -14$ m s^{-1}, $U = 50$ m s^{-1}, $T = 12.8$ K, $B = 4.3 \times 10^{-4}$ s^{-2}. Contours: $\Delta T = 2$ K, $T^* = 11.3$ K, $Z = 7.2$ km.

storm. The two main vortices merge at 900 days to produce a 50° long anticyclone that propagates at a rapid one degree per day ($c = -14$ m s^{-1}). Meanwhile, the easterly jet, being more stable, has only decreased to -36 m s^{-1}.

g. *Three vortices by eight mergers in a 180° domain*

Although vortex genesis takes a variety of paths, it usually ends with a single large anticyclone. We now present an example that either is an exception to this rule or does not realize it within a reasonable time. Such flows may be more relevant to Jupiter's Ovals than its GRS. Case G7 shows how an initial state with numerous vortices evolves toward an end state of three anticyclones. Since this is the most spectacular flow in our series, it is fully documented in Figs. 33–36. The vortices are smaller[8] and more numerous than in other cases, and from them we conclude that size is determined more by jet amplitude than by jet width through the contribution of B_J to the local Rossby radius of deformation.

For variety, the jet amplitudes are set at half the observed strength. Consequently, the instability produces a disturbance of wavenumber 16 initially, from which 11 full vortices grow (Figs. 33 and 34). Then, after a series of eight mergers, four of each type, the system reduces to a three-vortex state that may persist or may be evolving too slowly to be detected at 2500 days.

The paths added in Fig. 33 show where the final trio originates in the initial perturbation and provide a reference frame for describing the overall evolution. The main vortex, labeled M, originates clearly but unusually at the back of the pack, while the other two, A and B, emerge somewhat ambiguously from pairs of vortices. In particular, vortex A arises from the merger of the one so marked and its westward partner at 350 days, but either one may be regarded as the nucleus because the resulting storm is centered between the pair. Vortex B, however, forms from the merger of the one so marked and its eastward partner at 550 days, and the B vortex is considered to be the nucleus because the resulting storm adheres to its path. The small central vortex C, the last to be absorbed, is also tracked in Fig. 33.

[8] Because of this smallness, the $\Delta\lambda \sim 1°$ resolution is used.

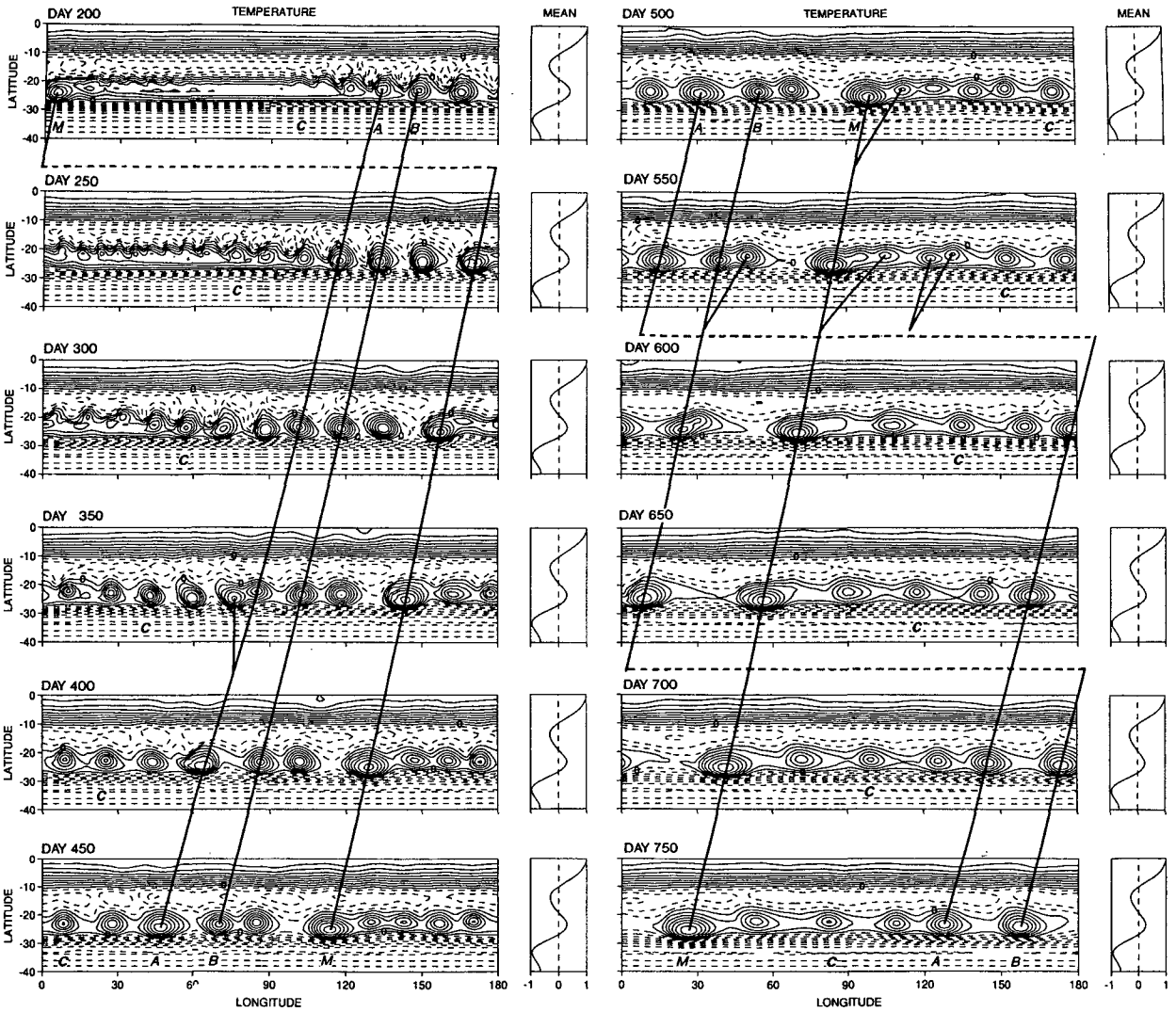

FIG. 33. Vortex genesis solution G7, generation of three long-lived anticyclones by eight mergers in a 180° domain. For Jovian $P_3(N180)$ parameters and geostrophic sinusoidal jet streams, as in Table 3. Labels M, A, and B refer to the main and major vortices; C refers to the

Initially, the localized perturbation spreads out into a wave packet and produces a group of five vortices at 200 days that come to dominate the evolution. Weaker storms form ahead of this group and by 350 days have caught the M vortex from the east to start the self-interaction of this 11-vortex system. The main merger phase begins when vortex M reels in the first and second of the four small storms in the leading group at 500 and 550 days, while the other two small storms merge, and vortex B absorbs its partner (Figs. 33 and 34). By 600 days, the flow has simplified into the three major vortices and the three minor storms.

The six-pack configuration propagates steadily westward until vortex M reels in a small storm at 900 days,[9] and vortex A sweeps up another at 1000 days (Fig. 33). The resulting group of three major vortices and the sole surviving minor storm C persists until 1500 days when vortex M reels in C (Fig. 34). The final trio then remains centered at $\phi = -23°$ and evolves so slowly that the final outcome remains unpredictable. During the last phase calculated, the gap between vortices M and B increases over 1500–2000 days but then remains constant, whereas the gap between vortices A and B decreases continuously but very slowly. This suggests that

[9] After 900 days the plots in Fig. 33 are no longer uniformly sampled, so see Fig. 34 for a more continuous representation.

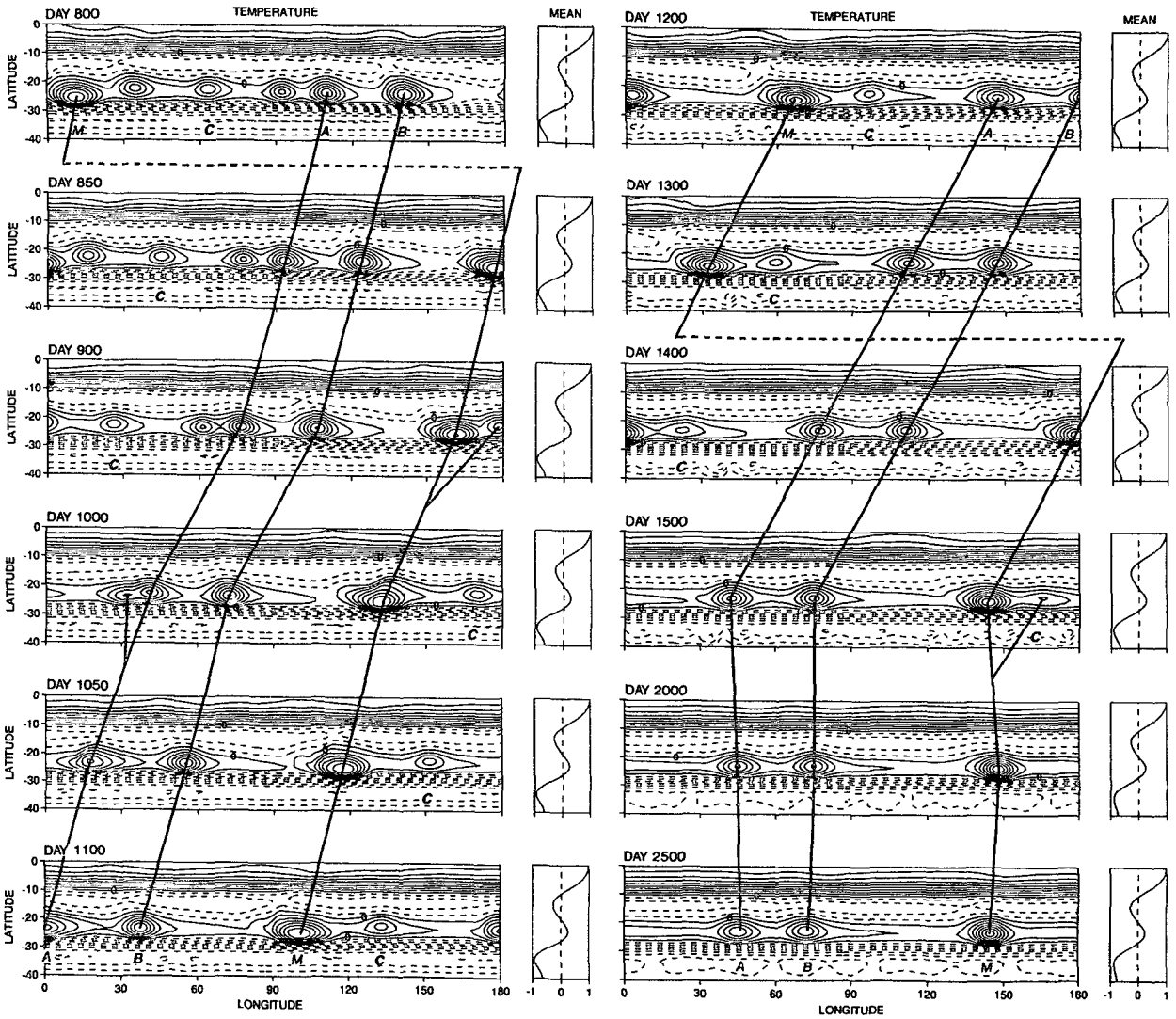

FIG. 33. (*Continued*) longest surviving core. Properties: $c = -4.5$ m s^{-1}, $U = 30$ m s^{-1}, $T = 13$ K, $B = 6.7 \times 10^{-4}$ s^{-2}. Contours: $\Delta T = 1$ K, $T^* = 8.5 - 8.4$ K, $Z = 7.2$ km.

vortices A and B may well merge, but only after another 1000 days or more, and they could give a system with two near-equal anticyclones that may or may not merge after an even longer period. Thus, any final state with a few well-separated vortices seems to be possible and depends as much on evolution as on origin.

The final vortices extend to depths that depend on their amplitudes and take on an exponential, not eigenmodal, variation (Fig. 35). The vertical motion produced by the propagation dominates the w field and extends deeply into the abyss. The flow scales remain low but relevant: $c = -4.5$ m s^{-1}, $U = 30$ m s^{-1}, $T = 13$ K, and $B = 7 \times 10^{-4}$ s^{-2} (Fig. 36). The jets hold their strength throughout, with only the E_1 easterly dropping to -10 m s^{-1}, and with a narrow E_0 equatorial countercurrent of -15 m s^{-1} arising from the wave action.

9. Genesis 2: The Galilean variations

The solutions presented in sections 4–8 describe generic vortex modes and the generic structures that favor their prolonged existence. Theoretically, these modes can exist for a wide range of values for the vertical scales h and H, provided that their relative ratio $h:H$ remains small, $\leqslant 1/20$. For example, the above solutions with $h \sim 50$ km and $H \sim 1000$ km are identical in form to those with $h \sim 500$ km and $H \sim 10\,000$ km if the temperatures are reduced accordingly by a factor of 10

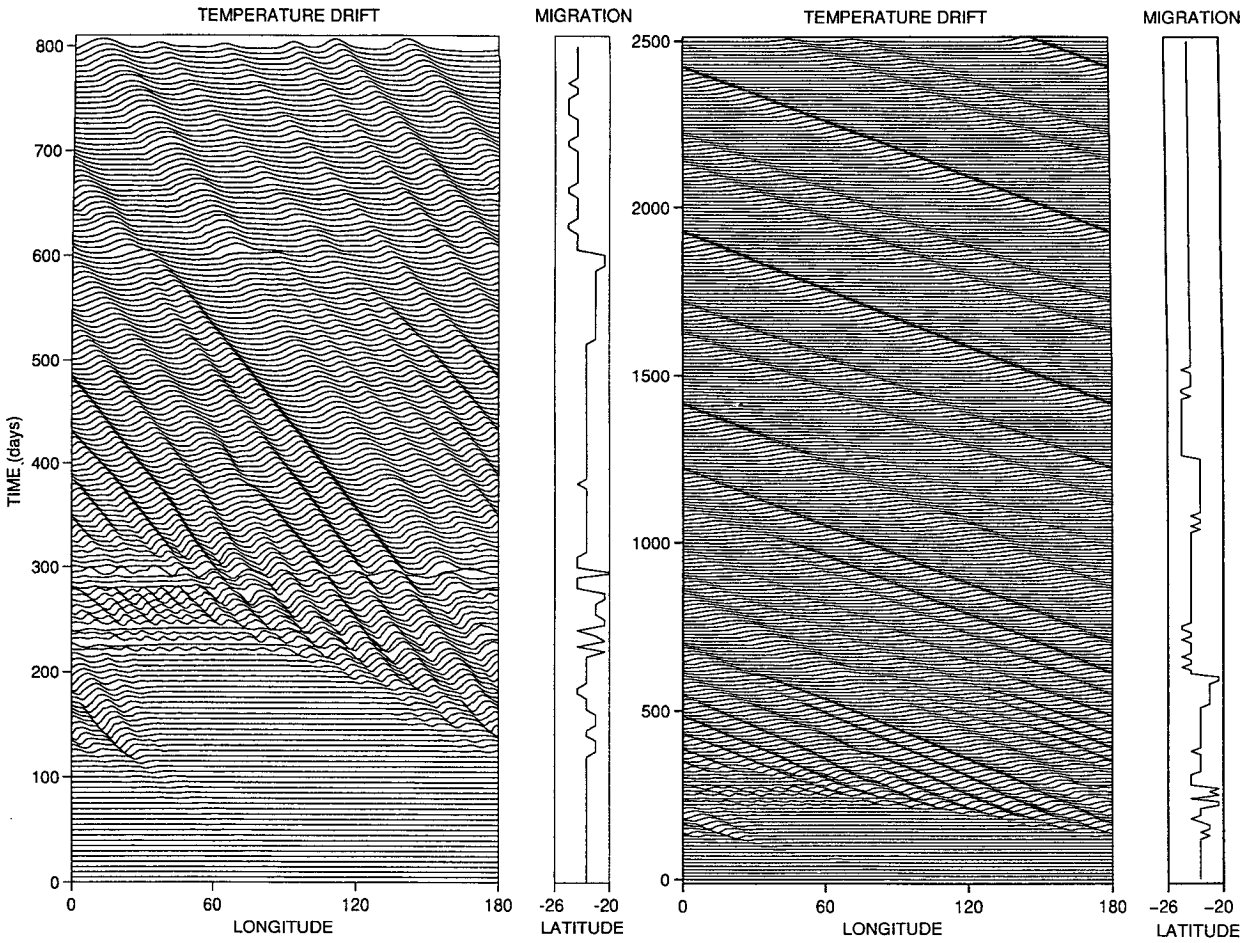

FIG. 34. Time sections for the genesis solution G7. Close-up on the left side illustrates the initial mergers. Temperature is sampled near the top surface at the latitude, shown on the right, of the vortex maximum. Scale: on the left, maximum $T = 5.5$ K $\equiv 2\times$ vertical increment; on the right, maximum $T = 5.9$ K $\equiv 1.2\times$ vertical increment.

to maintain similar velocities. This generality, together with the absence of adequate temperature observations and of a reliable estimate for an absolute vertical scale, limits the direct application of the vortex theory to Jupiter. However, observations just made by the *Galileo* spacecraft probe may have altered this situation, and we now consider to what extent the new data provide a definitive vertical scale and affect our analysis and conclusions.

Essentially, the *Galileo* velocity sample, derived from Doppler measurements of the probe's descent through the atmosphere at a latitude of 6.5°N, shows that the "winds were fairly constant" and that "wind speed increased with depth," according to D. Atkinson (see Carlowicz 1996). These measurements extended to about 100 km below the tropopause, thus sampling the outer $1/700$th of the planet's envelope. Before applying this data to models, we need to consider how representative the sample really is and whether it relates more to local than global conditions or to weather more than climate. In particular, we note that the flow measurement is Lagrangian and not Eulerian; that it is limited in time and longitude and so does not define the mean current at $\phi = 6.5°$; that it incorporates a strong eddy component in a very turbulent region, while remembering that on Earth eddies are often strongest at depth even though jets peak aloft; and that the sample is from a complex transitional zone between the equatorial and subtropical regimes that, as on Earth, may differ completely from the midlatitude regime in its structure. Furthermore, given that the winds must eventually vanish at some depth, the absence of any decline suggests that the probe did not go deep enough to be definitive. What the data primarily suggests is that the active layer has a depth of about 500 km rather than the 50 km often invoked. Dynamically, this has quantitative, but not fundamental, consequences.

Despite these limitations, we will take the data at face value and assume it represents the global and climatological state, not just the local weather, and proceed to examine whether our generic vortex modes and structures can be modified to comply with it while still maintaining their basic character. To do this, we examine the behavior of vortices generated by baroclinically unstable jets with flat or reversing $U_J(z)$ profiles extending over the top of the active layer to a depth $d \sim 100$ km. For convenience, we refer to this uppermost region as the "mixed layer," further extending the oceanic connection. Clearly, a very thin mixed layer with $d \ll h \ll H$ would not alter the EXP or LIN systems significantly and would only modify vortex behavior slightly. The question is whether a substantial mixed layer can be accommodated or whether vortices quickly collapse in its presence.

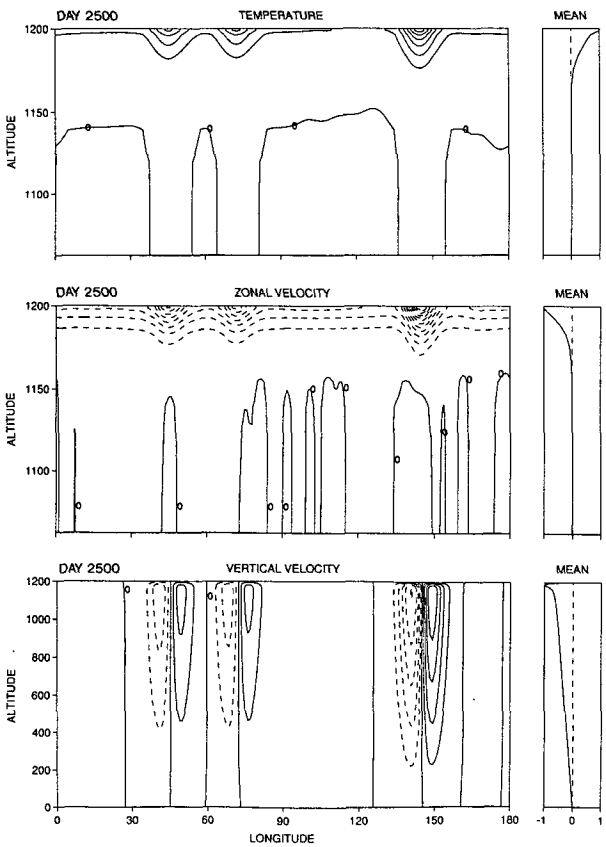

FIG. 35. Vertical sections for the genesis solution G7, sampled at latitudes near the vortex center. Contours: (a) $\Delta T = 2$ K, $T^* = 3.8$ K, $\phi = -24°$; (b) $\Delta u = 2$ m s^{-1}, $u^* = 8.3$ m s^{-1}, $\phi = -21°$; (c) $\Delta w = 0.1$ cm s^{-1}, $w^* = 0.001$ cm s^{-1}, $\phi = -24°$.

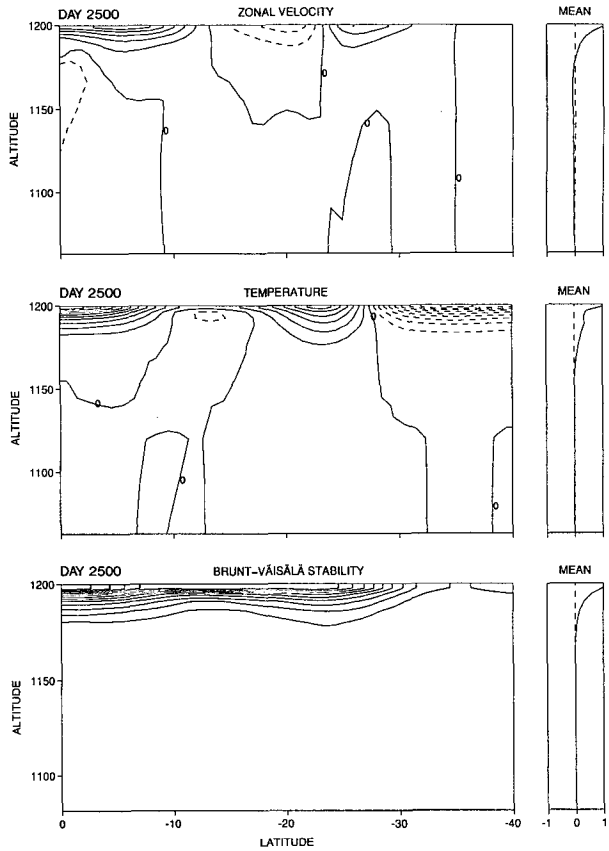

FIG. 36. Vertical sections for the genesis solution G7, sampled at longitudes near the vortex center. Contours: (a) $\Delta u = 10$ m s^{-1}, $u^* = 14$ m s^{-1}; (b) $\Delta T = 2$ K, $T^* = 1.3$ K; (c) $\Delta B = 0.5 \times 10^{-4}$ s^{-2}, $B^* = 3.8 \times 10^{-4}$ s^{-2}; $\lambda = 145°$.

To include a substantial mixed layer, we first extend the fluid domain to a depth $H = 10\,000$ km, which is an order of magnitude greater than before and one near which Jupiter makes its transition to a metallic state (Audouze and Israël 1994). Then, for an exponential structure with $N = 100$, we have an active layer to a depth $h = 500$ km. When such a structure is modified to include a mixed layer, a variety of calculations show that the vortices remain coherent and prolonged provided the mixed layer does not exceed 100 km in extent,[10] or, more generally, provided that $d \leq h/5$ and $h \leq H/20$.

[10] This limit can be extended to a maximum of 150 km by using $H = 15\,000$ km and $N = 60$, but we stay with the minimum values needed to comply with the *Galileo* data. Presumably, the limits of the Boussinesq model noted in section 2 are no greater when $h = 500$ km than when $h = 50$ km and it still represents the main dynamical processes correctly. Although the primitive equation limit that $H/a \ll 1$ may not be as well met, this should not affect motions confined to the active layer.

TABLE 4. Vortex genesis cases in low latitudes for variant structures. Constant parameter values are $H = 10\,000$ km, $N = 100$, $\phi = -40{:}0°$, $\lambda = 0{:}180°$; resolution $R\ (\lambda, \phi, z) = 98 \times 42 \times 20$, $\Delta\phi = 1°$, $\Delta\lambda \sim 2°$, $\Delta z \sim e^{5z'}$, $\Delta t = (1/50)$ day, $\nu_4 = -10^{17}$ m^4 s^{-1}, $\nu_2 = 10^{-8}$ m^2 s^{-1}. Jet profiles are defined, as in Table 2, by the latitudes Φ_J where the flow vanishes, with $\Phi_7 = [0, -6, -14, -21, -28, -40]$, $\Phi_{8b} = [0, -6, -13, -21, -29, -40]$, $\Phi_{9.5} = [0, -9, -14, -23, -33, -40]$. The superscript (a) denotes easterly jets with a slower exponential rate, $e^{Nz'/1.3}$. In case A2, the function $f(e^{Nz'})$ denotes an exponential form that is flattened over the top four grid points to give constant $U_J(z)$ and $B_s(z)$ distributions over the upper 100 km. In case A4, the sech distribution has a maximum at the scaled depth $d' = -0.6$ to give reversing $U_J(z)$ and $B_s(z)$ distributions of the upper 100 km. Note that the integral in A3 is simply $\int (\text{sech } Nz')\, dz = 1 + (2/\pi) \tan^{-1} (\sinh Nz')$.

Case	Static stability $T_s - 1$	Jet structure $U_J(z)$	Jet amplitudes $W_1 + E_1 + W_2 + E_2$	Jet profiles Φ_J
A1	$5\, e^{Nz'}$	$e^{Nz'}$	$100 - 60^{(a)} + 30 - 12^{(a)}$	$\Phi_{9.5}$
A2	$6 \int f(e^{Nz'})\, dz$	$f(e^{Nz'})$	$105 - 65 + 45 - 15$	Φ_7
A3	$3.5 \int (\text{sech } Nz')\, dz$	sech Nz'	$105 - 55 + 40 - 15$	Φ_{8b}
A4	$3 \int [\text{sech } N(z' - d')]\, dz$	sech $N(z' - d')$	$105 - 65 + 50 - 15$	Φ_7

We present four solutions that illustrate the essential effects of a mixed layer on vortices in hyperbolic structures, cases A1–A4 in Table 4. The first case A1 has the generic EXP structure to provide a reference for the A2–A4 cases and to confirm that solutions can be rescaled linearly in the vertical. A mixed layer is introduced in case A2 by resetting the values of the exponential function at the top three grid points to the value at the fourth and renormalizing. This flattened exponential function, denoted as $f(e^{Nz'})$ or FEXP, produces uniform $U_J(z)$ and $B_s(z)$ profiles over the upper 100 km (see Fig. 41).

For the second pair of solutions, a new generic structure sech Nz' is first introduced in case A3. This function, denoted as SECH, is almost identical to $e^{Nz'}$ in the abyss and the lower half of the active layer but deviates significantly in the upper half to produce a smooth approach to a flat flow profile. This form is modified in case A4 to sech $N(z' - d')$, denoted as DSECH, so that the jets peak at the nondimensional depth $d' = d/H$ and have reversed shears over the mixed layer (see Fig. 46).

All cases in Table 4 are chosen so as to generate a single vortex, either from the beginning or after merg-

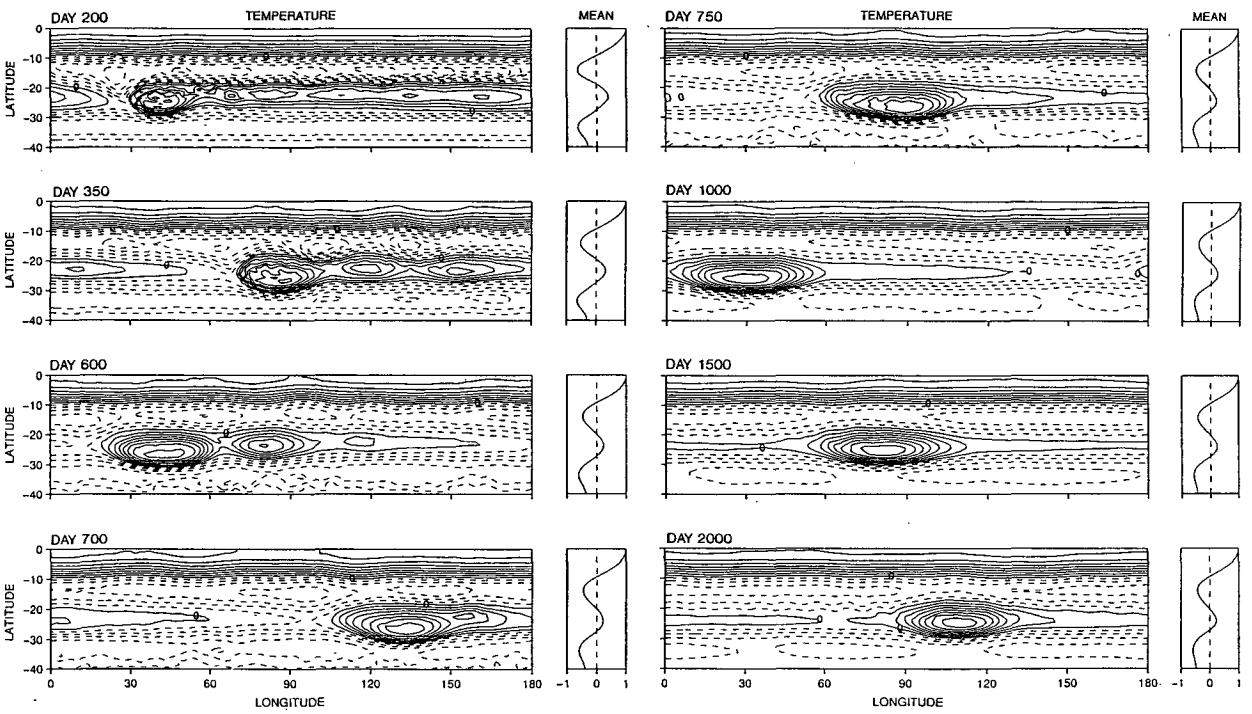

FIG. 37. Vortex genesis solution A1, generation of a single long-lived anticyclone ab initio in a deep EXP system from baroclinically unstable currents. For Jovian N100 parameters and geostrophic sinusoidal jet streams, as in Table 4. Properties: $c = -13$ m s^{-1}, $U = 64$ m s^{-1}, $T = 1.5$ K, $B = 5 \times 10^{-6}$ s^{-2}. Contours: $\Delta T = 0.2$ K, $T^* = 7.1 - 6.9$ K, $Z = 60$ km.

ers. But multiple vortex states also occur for these variant structures. The specific way in which the mixed layer, with a flat or reversing flow, is included is not critical provided the depth is limited and the same layer is applied to both U_J and B_s. Consequently, the vortices in the generic EXP and SECH systems evolve and behave in essentially the same way as each other, while the vortices in the modified FEXP and DSECH systems evolve in another way, to provide a subtle observational test for the planetary structure.

a. *Genesis in the deep EXP system*

In the reference case A1 for the 10^4 km deep EXP system in Fig. 37, the baroclinically unstable easterly jet produces a single large vortex over the 100–300 day period when the leading edge of the initial localized perturbation forms a closed front. The lengthy tail contains three cores, two of which continue to develop slowly until they are absorbed by the vortex at 400 and 700 days. After the mergers, the vortex adjusts into a balanced form by 1000 days and then propagates steadily and unchanged for the next 1000 days.

This A1 solution generally resembles that for the single vortex genesis in case G2 for the 10^3 km deep system in section 8b, except that the temperature variations are an order of magnitude weaker, reaching only 2.5 K in Fig. 37. Profiles of the main jets in Fig. 38 confirm that they maintain their form and reach a depth of $h \sim 500$ km, as does the vortex temperature field, which again takes on an exponential form rather than the first baroclinic mode. Overall, the vertical structure of the final state matches that of the G7 case in Fig. 36, apart from the greater vertical scale.

b. *Genesis in the FEXP system*

In the FEXP system, with its vertically uniform mixed-layer flows, the initial development of the vortices follows a different path from those seen in the generic EXP system (Fig. 39). Specifically, the first vortex to emerge, seen at $\lambda = 110°$ at 150 days, does so in the tail end of the perturbation and precedes the second vortex, seen at $\lambda = 140°$ at 150 days, that emerges in the head of the disturbance and becomes the dominant anticyclone. Subsequently, one minor storm forms ahead of the first vortex and three such form behind the main vortex. The leading pair in the triplet merge at 300 days to produce a storm matching the main one, while its remaining member just fades away. The two major vortices then proceed to merge over 400–500 days. The first vortex also fades away by 700 days and this leaves just the main vortex to chase and catch the remaining minor storm at 1800 days, in the only classic merger type seen in the A1–A4 solutions. The final vortex propagates steadily thereafter, maintaining its amplitude but becoming slightly smaller by 3000 days.

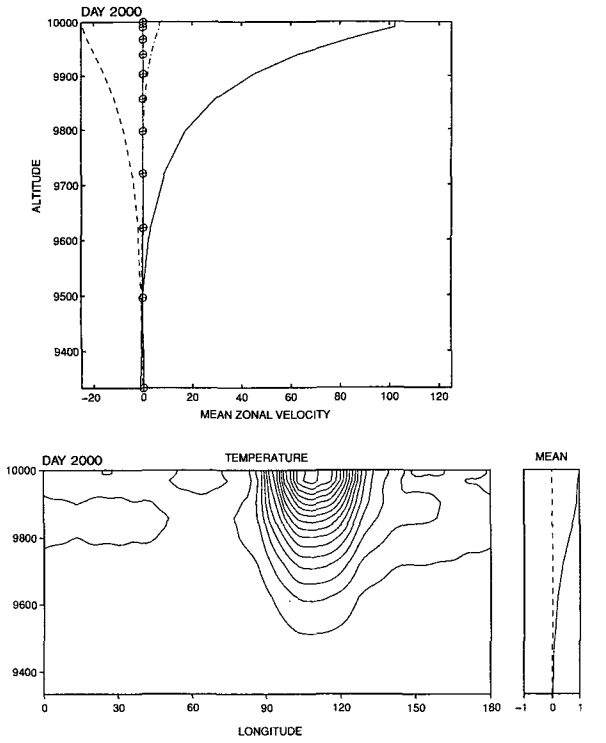

FIG. 38. (Top) Vertical structure of the mean zonal flow for the genesis solution A1. The W_1, E_1, and W_2 jets are sampled at $\phi = -(7, 17, 25)°$ and plotted with solid, dashed, and dash–dot lines. Crosses mark the gridpoint distribution for the $\Delta z \sim e^{5z'}$ spacing, for an upper level subdomain; Units: km, m s^{-1}. (Bottom) Vertical section for the genesis solution A1. Sampled at a latitude near the vortex center; contours: $\Delta T = 0.1$ K, $T^* = 0.35$ K, $\phi = -24°$.

In the vertical, all the major jets retain their uniformity in the mixed layer (Figs. 40 and 41). The temperature field reaches a peak of 1.3 K at a depth of 150 km but has no latitudinal variations at the top and produces a complex Brunt–Väisälä stability distribution in the mixed layer. Again the vortex structure follows that of the jets rather than the first baroclinic eigenmode, thus vanishing at the top (Fig. 41).

c. *Genesis in the SECH system*

In the generic A3 SECH case in Fig. 42, the evolution generally resembles that seen in the EXP system (cf. Fig. 37) in that the main vortex forms out of the frontal occlusion at the leading edge of the perturbation. Three cores also arise and grow to give a complex tail. The main vortex absorbs the first pair of these at 300 and 500 days, but the assimilation of the final one proceeds extremely slowly over 800–1800 days. This reluctance to merge was also seen in the G7 solution. The final A3 vortex maintains its strength and size almost as well as its A1 EXP counterpart, suggesting that the SECH structure forms a viable alternative system for prolonged vortices.

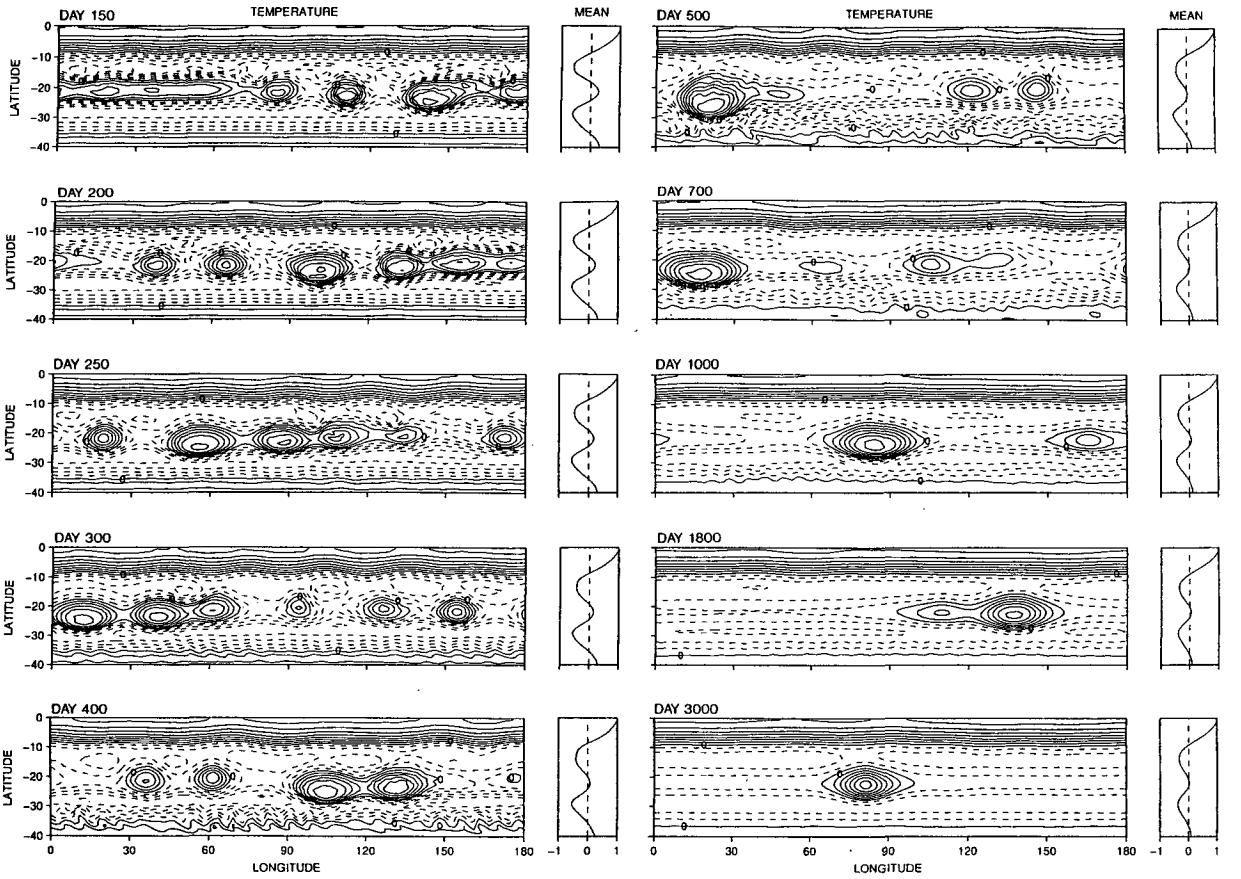

FIG. 39. Vortex genesis solution A2, generation of a single vortex by three mergers in a deep FEXP system. For Jovian N100 parameters and geostrophic sinusoidal jet streams, as in Table 4. Properties: $c = -13$ m s^{-1}, $U = 52$ m s^{-1}, $T = 1.5$ K, $B = 2 \times 10^{-6}$ s^{-2}; contours: $\Delta T = 0.2$ K, $T^* = 1.41 - 1.46$ K, $Z = 143$ km.

In the vertical, the A3 jets maintain their smooth approach to a zero shear aloft (Fig. 43). The vortex temperature varies like the mean field, decreasing smoothly upward from a peak of 1.0 K at the 100-km depth but without vanishing at the top.

d. Genesis in the DSECH system

Although the DSECH structure departs fundamentally from the generic forms by reversing the vertical jet shears and the horizontal baroclinicities over the mixed layer, prolonged vortices are still possible provided the layer is no deeper than 100 km. In such a case, A4 in Fig. 44, the vortices form rapidly with the first emerging at 100 days at $\lambda = 160°$ in the *tail* of the perturbation and the second forming in the *head* of the perturbation at 150 days at $\lambda = 150°$. Whereas only one dominant vortex usually forms in the generic systems, the formation of two in mixed-layer systems seems to be typical behavior (cf. Fig. 39). Three of the four cores that form the A4 vortex tail at 150 days continue to grow and proceed to merge with the main vortex at 200, 400, and 600 days. The small vortex propagates faster than the main and the two eventually merge at 1000 days. Although balanced, the final vortex gradually shrinks in longitudinal size over the next 2000 days while keeping its amplitude at 1.2 K.

In the vertical, both the final vortex and equatorial jets display reversed shears and baroclinicities in the mixed layer (Figs. 45 and 46). These reversed baroclinicities produce minima in the Brunt–Väisälä stability aloft. However, of the zonal mean flows, only the W_1 jet fully maintains the original form, as the E_1 and W_2 jets tend to develop vanishing shears aloft (Fig. 46).The vortex itself again adopts the same structure as the jets, thus activating both the first and second baroclinic eigenmodes, whose interactions may be the cause of the slow shrinkage (Fig. 46).

Overall, it appears that vortices can flourish in systems with reversed shears in the mixed layer but that they do not persist—without renewal—as well as those with flat shears or with no mixed layer. Thus the basic modes for generic exponential structures

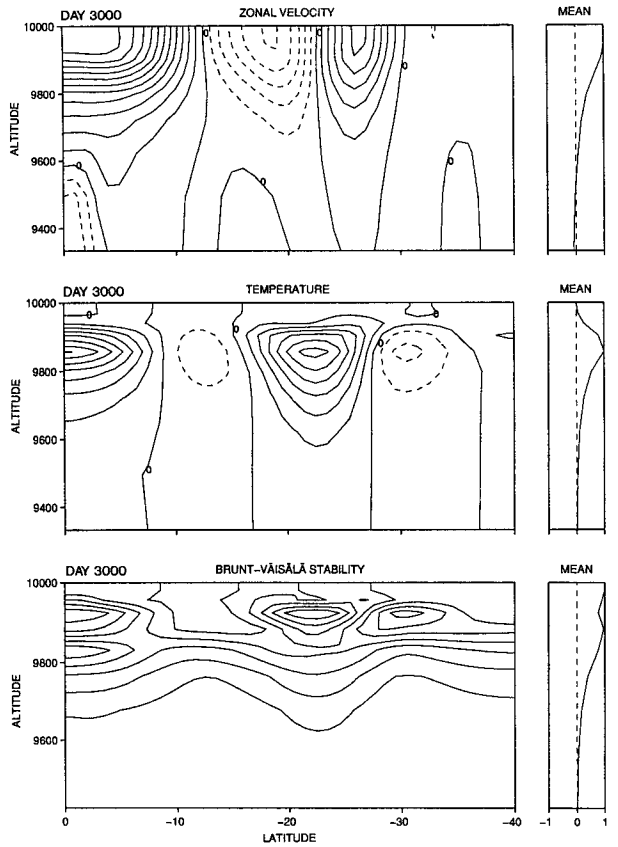

FIG. 40. Vertical sections for the genesis solution A2, sampled at a longitude near the vortex center. Contours: (a) $\Delta u = 10$ m s^{-1}, $u^* = 23$ m s^{-1}; (b) $\Delta T = 0.2$ K, $T^* = 0.35$ K; (c) $\Delta B = 5 \times 10^{-7}$ s^{-2}, $B^* = 2.3 \times 10^{-6}$ s^{-2}; $\lambda = 82°$.

can be modified to comply with the *Galileo* data and, therefore, are not contradicted by it. The calculations suggest, however, that the structure implied by the data can persist at the latitude where it was taken but that when it is imposed elsewhere, it tends to relax toward greater uniformity. Although Jupiter could have an FEXP or DSECH vertical structure, with $d \sim 100$ km, $h \sim 500$ km, and $H \sim 10^4$ km, it is uncertain whether the observations at $\lambda = 6.5°$ really have a global relevance. Consequently, we still lack an estimate of an absolute vertical scale that is more accurate than the range $50 \leq h \leq 500$ km suggested by our calculations.

10. Conclusions

The parametric behavior of planetary vortices has been derived for atmospheres with static stability structures primarily of the exponential form $e^{Nz'}$ by varying the rate N in a three-dimensional primitive equation model. Our numerical model allows vortices to exist indefinitely when they are physically capable of doing so. Vortices are found to be absolutely stable when they are generally large compared to the Rossby radius, thin compared to the abyssal depth, anticyclonic, and possess a first baroclinic eigenmodal or exponential structure. The vortices are essentially nonlinear baroclinic Rossby waves and are an extension of the Rossby vortices of the shallow-water system. Such anticyclones are generated naturally by baroclinically unstable easterly jets and can exist at all latitudes under conditions that vary from midlatitudes to low latitudes to the equator.

At the equator, anticyclones are stable when they have the Hermite latitudinal form, the Korteweg–deVries longitudinal form, and the first baroclinic eigenmodal vertical form for exponential stratifications as derived by Marshall and Boyd (1987). Only vortices based on the first-order Hermite mode have been analytically defined and numerically studied but are the most stable and the most likely to exist for a wide range of parameters. In fact, this Rossby soliton exists indefinitely for both Jovian and oceanic parameters. The numerical solutions, unlike the analytical, let the vortex generate a barotropic mode that is substantial but is distributed so as not to feedback onto the storm. Furthermore, when unbalanced vortices are inserted into

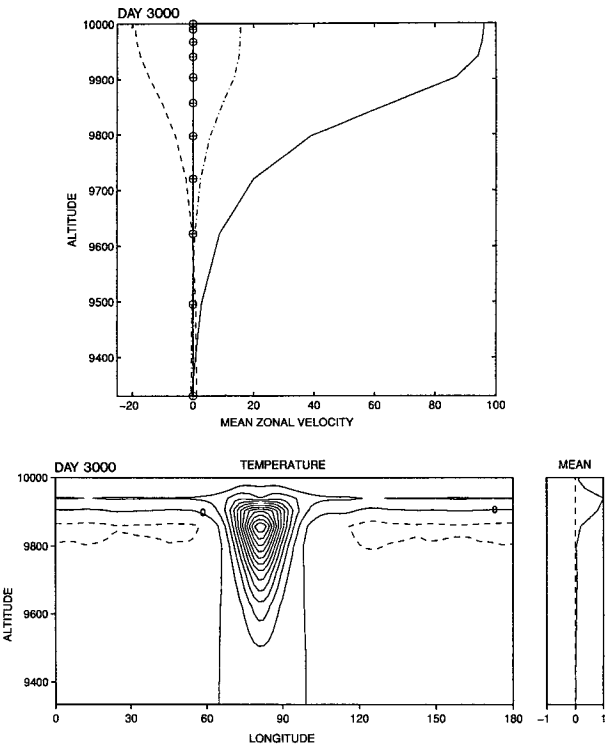

FIG. 41. (Top) Vertical structure of the mean zonal flow for the genesis solution A2. The W_1, E_1, and W_2 jets are sampled at $\phi = -(7, 17, 25)°$ and plotted with solid, dashed, and dash–dot lines. Crosses mark the gridpoint distribution. For an upper-level subdomain. Units: km, m s^{-1}. (Bottom) Vertical section for the genesis solution A2. Sampled at a latitude near the vortex center. Contours: $\Delta T = 0.1$ K, $T^* = 0.13$ K, $\phi = -23°$.

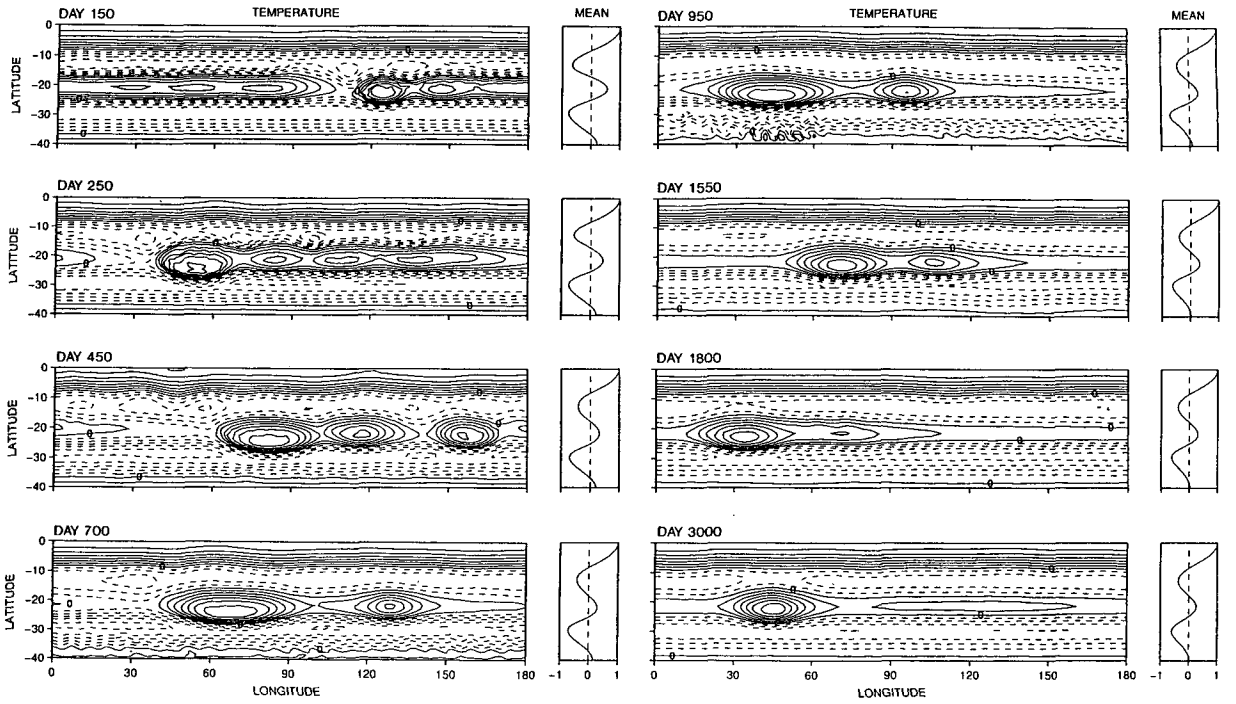

FIG. 42. Vortex genesis solution A3, generation of a single vortex by three mergers in a deep SECH system. For Jovian N100 parameters and geostrophic sinusoidal jet streams, as in Table 4. Properties: $c = -11$ m s^{-1}, $U = 57$ m s^{-1}, $T = 1.0$ K, $B = 3 \times 10^{-6}$ s^{-2}; contours: $\Delta T = 0.15$ K, $T^* = 0.95 - 0.99$ K, $Z = 96$ km.

the numerical model, they adjust by shedding secondary vortices with which they later undergo quasi-soliton interactions. Thus, baroclinic Rossby solitons appear to be robust and not too dependent on being exactly like the analytical forms.

Equatorial anticyclones can also be generated quite easily by waves emanating from low-latitude disturbances and can also exist in modified form when embedded within zonal currents. These solutions confirm that a connection exists between the shallow water and baroclinic phenomena when the latter have an exponential structure. This leads us to look for connections at other latitudes with the preliminary set of parameters and structures, $P_1(N20)$, suggested for Jovian studies by the equatorial analysis.

In midlatitudes, the largest Rossby vortices with the shallow P_1 structures are quasi-stable in the sense that they remain coherent but slowly lose amplitude as they migrate equatorward. Migration, followed by a rapid dispersion in low latitudes, is the main cause of P_1 vortex collapse. Medium and small vortices migrate even faster and, thus, collapse more quickly. This variation in behavior corresponds to that seen in the shallow-water model and also displays features associated with PG, IG, and QG dynamics. In the shallow-water system, however, the large vortices are absolutely stable, whereas in the PE system they achieve that status only when $N \geq 90$. The difference occurs because large P_1 vortices generate a barotropic mode that forces migration.

In low latitudes, the evolution in the P_1 regime is determined more by dispersion than by migration, so vortex lives are shorter than in midlatitudes. Zonal jets, especially easterlies, can prolong vortex existence but not indefinitely. Vortices that are temporarily blocked by an easterly jet become smaller until they can tunnel through the jet and resume their equatorward migration. Although stronger jets block migration more, their amplitudes are limited by baroclinic instability to levels that still allow vortices to get through, at least in the P_1 regime.

The best way to make vortices less migratory and more long-lived is by making them thinner relative to the abyss. Thus, in the $P_2(N60)$ regime, thin vortices migrate so slowly they can be blocked by a weak easterly jet and made conditionally permanent. Furthermore, in the $P_3(N90+)$ regime,[11] very thin vortices do not migrate at all, so they are absolutely stable in middle and low latitudes. Coexistence and genesis then replace blocking as the main role of the jets when N becomes large enough.

[11] Although absolute stability requires that $N \geq 90$ in low latitudes, it may occur for $N \sim 50$ in midlatitudes; this issue was not examined.

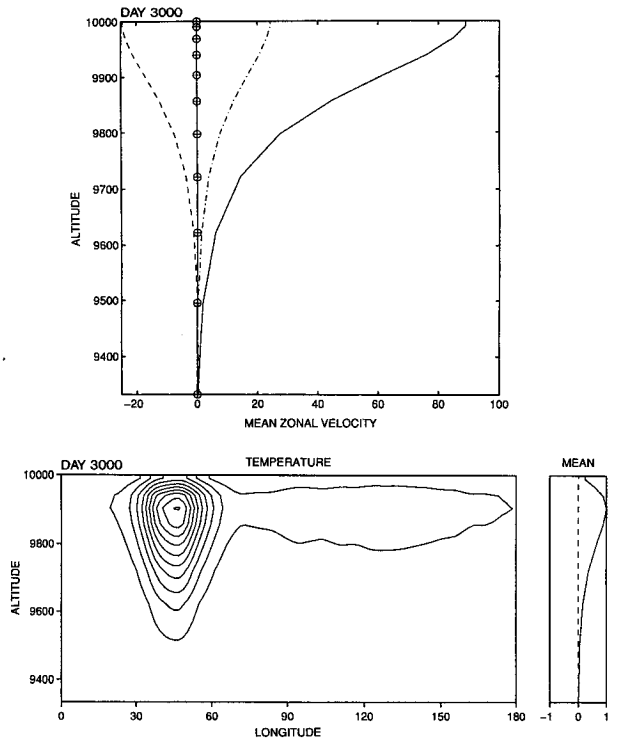

FIG. 43. (Top) Vertical structure of the mean zonal flow for the genesis solution A3. The W_1, E_1, and W_2 jets are sampled at $\phi = -(7, 17, 25)°$ and plotted with solid, dashed, and dash–dot lines. Units: km, m s^{-1}. (Bottom) Vertical section for the genesis solution A3, sampled at a latitude near the vortex center; contours: $\Delta T = 0.1$ K, $T^* = 0.24$ K, $\phi = -23°$.

Very thin, steeply exponential (EXP) vortices in the P_3 regime can also be represented by confined linear-z (LIN) distributions for the velocity and the stability B_s in the upper layer. This alternative L_3 structure for stable vortices also has different baroclinic instability properties that are useful for generating jets (see Part II). Very thin vortices of the EXP or LIN form also remain absolutely stable when embedded in alternating jet streams of identical form and limited amplitude.

When they are strong, easterly jets become baroclinically unstable in the P_3 and L_3 regimes and energize wave packet perturbations into solitary long waves or vortices if the preferred scale exceeds the Rossby radius sufficiently. A large variety of evolutionary paths are possible but most result, after a series of mergers and enough time, in a single vortex end state.[12] Single vortex states can also arise at the start and persist thereafter, but they are harder to realize. The scale of the vortices generated by an instability depends more on the jet amplitude than on the jet width. Exceptions to the merger rule do occur, with multivortex end states occurring when the merger timescale is too long to be realized or when the vortices are too equally matched to approach each other. Interactions may even lead to vortex collapse if the components are so strong that their combination cannot reach a balanced equilibrium.

Vortex behavior in the P_3 regime differs significantly from its shallow-water prototype. For example, in the PE model the vortices are generated by the baroclinic instability of an easterly jet, whereas in the reduced-gravity SW model the nature of the shear instability is somewhat ambiguous. The propagation speed is the ambiguous quantity for the PE model, being as much determined by local flow fields as by the planetary long-wave speed c_β. This complexity also helps make the vortex interactions more varied. In the shallow-water system, the mergers are relatively simple; the stronger vortices move faster than the weaker ones and eventually catch and absorb them. Although this also happens in the PE system, the strong vortices can also reel in the weaker ones trailing behind them. Proximity and advection seem to be as important as propagation in determining the character of the interactions.

Vortex behavior also serves a wider purpose: the selective existence of stable vortices allows them to be used effectively, both qualitatively and quantitatively, as an atmospheric probe to examine Jupiter's atmospheric structure. The vortex stability characteristics primarily give the thermal $T(z)$ structure, while the coexistence with jets yields the flow $u(z)$ structure, and genesis suggests a timescale of about 1000 days. Working with realistic levels of c, u, T, and B could make the probe quantitative, but selecting representative values for these quantities still involves arbitrary assumptions and produces ambiguous estimates.

Indeed, the existence of the conditionally stable P_2 vortices and the absolutely stable P_3 vortices implies that Jupiter's atmosphere is thin and confined to a layer of thickness h above an abyss of depth H such that $h/H \leqslant 1/20$. The vortex solutions, however, are rescalable in the vertical, so they do not allow us to deduce absolute values of h and H. The recent *Galileo* spacecraft observation suggesting that the winds are uniform or increase downward over the upper 100 km of the troposphere at $\lambda = 6.5°$ relates to this problem but, given that the data do not represent the mean conditions at that latitude and come from a complex zone that may not be globally representative, does not resolve this issue. However, if the data are assumed to have global and climatological relevance, the vortex theory can be made to comply with the observations by introducing a shallow mixed layer of depth $d \ll h$ aloft, represented by truncated $e^{Nz/H}$ or by sech $N(z - d)/H$ hyperbolic structures. Vortex coherence and longevity are maintained in such systems and suggest that Jupiter's atmosphere has layers with $d \sim 100$ km, $h \sim 500$ km,

[12] Because of this tendency, we can use small domains to study basic behavior and then extrapolate to large domains where timescales are often impractically lengthy.

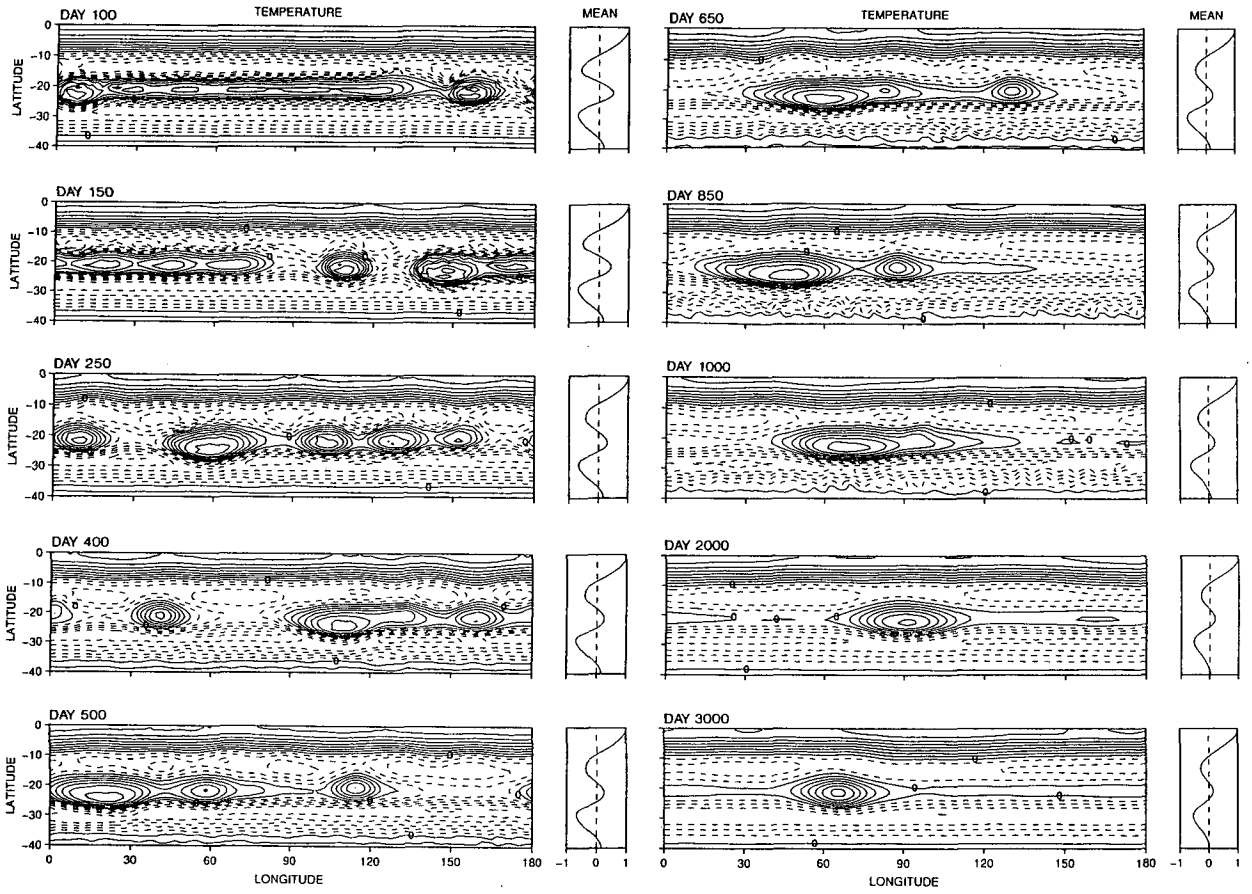

FIG. 44. Vortex genesis solution A4, generation of a single vortex by four mergers in a deep DSECH system. For Jovian N100 parameters and geostrophic sinusoidal jet streams, as in Table 4. Properties: $c = -14$ m s^{-1}, $U = 51$ m s^{-1}, $T = 1.2$ K, $B = 4 \times 10^{-6}$ s^{-2}; contours: $\Delta T = 0.15$ K, $T^* = 1.1$ K, $Z = 143$ km.

and $H \sim 10\,000$ km, a depth near which the transition to a metallic state occurs.

The baroclinic P_3 and L_3 vortices also extend the shallow-water model for Jupiter's Great Red Spot. They imply that the GRS was generated by the baroclinic instability of the easterly jet E_1 and is maintained by a continuing instability and by eddy absorption. Such vortices can exist freely, however, if dissipation is negligible. Evolution, particularly the interaction history, primarily determines the number of vortices that exist in a zone. But the uniqueness of the GRS could be due to its initial emergence as such or could be the result of a series of mergers. The Large Ovals are smaller because they lie in latitudes where the Rossby radius is smaller and the jets are narrower, and remain multiple because their interaction times are so long (see Part II for their simulation). At the equator, Jupiter's plumes could be related to the Rossby soliton of MB87 if allowance is made for the superrotating current.

To be more specific, four stages of GRS existence have been observed (see section 9 of Williams and Wilson 1988). In the high-drift Cassini phase, the vortex was smaller and had a propagation speed of -10 m s^{-1} in 1665 that is in close agreement with our PE solutions. The changes in size and drift speed that occurred during the other phases are significant and complex but consistent with the finding that the drift rate of the P_3 vortices depends as much on the local amplitudes as on the planetary c_β factor. Although the GRS is a low-latitude vortex, its stability does not depend on the adjacent easterly and westerly jets if it lies in the P_3 regime. The spots on Saturn may be less prolonged because their structure puts them in the P_2 regime or because seasonal shifts in the jets destroy their internal balance. The large anticyclone seen on Neptune (Sromovksy et al. 1993) could easily be stable without jets to support it if it lies in the P_3 regime, but its origin would then be mysterious.

The PE solutions also generally support the hypothesis, first put forward in Williams (1975a), that close dynamical ties exist between Jupiter's atmosphere and Earth's oceans. The connections occur because both systems have a small Rossby radius that leads to a wide range of dynamical scales and be-

cause both seem to have exponential-like structures that concentrate their motions in an upper thermocline layer and, perhaps, also in a mixed layer. These connections exist despite geometric and energizing differences. So is Jupiter some sort of primeval or primitive ocean—but larger, deeper, and simpler than Earth's? The answer depends upon whether one distinguishes an ocean from an atmosphere primarily by its fluid composition or by the vertical distribution of its motions.

Jupiter's vortices last longer than the Gulf Stream's because its abyss is deeper and its flow environment is simpler and more benign. Whatever the physical connection, the ocean studies of MB87 give us the theoretical connection between the shallow-water and three-dimensional modes at the equator that provides the key to the dynamics of exponential systems such as Jupiter may have. We have extended that connection from the equator to all latitudes, from low vertical rates ($N = 8$) for the ocean to high rates ($N \geq 100$) for the planets, and from solitons to vortices and jets.

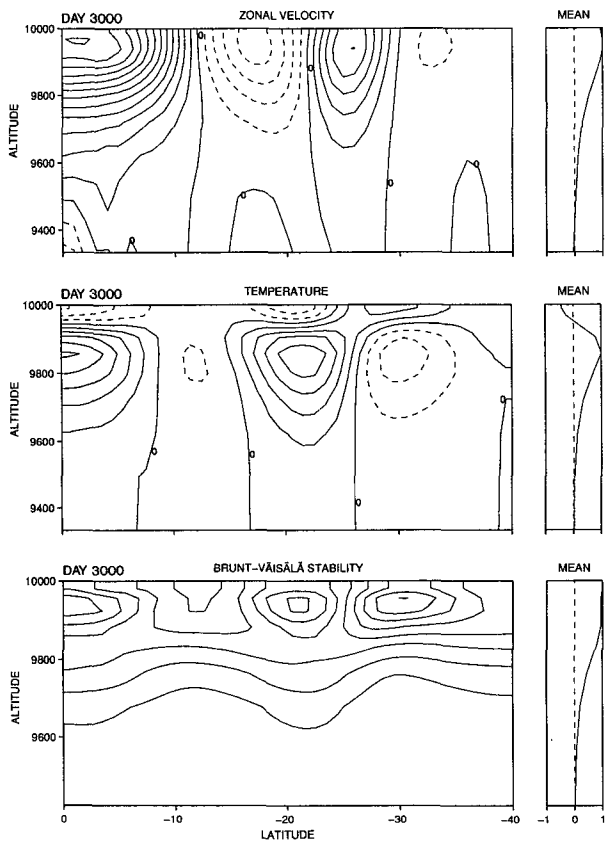

FIG. 45. Vertical sections for the genesis solution A4, sampled at a longitude near the vortex center. Contours: (a) $\Delta u = 10$ m s^{-1}, $u^* = 24$ m s^{-1}; (b) $\Delta T = 0.2$ K, $T^* = 0.22$ K; (c) $\Delta B = 5 \times 10^{-7}$ s^{-2}, $B^* = 2.1 \times 10^{-6}$ s^{-2}; $\lambda = 66°$.

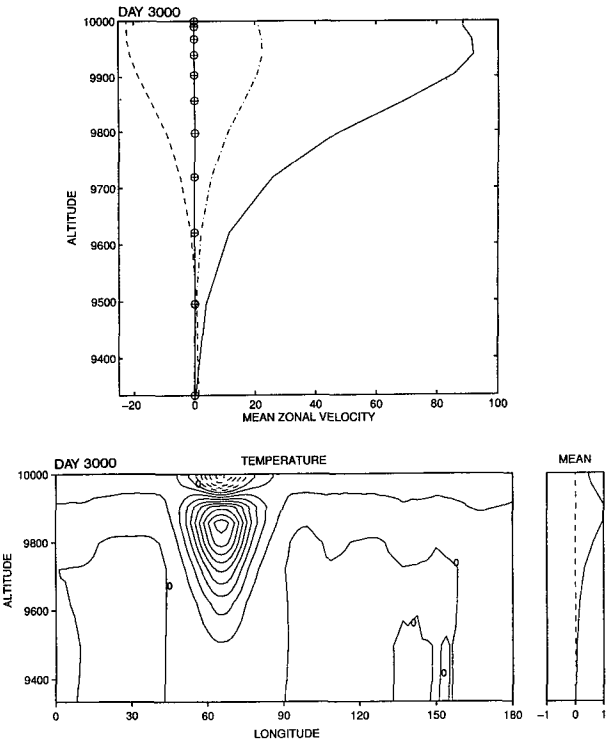

FIG. 46. (Top) Vertical structure of the mean zonal flow for the genesis solution A4. The W_1, E_1, and W_2 jets are sampled at $\phi = -(7, 17, 25)°$ and plotted with solid, dashed, and dash–dot lines. Units: km, m s^{-1}. (Bottom) Vertical section for the genesis solution A4, sampled at a latitude near the vortex center. Contours: $\Delta T = 0.1$ K, $T^* = 0.16$ K, $\phi = -22°$.

In this paper we present solutions that address basic issues concerning vortex stability and vortex genesis. In Part II, we use what we have learned from these solutions to address two more basic issues that need to be solved to complete our model for the Jovian circulation, those concerning multiple jet genesis and superrotation onset. There, we examine first how the jets assumed in this paper can be produced by standard processes in fluids driven by simple heating arrangements. This leads to a study of the simultaneous genesis of the multiple jets and vortex sets that lie in the three zones containing Jupiter's major ovals. Then, at last, we come to the mystery of the origin of the equatorial superrotation and offer a simple but fundamental explanation.

Acknowledgments. For perceptive comments that helped improve this paper, I am most grateful to Kirk Bryan, Stephen Garner, Stephen Griffies, Ray Pierrehumbert, and Peter Rhines. I am further indebted to William Hurlin, Ron Pacanowski, and the late Michael Cox for modeling advice, and to R. Saravanan and The MathWorks Inc. for assistance in developing the graphics packages. A special thanks goes to Wendy Marshall for typing and to Catherine Raphael and Jeffrey Varanyak for drafting. This study also benefitted from the

discussions I had with Toshio Yamagata during my tenure of a fellowship awarded by the Japan Society for the Promotion of Science.

REFERENCES

Anderson, D. L. T., and P. D. Killworth, 1979: Nonlinear propagation of long Rossby waves. *Deep-Sea Res.*, **26,** 1033–1049.

Audouze, J., and G. Israël, 1994: *The Cambridge Atlas of Astronomy.* 3d ed. Cambridge University Press, 473 pp.

Boyd, J. P., 1980: Equatorial solitary waves. Part 1: Rossby solitons. *J. Phys. Oceanogr.*, **10,** 1699–1717.

——, 1983: Equatorial solitary waves. Part 2: Envelope solitons. *J. Phys. Oceanogr.*, **13,** 428–449.

Bryan, K., 1969: A numerical method for the study of the circulation of the World Ocean. *J. Comput. Phys.*, **4,** 347–376.

Carlowicz, M., 1996: Jupiter's atmosphere defies predictions. *Eos, Trans. Amer. Geophys. Union,* **77,** 33–44.

Carlson, B. E., A. A. Lacis, and W. B. Rossow, 1994: Belt-zone variations in the Jovian cloud structure. *J. Geophys. Res.*, **99,** 14 623–14 658.

Charney, J. G., and G. R. Flierl, 1981: Oceanic analogues of large-scale atmospheric motions. *Evolution of Physical Oceanography,* B. A. Warren and C. Wunsch, Eds., MIT Press, 504–548.

Cushman-Roisin, B., G. G. Sutyrin, and B. Tang, 1992: Two-layer geostrophic dynamics. Part I: Governing equations. *J. Phys. Oceanogr.*, **22,** 117–127.

Feldstein, S. B., 1991: A comparison of the weakly nonlinear instability of westerly and easterly jets in a two-layer beta-plane model. *J. Atmos. Sci.*, **48,** 1701–1717.

Flierl, G. R., 1987: Isolated eddy models in geophysics. *Annu. Rev. Fluid Mech.*, **19,** 493–530.

Gal-Chen, T., 1988: A theory for the retrievals of virtual temperature from remote measurements of horizontal winds and thermal radiation. *Mon. Wea. Rev.*, **116,** 1302–1319.

Garbow, B. S., J. M. Boyle, J. J. Dongarra, and C. B. Moler, 1977: *Matrix Eigensystem Routines—EISPACK Guide Extension.* Springer-Verlag, 343 pp.

Gierasch, P. J., and B. J. Conrath, 1993: Dynamics of the atmospheres of the outer planets: Post-*Voyager* measurement objectives. *J. Geophys. Res.*, **98,** 5459–5469.

Gill, A. E., 1982: *Atmosphere–Ocean Dynamics.* Academic Press, 662 pp.

——, J. S. A. Green, and A. J. Simmons, 1974: Energy partition in the large-scale ocean circulation and the production of mid-ocean eddies. *Deep-Sea Res.*, **21,** 499–528.

Greatbatch, R. J., 1985: Kelvin wave fronts, Rossby solitary waves and the nonlinear spin-up of the equatorial oceans. *J. Geophys. Res.*, **90,** 9097–9107.

Held, I. M., and A. Y. Hou, 1980: Nonlinear axially symmetric circulations in a nearly inviscid atmosphere. *J. Atmos. Sci.*, **37,** 515–533.

James, I. N., 1994: *Introduction to Circulating Atmospheres.* Cambridge University Press, 422 pp.

Killworth, P. D., 1979: On the propagation of stable baroclinic Rossby waves through a mean shear flow. *Deep-Sea Res. Part A,* **26,** 997–1031.

Marshall, H. G., and J. P. Boyd, 1987: Solitons in a continuously stratified equatorial ocean. *J. Phys. Oceanogr.*, **17,** 1016–1031.

Matsuno, T., 1966: Quasi-geostrophic motions in the equatorial area. *J. Meteor. Soc. Japan,* **44,** 25–43.

McWilliams, J. C., 1991: Geostrophic vortices. *Nonlinear Topics in Ocean Physics,* A. R. Osborne, Ed., North-Holland, 5–50.

Moler, C. B., and G. W. Stewart, 1973: An algorithm for generalized matrix eigenvalue problems. *SIAM J. Numer. Anal.*, **10,** 241–256.

Needler, G. T., 1967: A model for thermohaline circulation in an ocean of finite depth. *J. Mar. Res.*, **25,** 329–342.

Nezlin, M. V., and G. G. Sutyrin, 1994: Problems of simulation of large long-lived vortices in the atmospheres of the giant planets (Jupiter, Saturn, Neptune). *Surv. Geophys.*, **15,** 63–99.

Panetta, R. L., 1993: Zonal jets in wide baroclinically unstable regions: Persistence and scale selection. *J. Atmos. Sci.*, **50,** 2073–2106.

Pierrehumbert, R. T., and K. L. Swanson, 1995: Baroclinic instability. *Annu. Rev. Fluid Mech.*, **27,** 419–467.

Rahmstorf, S., 1993: A fast and complete convection scheme for ocean models. (Unpublished manuscript) *Ocean Modelling,* **101,** 9–11.

Rhines, P. B., 1975: Waves and turbulence on a beta plane. *J. Fluid Mech.*, **69,** 417–443.

——, 1989: Deep planetary circulation and topography: Simple models of midocean flows. *J. Phys. Oceanogr.*, **19,** 1449–1470.

——, 1994: Jets. *Chaos,* **4,** 313–339.

Smagorinsky, J., 1958: On the numerical integration of the primitive equations of motion for baroclinic flow in a closed region. *Mon. Wea. Rev.*, **86,** 457–466.

Smith, R. D., J. K. Dukowicz, and R. C. Malone, 1992: Parallel ocean general circulation modeling. *Physica D: Amsterdam,* **60,** 38–61.

Sromovsky, L. A., S. S. Limaye, and P. M. Fry, 1993: Dynamics of Neptune's major cloud features. *Icarus,* **105,** 110–141.

Vallis, G. K., and M. E. Maltrud, 1993: Generation of mean flows and jets on a beta plane and over topography. *J. Phys. Oceanogr.*, **23,** 1346–1362.

Welander, P., 1959: An advective model of the ocean thermocline. *Tellus,* **11,** 309–318.

Williams, G. P., 1975a: Some ocean–Jupiter connections. *Mode News,* **78,** 1–4.

——, 1975b: Jupiter's atmospheric circulation. *Nature,* **257,** 778.

——, 1978: Planetary circulations: 1. Barotropic representation of Jovian and terrestrial turbulence. *J. Atmos. Sci.*, **35,** 1399–1426.

——, 1979: Planetary circulations: 2. The Jovian quasi-geostrophic regime. *J. Atmos. Sci.*, **36,** 932–968.

——, 1985a: Geostrophic regimes on a sphere and a beta plane. *J. Atmos. Sci.*, **42,** 1237–1243.

——, 1985b: Jovian and comparative atmospheric modeling. *Advances in Geophysics,* Vol. 28A, Academic Press, 381–429.

——, 1988a: The dynamical range of global circulations—I. *Climate Dyn.*, **2,** 205–260.

——, 1988b: The dynamical range of global circulations—II. *Climate Dyn.*, **3,** 45–84.

——, and J. L. Holloway, 1982: The range and unity of planetary circulations. *Nature,* **297,** 295–299.

——, and T. Yamagata, 1984: Geostrophic regimes, intermediate solitary vortices and Jovian eddies. *J. Atmos. Sci.*, **41,** 453–478.

——, and R. J. Wilson, 1988: The stability and genesis of Rossby vortices. *J. Atmos. Sci.*, **45,** 207–241.

Yamagata, T., 1982: On nonlinear planetary waves: A class of solutions missed by the traditional quasi-geostrophic approximation. *J. Oceanogr. Soc. Japan,* **38,** 236–244.